Tribological Performance of Positive Surface Textured Sliding Contact under Mixed Lubrication– An Experimental and Numerical Approach

A thesis submitted in the partial fulfillment of the requirements for the award of the degree of

DOCTOR OF PHILOSOPHY

By

Mr. P. Venkateswara Babu

(Roll No. 714128)

Under the supervision of

Dr. Syed Ismail

and

Dr. B. Satish Ben

DEPARTMENT OF MECHANICAL ENGINEERING

NATIONAL INSTITUTE OF TECHNOLOGY WARANGAL

WARANGAL-506 004, TELANGANA, INDIA

2020

Dedicated to

My beloved Parents and Teachers

NATIONAL INSTITUTE OF TECHNOLOGY WARANGAL

DECLARATION

This is to certify that the thesis entitled "**Tribological Performance of Positive Surface Textured Sliding Contact under Mixed Lubrication– An Experimental and Numerical Approach"**, is a bonafide work done by me under the supervision of Dr. Syed Ismail and Dr. B. Satish Ben and was not submitted elsewhere for the award of any degree.

I declare that this written submission represents my idea in my own words and where others ideas or words have not been included. I have adequately cited and referenced the original sources. I also declare that I have adhered to all principles of academic honesty and integrity and have not misinterpreted or fabricated or falsified any idea/data/fact/source in my submission. I understand that any violation of the above will be a cause for disciplinary action by the Institute and can also evoke penal action from the sources which have thus not been properly cited or from whom proper permission has not taken when needed.

Date:

Place:

P. Venkateswara Babu
Research Scholar
Roll No. 714128

NATIONAL INSTITUTE OF TECHNOLOGY WARANGAL

CERTIFICATE

This is to certify that the thesis entitled "**Tribological Performance of Positive Surface Textured Sliding Contact under Mixed Lubrication– An Experimental and Numerical Approach"** that is being submitted by **Mr. P. Venkateswara Babu** in partial fulfillment for the award of the degree of Doctor of Philosophy (PhD) in the Department of Mechanical Engineering, National Institute of Technology Warangal, India, is a record of the bonafide research work carried out by him under our guidance and supervision. The results of embodied in this thesis have not been submitted to any other University or Institute for the award of any degree or diploma.

Date:

Place:

Dr. Syed Ismail
Assistant Professor
Department of Mechanical Engineering
NIT Warangal

Dr. B. Satish Ben
Associate Professor
Department of Mechanical Engineering
NIT Warangal

ACKNOWLEDGEMENTS

I would like to express my sincere gratitude to my supervisors, **Dr. Syed Ismail and Dr. B. Satish Ben** for their invaluable guidance and motivation throughout my Ph.D. I am highly indebted to them for their expertise while sharing their knowledge, understanding, encouragement and patience. I am immensely thankful to them for their valuable advices, correcting all my manuscripts, progress reports, thesis reports with great concern and commitment and spending their precious time with good discussions regarding my research work.

I wish to sincerely thank university authorities, **Prof. N. V. Ramana Rao**, Director, National Institute of Technology, Warangal and others who gave me an opportunity to carry out research work. I also sincerely thank **Prof. N. Selvaraj**, Head, Mechanical Engineering Department, National Institute of Technology, Warangal for his continuous support towards carrying out research work.

Thanks are also due to **Prof. P. Bangaru Babu**, former Head, Mechanical Engineering Department, National Institute of Technology, Warangal for providing necessary departmental facilities and services during successful completion of research work. I wish to express my sincere and whole hearted thanks and gratitude to **Prof. R. Narasimha Rao** and **Dr. G. Brahmaraju** (DSC members) for their kind help, encouragement and valuable suggestions for the successful completion of research work. I wish to thank **Dr. G. Raghavendra** for his extended help during this work.

I would like to express my sincere thanks to all my friends and colleagues specially, to **Dr. Mallikarjuna Rao**, **Dr. Kishore**, **Dr. Amrut Shrikant Mulay**, **Mr. Sri Chaitanya**, **Mr. Markandeyulu**, **Mr. Avinash Borgaonkar**, **Mr. Nagendra Prasad**, **Mr. Ramana Reddy**, **Mr. Satish**, **Mr. Shyam Kumar**, **Mr. Yogesh Thakre**, **Mr. Shyam Sundar Patel**, **Mr. Subhash Chandra bose, Mr. Rakesh, Mr. Sasidhar, Mr. S V Ramakrishna, Mr. Ajay Kumar, Mr. Murali, Mr. Narasimha Rao, Mr. Srikanth, Mr. Sudheer, Mr. Riyaz, Mr. Sasi Kaye, Mr. Habeeb Rahman, Mr. Naresh Babu, Mr. Ramanjulu and Mr. Narayana.** I would like to thank **Mr. Yellaiah**, Tribology Lab technician for his support during the completion of the research work.

Words are inadequate to express my thanks to all my family members, my father **Mr. P. Gangulappa**, mother **Mrs. P. Subbamma**, sister **Ms. P. Swapna Kumari** and my wife **Mrs. P. Vasavi** for exhibiting patience during this long and arduous journey.

I want to express my sincere thanks to all those who directly or indirectly helped me at various stages of this work. Above all, I express my indebtedness to the "Almighty" for all his blessing and kindness.

P. Venkateswara Babu

Abstract

Energy efficiency is a major concern in all industries as well in society because of limited resources and pollution related problems. Friction is one of the major sources which can affect energy efficiency and approximately one-third of the energy resources are consumed worldwide to overcome friction between mechanical components. This is the case in particular with internal combustion (IC) engines, in which friction in the piston assembly contributes approximately to 50-60% of the total engine friction [74, 75]. Sliding contacts in the boundary or mixed lubrication regimes experience heavy friction losses due to the presence of thin oil films. Therefore, solutions to reduce friction between the mechanical components are considered crucial in improving energy efficiency. Lubrication improvement and surface modification are key factors in minimizing friction of mechanical tribo-systems. The surface modification techniques such as surface texturing of components have been remarkable in improving the tribological behavior of the sliding pairs, particularly at instances such as boundary or mixed lubrication regimes.

Proper lubrication is one of the key factors to improve the tribological behavior of interacting sliding surfaces under lubricated conditions. Therefore, in order to select the appropriate lubricant, different lubricants which are commercially available, such as SAE20W-50, SAE15W-40 and SAE10W-30, were tested on four ball tester. Based on the experimental results, SAE15W-40 was selected to lubricate the contact. Square-shaped positive textures are fabricated by using a new masking method followed by chemical etching process, which is simple and efficient to produce the required geometry. Afterward, experimental tests were conducted on pin on disc friction and wear test rig to evaluate the friction and wear properties of the developed textured parallel sliding contact. The parameters that have been varied in the present work are texture area density, height and normal load. In order to assess the lubrication regimes, Stribeck curves were drawn with friction coefficient as a function of lubrication parameter. The results showed that the contact was operating in the mixed lubrication regime. Furthermore, minimum friction coefficient and wear rate were obtained at a normal load of 5 N, texture area density of 0.1 and, a texture height of 10 µm at a constant sliding velocity of 1.67 m/s. For these conditions,

friction coefficient and wear rate reduced by 85.4% and 88.9% respectively, in comparison with un-textured surfaces.

Furthermore, texture shape may also effect the tribological properties; however, conducting experiments for different texture shapes is costly and time-consuming. In this regard, a theoretical model of textured parallel sliding contact has been developed under mixed lubrication regime. The modified Reynolds equation (Patir-Cheng flow model) and asperity contact model (Greenwood-Tripp model) were solved for hydrodynamic and asperity pressures, respectively. The textured surfaces were modelled by considering the surface roughness effect on the fluid flow. The numerical result of the developed model was compared with the experimental results of square-shaped positive textures. The results indicated that simulation results were qualitatively in agreement with experimental results. In addition, the developed model was quantitatively validated with previously available literature.

The theoretical model developed has been used to investigate the impact of various texture parameters such as texture shape, area density and height on tribological performance parameters such as friction coefficient, hydrodynamic load support percentage, and minimum film thickness. In addition, the effect of sliding velocity on tribological performance parameters was investigated. The numerical simulation results depicted that an area density of 0.1 and a texture height of 5 μm exhibited lower value of friction coefficient for all the texture shapes. Sliding velocity showed a prominent effect on friction coefficient, hydrodynamic load support percentage, and minimum film thickness for all texture shapes. As for the texture shape's concern, elliptical shape was superior in improving frictional performance compared to other shapes. Furthermore, at an area density of 0.1, texture height of 5 μm and sliding velocity of 0.5 m/s, a maximum friction reduction of 87% was obtained with elliptical shape as compared to un-textured case.

Keywords: chemical etching; friction; parallel sliding contact; pin on disc; surface texture; tribological performance; wear

Table of Contents

List of Tables

List of Figures

List of Abbreviations

Abbreviation	Description
A_s	Total area occupied by the sample surface
A_t	Area occupied by a single texture
A_u	Area occupied by an imaginary unit cell
A', K', Z'	Parameters used in Greenwood and Tripp model (1970)
a	side length of the square-shaped texture
B	Unit cell size
b	Axial width of the sample surface
C_f	Boundary friction factor
d_1	Horizontal distance between the two consecutive textures
d_2	Vertical distance between the two consecutive textures
d_s	Sliding distance
E_1	Elastic modulus of the moving surface
E_2	Elastic modulus of the stationary surface
E'	Composite elastic modulus of the contact pair
F	Total frictional force
F_a	Asperity friction force
F_h	Hydrodynamic friction force
$F_{2.5}$	Statistical function
f	Friction coefficient
H	Oil film thickness ratio
h	Mean film thickness
h_T	Local film thickness
$\bar{h}_T$	Mean gap between the interacting rough surfaces
h_0	Minimum film thickness
h_r	Texture height ratio
h_t	Height of the texture
l	Length of sample surface
N	Number of textures

nx, nz	Number of grid points in x and z-directions
P_t	Pitch length between two consecutive textures
p	Local fluid film pressure or hydrodynamic pressure
$\bar{p}$	Mean fluid film pressure or hydrodynamic pressure
p_{asp}	Mean asperity contact pressure
q_x, q_z	Local fluid flows in x and z-directions
$\bar{q}_x$, $\bar{q}_z$	Mean expected flows in x and z-directions
$2r_p$	Base length of texture
S	Relative dimple depth
S_p	Texture area density
T	Frictional torque
U	Sliding velocity of the moving surface
W	Total load support of the contact system
W_1	Applied load
W_a	Load carried by asperities
W_h	Load carried by fluid film
W_f	Weight of the sample after the experiment
W_i	Weight of the sample before the experiment
x, z	Global coordinate system
β	Asperity mean radius of curvature
γ	Surface pattern parameter
δ_1, δ_2	Random roughness of amplitudes measured from the mean values
η	Asperity density
λ	Aspect ratio of texture
μ	Lubricant dynamic viscosity
v_1	Poisson's ratio of moving surface
v_2	Poisson's ratio of stationary surface
ρ	Density of the sample material
σ	Composite roughness of the sliding pair
σ_1	Surface roughness of moving surface
σ_2	Surface roughness of stationary surface

$\bar{\tau}$	Mean hydrodynamic shear stress
$ø_c$	Contact factor
$ø_f$, $ø_{fs}$, $ø_{fp}$	Friction induced flow factors
$ø_s$	Shear flow factor
$ø_x$, $ø_z$	Pressure flow factors in x and z-directions

Chapter 1

Introduction

This chapter describes the brief history and background of friction and wear. The definition and types of surface texture and its parameters are discussed. The chapter also discusses the role of surface textures in improving the tribological performance and its use in tribological applications. It also outlined the motivation of the present research work. At last, the organization of the dissertation is discussed.

1.1 Friction and wear

In general, friction is intrinsic, and is induced between sliding surfaces, which are in relative motion. Friction has a tendency to oppose relative motion between the sliding surfaces through loss of energy mostly in the form of heat, mechanical vibration and noise. Excessive friction can cause damage to the sliding surfaces, and as a result, the surfaces become worn out. Hence, in most of the mechanical applications, friction is an undesirable phenomenon.

The main reason for the existence of friction is that there is no perfectly smooth surface. In reality, no matter how well the surfaces are prepared, they have a small degree of roughness/waviness in the form of valleys and hills. When two surfaces slide against each other under the relative motion, the asperities on the surfaces interact with each other producing friction as a result. Wear can occur as a result of excessive friction. Thus, each time some material from the sliding surfaces is removed, the surface topography changes and new valleys and hills are generated, and the removed material from the surface can be called wear debris. Some of the wear debris remains at the contact and induces more resistance against the motion. As a result, the form of wear occur can be termed abrasive wear.

Therefore, the intrinsic roughness of the sliding surfaces could be the main reason for the existence of friction and thus wear. However, this friction and wear can be reduced by polishing the sliding surfaces to a fine degree. After some point, although the sliding surfaces are smooth enough, both friction and wear will start to increase again. This is because as the surfaces

become smoother, the attractive forces between the sliding surfaces increases; thus, the surfaces stick to each other. Therefore, some of the material from each surface is transferred to another surface and removes the surface films. This form of wear is called adhesive wear. Although other forms of wear may occur under different conditions; these two wear mechanisms are considered to be significant wear mechanisms. For example, corrosion wear occurs due to the chemical reaction of interacting surfaces with each other or with the environment.

For a long time, it has been discovered that introducing a third element between the sliding surfaces can substantially reduce friction and wear. These elements can keep the asperities of the interacting surfaces apart from each other and also protect the surfaces from unwanted contamination and chemical reaction. Such an element is known as lubricant. A lubricant can be solid, liquid or gas. In general, liquid lubricants such as oils are most common. The lubricating oils that are used in industries can be mineral, organic or synthetic oils. In addition, depending on the application, different additives can be added to the base oil to facilitate the required function of a lubricant.

Along with appropriate lubricants, improvements in the tribological behavior of interacting surfaces can also be achieved through surface engineering. Generally, surface engineering can be considered in two categories: surface coating and surface modification. In surface coating technique, a layer or layers of a material or materials are introduced on the surfaces that are in contact to improve the tribological properties such as friction and wear resistance. The coating process can also be attained by changing the chemical composition of the surface itself. The methods in which the surface is modified without changing its composition such as polishing, honing, heating or local melting are known as surface modification methods. In recent years, most of the researchers have focused on controlling friction and wear through the modification of surface topography by considering parameters such as surface roughness and skewness in a controlled manner. It is believed that surfaces with controlled micro-geometry such as surface textures can be emerging in improving tribological performance. The ranges of the tribological performance improvement in terms of friction coefficient through surface engineering can be seen in Table 1.1.

In addition to the processes mentioned above, the idea of introducing artificial and deterministic surface roughness in the form micro-features with specific shape, size, orientation

and distribution have been of increasing interest. It is believed that well designed micro-features can enhance the tribological performance parameters such as friction and wear of the interacting surfaces.

Table 1.1 Tribological performance improvement through surface engineering

Author	**Friction coefficient**			
	Plain surface	Surface texturing	Surface coating	Surface texture with coating
Vilhena etal. [1]	0.013-0.018	0.006-0.01	-	-
Wang et al. [2]	0.21-0.28	0.15-0.18	-	-
Jiang et al. [3]	0.122-0.181	-	0.11-0.137	-
Martins et al. [4]	0.027-0.034	-	0.02-0.025	-
Garrido et al. [5]	-	-	0.0845-0.1201	0.0587-0.0608
He et al. [6]	-	-	0.16-0.31	0.11-0.24
Hu et al. [7]	-	-	0.06-0.08	0.03-0.06
Ye et al. [8]	-	-	0.082-0.095	0.06-0.072

1.2 Surface textures

Several mechanisms may contribute to hydrodynamic lift in bearings according to the conventional theory of lubrication. These mechanisms are lubricant density variation, viscosity and thermal wedge, squeeze film effect, non-Newtonian effects, eccentric rotation and surface roughness/waviness.

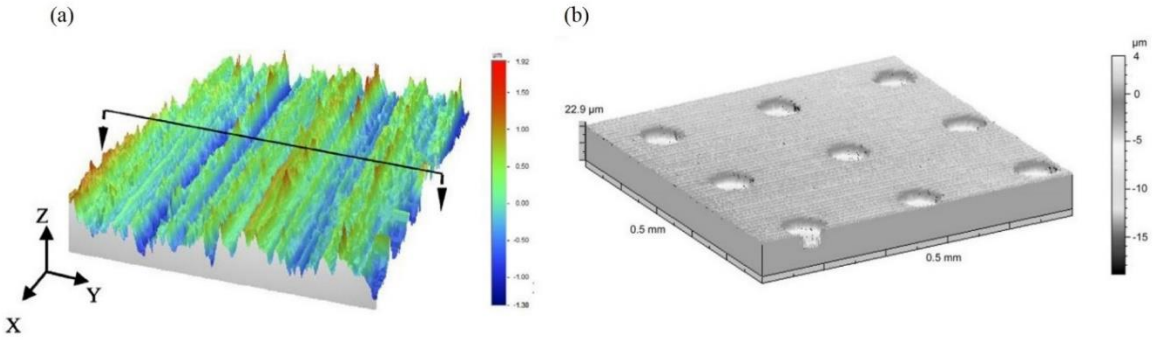

Fig.1.1 Types of surface roughness: (a) random surface roughness [9]; (b) deterministic surface roughness [10]

In recent years, many researchers have focused on surface roughness to achieve improvements in lubrication and tribological performance. The surface can be modified by random and deterministic surface roughness, as shown in Fig.1.1. The surface textures are micro-features that come under the category of deterministic surface roughness. Surface texturing is an effective and reliable method that can alter the surface topography to optimize tribological performance of the interacting sliding surfaces. The concept of surface texturing is inspired by nature. For example, shark skin boosts up the swim speed against drag force, and hence the swimsuits of Olympic athletes have v-shaped grooves which resemble the texture of shark skin [11].

In literature, different terminology has been used to describe intentionally created surface irregularities such as surface features, surface structures or geometries, surface topographies and surface textures. Surface textures can be classified as positive and negative textures, as shown in Fig.1.2. Generally, positive textures protrude out of the surface (see Fig.1.2 (a)), whereas negative textures recess into the surface (see Fig.1.2 (b)).

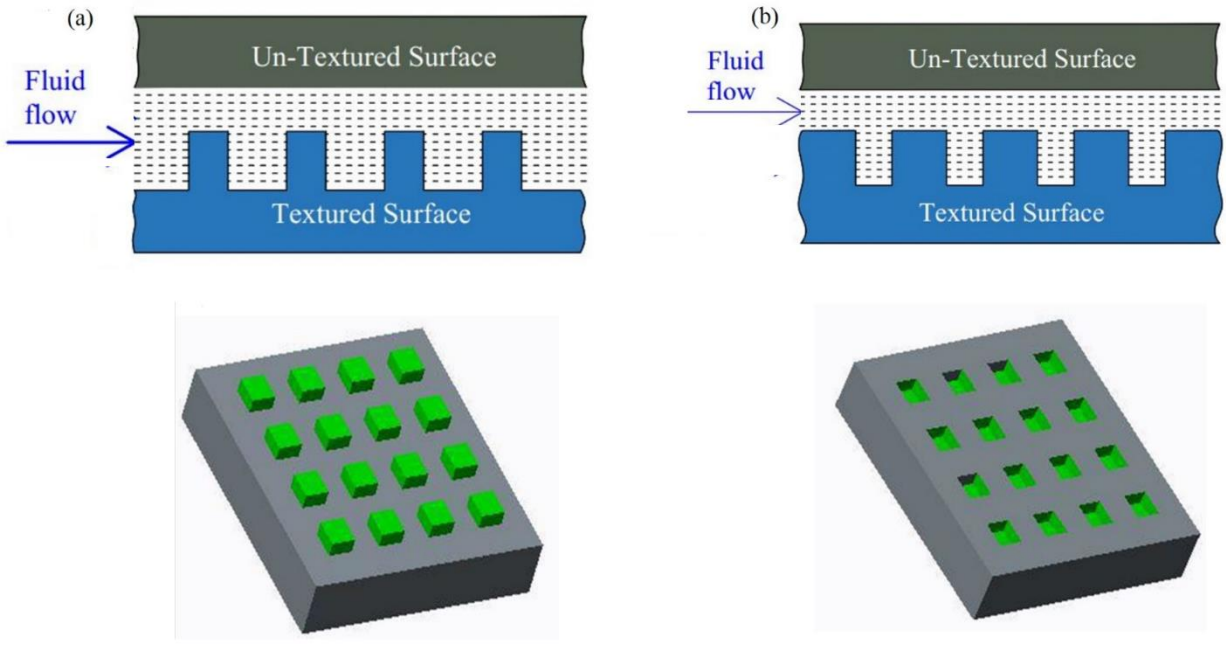

Note : (a) Positive textures; (b) Negative textures

Fig.1.2 Types of surface texture

The negative textures are described by different names in the literature such as dimples, pores, grooves, pits, pockets, while positive textures are called protrusions, bumps, asperities,

etc. Surface texture geometry and dimensions can vary in shape and range from some microns to a lot of microns in size. A typically fabricated texture shapes are shown in Fig 1.3. In recent years, many researchers have focused on different surface texture shapes and distributions. However, circular dimples are still the most commonly used because of the ease of manufacturing and lower costs.

In general, positive texture gives high preferential end flow and high hydrodynamic pressure but they are difficult to manufacture. Whereas, negative textures always ensure the availability of fluid film between the interacting sliding surfaces while acting as oil reservoir and they are easy to manufacture. However, the negative textures are weak in generating high hydrodynamic pressures at the contact.

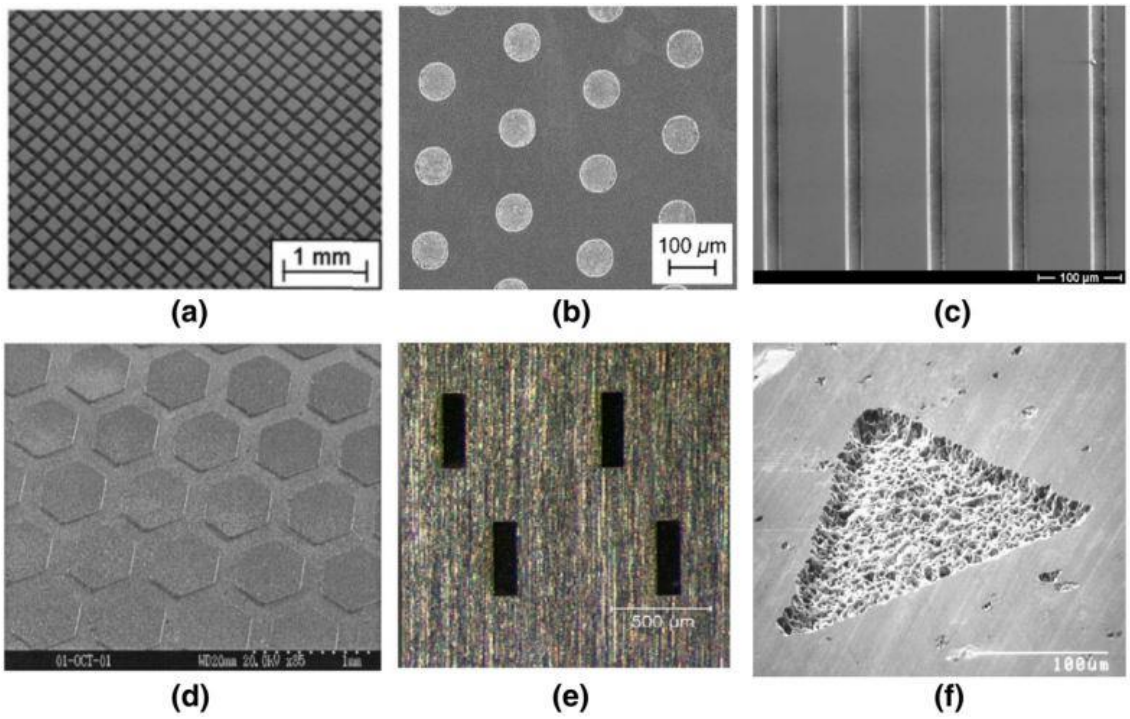

Fig.1.3 SEM images of different surface textures: (a) square-shape (positive) [12], (b) hemispherical shape (negative) [13], (c) grooves (negative) [14], (d) hexagonal shape (positive) [15], (e) square shape (negative) [16], (f) triangular shape (negative) [17].

1.2.1 Surface texture parameters

A parallel sliding contact with square dimples is explored in Fig.1.4 to describe the commonly used parameters of textured surfaces. An individual texture can be illustrated by parameters such

as shape, size, texture height/depth and its orientation related to sliding direction. The commonly used surface texture parameters are explained below:

Aspect ratio (λ): The aspect ratio is defined as dimple depth/height over diametric length ratio.

$$\lambda = \frac{h_t}{2r_p} \tag{1.1}$$

It is noticed that h_t is texture's height/depth in the case of positive/negative texture and $2r_p$ is diametric length.

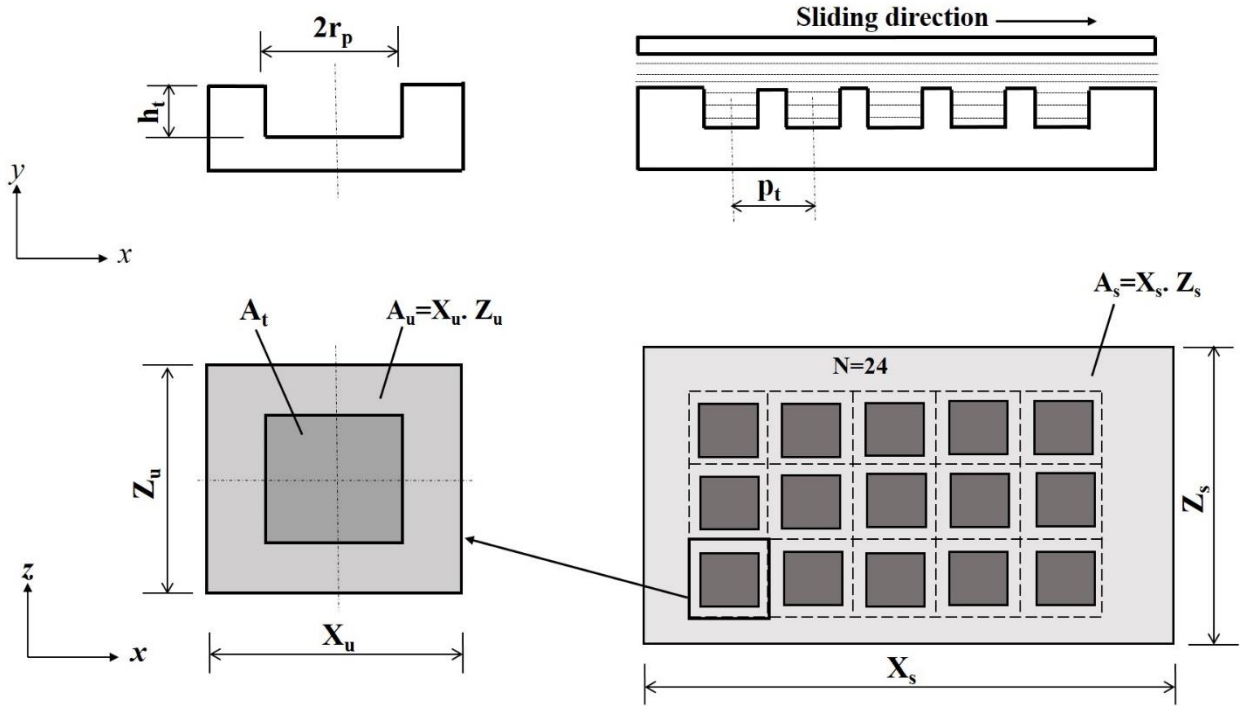

Fig.1.4 Schematic view of parallel sliding contact with square-dimples

Area density (S_p): The area density is defined as the area occupied by the textured portion to the total area of the considered surface.

$$S_p = \frac{A_t N}{A_s} = \frac{A_t}{A_u} \tag{1.2}$$

Where, N=number of textures, A_t=Area occupied by a single texture, A_s=total area occupied by the surface, A_u= Area occupied by an imaginary unit cell.

Relative dimple depth (*S*): The relative dimple depth of the texture is defined as the ratio of texture's depth/height to minimum film thickness.

$$S = \frac{h_t}{h_0} \tag{1.3}$$

Where h_0 is the minimum film thickness.

Height ratio (h_r): The texture's height ratio is defined as follows;

$$h_r = \frac{h_t + h_0}{h_0} = S + 1 \tag{1.4}$$

Pitch (P_t): It is the center distance between the two consecutive textures in sliding direction.

Although all the above-mentioned parameters considerably affect the overall performance of the mechanical systems, it is recognized that aspect ratio, area density, texture depth/height and shape are the most influential and important parameters of textured surfaces [18]. Therefore, most of the studies have been focused on optimization of these parameters.

1.2.2 Use of surface textures in tribological applications

In the mid-1960s, Hamilton et al. [19] studied the influence of surface irregularities on the lubrication performance of mechanical face seals. They investigated both asperities and cavities. Their results showed that by introducing the micro-surface irregularities on the sliding surfaces, an additional load carrying capacity had been developed. Afterwards, their work was continued by Anno et al. [20, 21]. Since then it is believed that micro-irregularities such as asperities and grooves can be implemented on the sliding surfaces to get a beneficial effect on lubrication performance of mechanical seals. Moreover, this concept was further developed by Etsion and his group [22, 23]. The authors utilized laser technology to produce surface textures in the form of micro-pores or dimples on the surfaces.

Since the 1990s, surface texturing has been gaining increasing attention in tribological applications due to its potency to improve lubrication, friction and wear performance of mechanical components in relative motion. In recent years, the idea of introducing micro-textures on the surfaces has increased in industrial applications in order to experience the beneficial effects of tribological performance. For example, in order to prevent the adhesion of

recording heads with contacting surface in magnetic storage discs, surface textures are provided in landing areas of the disc [24, 25]. Furthermore, in order to overcome the adhesion and stiction in the MEMS devices, surface texturing is employed to reduce adhesion and stiction [25]. Surface texturing has been applied to the surfaces of the functional tool in forming processes such as deep drawing [26], cold forging [27] and cold rolling [28] and this increased the tool life and reduced the lubricant consumption. In recent times, surface textures have been successfully employed on the rake face of cutting tools, and this yielded better lubrication conditions in an orthogonal machining operation [29, 30].

In addition, great breakthroughs have been achieved by means of surface texturing of many tribological surfaces such as mechanical seals [31-34], journal bearings/thrust bearings [35-39], PR-CL contact in IC engines [40-43]. Moreover, surface texturing has also been proposed in the applications such as engine power train and drive train components and wrist pin bearings, where the starved lubrication conditions may exist [44, 45].

1.2.3 Role of surface texturing in improving tribological performance

The mechanisms through which the surface texture enhances the tribological performance of sliding contacts are “lubricant replenishment”, “wear debris entrapping” and “additional hydrodynamic lift” [46-48]. A normally grounded surface roughness cannot hold the lubricant in place since there is no physical mechanism to entrap the lubricant or wear debris effectively. It is believed that well-designed textured surface can improve the tribological behavior of sliding contacts. The mechanisms of surface texture can be seen in Fig.1.5. The first mechanism is related to lubricant starvation, i.e., the inadequate lubricant present at the inlet of the contact causes a reduction in film thickness, which can be found in automotive PR-CL contacts at piston reversals. In general, starvation occurs when the lubricant is pushed away from the contact during one pass and does not flow back into the contact in time for the next pass. In such situations, textures on the surfaces act as “micro-reservoirs” and increase the lubricant flow back into the contact- this process is known as “lubricant replenishment.” Many researchers have investigated this mechanism [44, 46-50].

The other mechanism is “wear debris entrapment” in which surface textures reduce the wear by removing the wear debris from the contact zone through accumulating in the pockets; otherwise, the debris remains at the contact and accelerates the wear of the components. Several

studies have identified that surface textures can remove wear particles from the contact zone and help in delaying the wear process through debris entrapment, which results in prolonged life of the components [14, 51-53]. The role of surface texture in improving tribological performance is mainly based on the contact conditions as well as operating lubrication regime. In the case of hydrodynamic or mixed lubrication, these micro-features (surface textures) act as Rayleigh step bearings to generate additional hydrodynamic lift by forming convergent clearances [54-57]. In the case of boundary lubrication, these micro-features acts as secondary lubricant reservoirs and supply lubricant to the desired locations [13, 58, 59]. In boundary lubrication, these intentionally created undulations trap the wear debris and hence decrease ploughing between interacting surfaces. As a result, abrasive wear and friction can be reduced [35, 60-62].

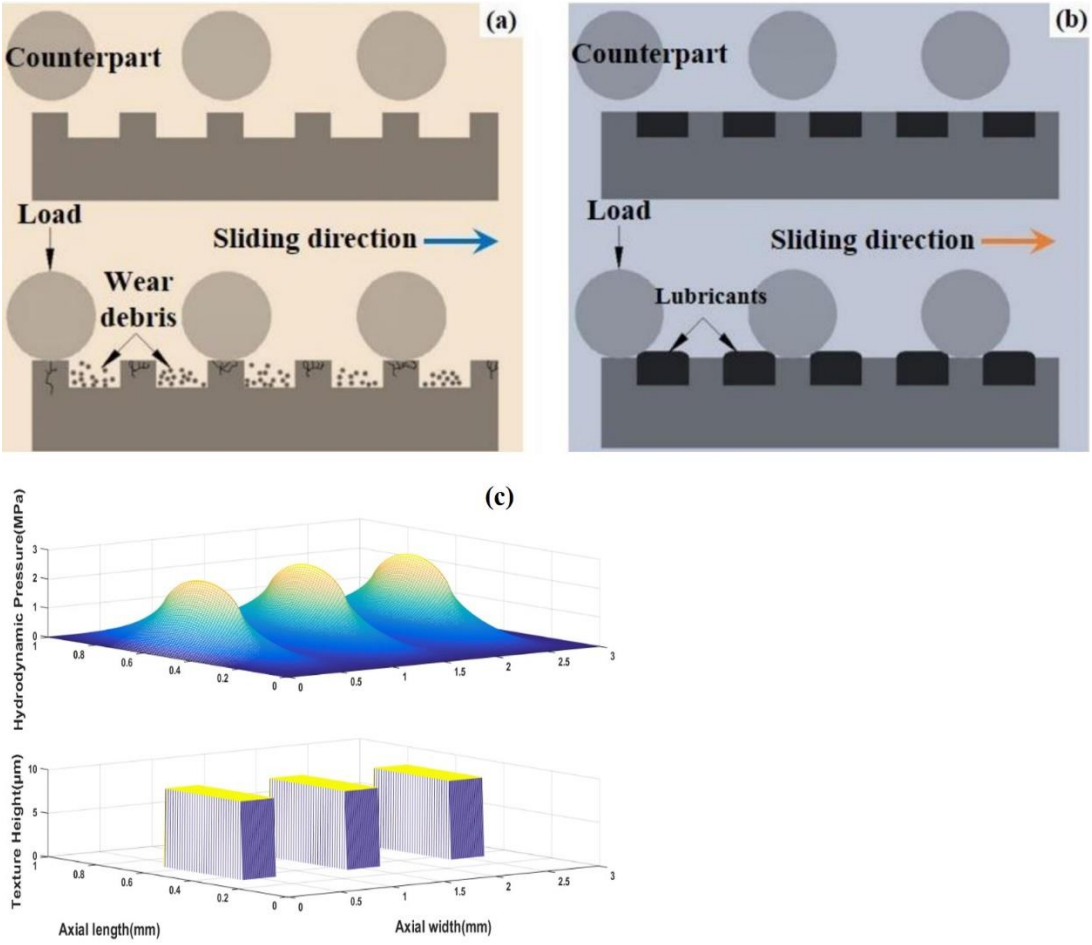

Fig.1.5 Mechanisms of surface texture in improving tribological performance [63]: (a) capturing Wear debris; (b) lubricant reservoir; (c) generating hydrodynamic pressure

In addition to the above-said mechanisms, the lubricant present in micro-pockets can prevent the abnormal temperature rise due to dry sliding conditions during the start or stop operations of the contact [13]. Furthermore, it is reported that the leading edge of each texture becomes worn out during the initial stages of sliding and acts as an inclined surface which promotes hydrodynamic lift at the contact [64]. This leading-edge concept was reported by Hupp [64] with the help of experimental data, which indicates that the initial startup friction coefficient is much more than the average friction coefficient values. Furthermore, another mechanism of surface textures is based on the occurrence of cavitation. In general, local cavitation may occur in the diverging clearance of micro-pocket due to asymmetric hydrodynamic pressure distribution over each pocket, which offers a substantial amount of load-carrying capacity. In general, for incompressible fluids, pressure increases in convergent regions, whereas it decreases in diverging regions. Theoretically, the cavity induced in the diverging region is an isobaric region owing to the pressure generated in this region which cannot be lower than cavity pressure. Because of this, the pressure rise in convergent regions is more than the pressure drop in divergent regions; as a result, an additional load carrying capacity can be generated [65, 66]. This beneficial effect of generating the additional load support by hydrodynamic action is called micro-hydrodynamics of surface textures [67]. Surface texturing can also have a significant effect in expanding the boundaries of hydrodynamic lubrication regime under boundary or mixed lubrication conditions [68-70]. In addition to these, the reduction of stiction and micro-plasto-hydrostatic lubrication effects are also reported as the beneficial outcomes of surface texturing [71].

1.3 Motivation of the present work

Energy efficiency is a major concern in industries as well in society because of insufficient resources and pollution related problems [72]. In recent days, approximately one-third of the energy resources are consumed worldwide to overcome the friction between mechanical components [73]. This is the case in particular with IC engines, in which friction in the piston assembly contributes approximately to 50-60% of the total engine friction [74, 75]. Therefore, solutions to reduce friction between the mechanical components are considered crucial in improving energy efficiency. In this context, tribology plays a crucial role in reducing friction and wear between the mechanical components which are in relative motion. Tribological

solutions may include but are not limited to surface treatments of components, such as applying coatings to the surfaces [76], chemical modifications [77] and surface texturing [13, 62, 77-79]. Among all the methods, surface texturing has evolved as a prominent method for improving tribological performance of interacting surfaces. This motivates to do the research work in the area of surface texturing to improve the tribological performance of sliding sufaces.

1.4 Scope of the work

It is crucial to understand the fundamental concept of surface texturing and mechanisms behind the improvement in friction and wear performance. The surface texture geometry and fabrication methods also play a key role in deciding the performance of textured surfaces. Surface textures are classified as positive and negative textures. Considerable work have been reported on negative textures, while a lot of scope is available for fabrication of positive textures and its investigation on tribological behavior of sliding contacts. In numerical modelling, most of the researchers have focused on modelling the textured surfaces in pure hydrodynamic lubrication regime. There is a scope for the numerical study of positive textured surfaces in mixed lubrication regime to predict more accurately the tribological characteristics of interacting sliding pairs. Furthermore, the effects of surface roughness of the sliding surfaces on fluid flow may be included while modelling the textured sliding contacts.

1.5 Thesis organization

The thesis is organized into seven chapters, and the contents of each chapter are summarized as follows:

Chapter 1 deals with the significance of surface texture concerning the tribological performance of mechanical components. It describes the history and background, classification of surface textures and its parameters, applications, mechanisms of surface textures and also rationale for the present research.

Literature review on surface texturing and its industrial applications are discussed in **chapter 2**. The literature on experimental and numerical investigation of surface textures and its beneficial effect on the tribological performance of various sliding pairs has also been discussed. The objectives of the present work have also been outlined.

Chapter 3 provides different fabrication techniques to produce surface textures. The fabrication technique of chemical etching method to produce square-shaped positive texture with varying area density and texture height is presented. The effect of etching concentration and etching time on texture height has been highlighted.

The selection of materials and appropriate lubricant to lubricate the parallel sliding contact is presented in **chapter 4**. The sliding experiments were conducted with square-shaped textures under lubricated condition and worn surfaces were analyzed. The experimental results of square-shaped positive textures on the tribological performance have been studied, and the results are compared with un-textured reference.

Chapter 5 addresses the development of numerical code for surface textured parallel sliding contact under mixed lubrication regime. The modified Reynolds equation proposed by Patir-Cheng and asperity contact model proposed by Green Wood-Tripp are discussed.

The developed numerical code is used to optimize the tribological properties of the parallel sliding contact. The effect of surface texture geometric parameters such as texture shape, area density and height through the developed numerical code is discussed in **chapter 6**.

Chapter 7 summarizes the concluding remarks of the present research work carried out. The chapter also provides future recommendations based on the present work.

Chapter 2

Literature review

Lubrication improvement and surface modification are key factors in minimizing the friction of mechanical tribo systems [80]. Surface texturing has been found to be a potential method which can purposefully modify the surface topography in a pre-determined manner by generating specific features to improve the lubrication conditions and hence the tribological performance of mechanical components, which are in relative motion [81]. The chapter presents a brief literature review of experimental and numerical studies of the textured surfaces. This chapter also provides a summary of literature review and objectives of the present work.

2.1 Impact of surface texture on tribological performance: Experimental studies

Many researchers have studied the impact of surface texturing on tribological performance under different lubricated sliding conditions and drawn different conclusions. Kovalchenko et al. [82] performed experiments on smooth and laser textured surfaces at different load and speed conditions in the presence of low and high viscous oils on pin-on-disc apparatus. They found that laser textured surfaces exhibited maximum reduction in friction compared to smooth surfaces with high viscous oils at higher loads and speeds. Henry et al. [83] studied the influence of square-shaped dimples on load support and frictional performance of parallel thrust pad bearing. Their results showed that textured bearings reduced the friction by up to 30% at low loading conditions, while for heavy loading conditions, the effect of textured bearing was found detrimental when compared with un-textured bearings. Furthermore, an experimental investigation of micro-texture parameters on friction performance was reported by Wakuda et al. [13]. Their results showed that the texture size and area density were found to be significant on the tribological properties, while texture shape had no effect. A maximum reduction in friction was observed for a texture size of 100 μm and an area density below 20%. On the contrary, Galda et al. [69] observed that texture shape, size, and area density were critical factors in

friction and wear reduction of sliding contacts under lubricated conditions. Etsion et al. [84] investigated the laser surface textured parallel thrust bearing on the performance characteristics such as clearance and friction. Spherical shaped dimples were tested under hydrodynamic lubrication conditions for various load and speed conditions. Their results showed 50% reduction in friction coefficient and also a drastic increase of clearance of about three times with textured bearings when compared with un-textured bearings. Furthermore, Dumitru et al. [85] investigated micro-dimpled steel disks under mixed lubrication regime. The array of micro-dimple patterns were arranged in the form of micro holes as shown in Fig.2.1. The dimple diameter and depths were varied in a range of 50-100 μm and 5-8 μm, respectively. The spacing between the dimples varied in the range of 30-60 μm. The authors measured the lifetime of the textured sample in terms of the sliding distance at which the friction coefficient increases rapidly and reached the friction coefficient of an un-textured sample. Their results showed eight times improvement in lifetime of the textured sample compared with un-textured sample.

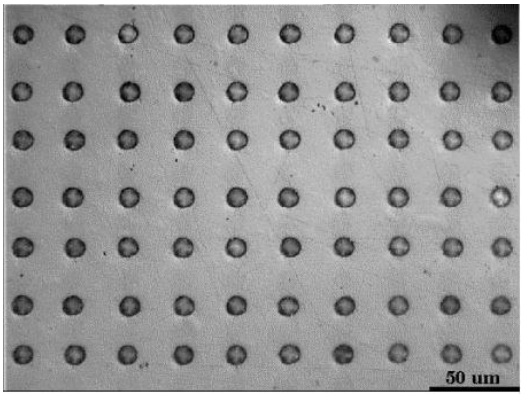

Fig.2.1 Micro-dimples arranged in square pattern [85]

On the other hand, Wang et al. [86] investigated the effects of triangular-shaped dimples on tribological behavior of lubricated point contacts. The authors utilized laser ablation process to produce triangular-shaped dimples on steel disks by varying coverage ratio and depth. The image of textured steel disk for different coverage ratios is shown in Fig.2.2. Their results suggested the lowest value of friction coefficient was obtained at optimum parameters of texture depth 10-15 μm and coverage ratio 10%. In addition, the sliding direction perpendicular to the base of triangular texture had a prominent effect in reducing friction.

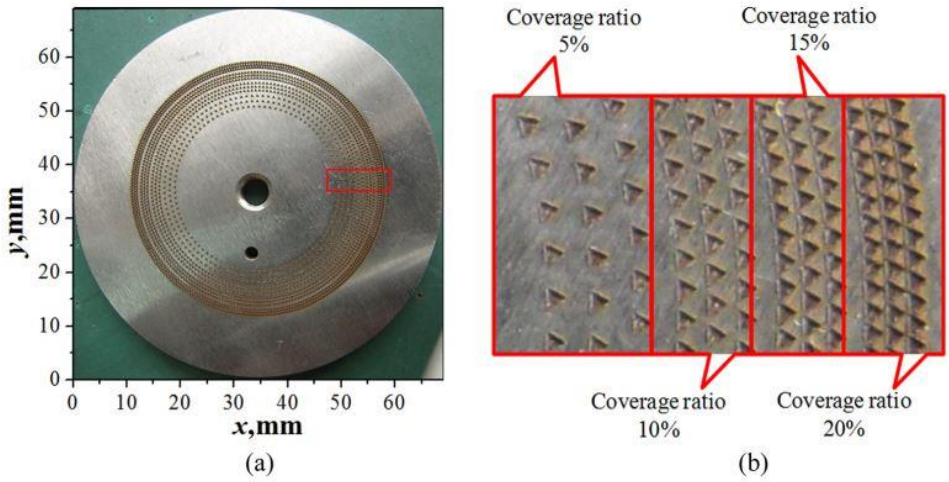

Fig.2.2 The textured steel disk with triangular-shaped dimples [86]

Furthermore, in order to study the effects of the texture size, depth and density on the frictional performance of sliding contact, Echávarri Otero et al. [87] conducted experiments on ball-on-disc tribometer under high load and low-speed conditions. Elliptical textures have been fabricated on disc surface (see Fig.2.3) by photolithography and chemical etching methods. The experimental results have been used to optimize the texture parameters by using artificial neural networks. A minimum friction coefficient was found at optimum texture parameters of the density of 5%, depth of 78 µm, major and minor axes of size 600 µm and 150 µm, respectively. Furthermore, Varenberg [88] studied the effect of groove width and depth on friction and wear reduction. They found that wider grooves reduced the friction more compared to smaller grooves. This may be due to more wear debris captured with wider grooves. In addition, reduction in friction was achieved with increase of groove depth to a certain point, and after that no effect of groove depth on friction reduction was observed. This is because once the depth of the groove reached a certain point below which the lowest particle had a size of wear debris, then wear debris may not reach the bottom and thus, there is no beneficial effect in creating deeper grooves.

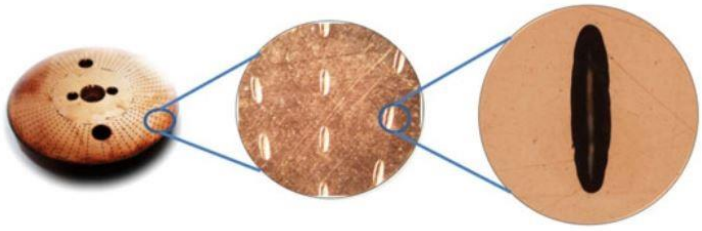

Fig. 2.3 Elliptical textured disc surface fabricated by chemical etching method [87]

Meng et al. [16] investigated the effect of rectangular dimpled parallel sliding surfaces for friction reduction. The laser textured rectangular dimples with a length 400 μm, width of 100 μm and depth of 25 μm (see Fig.2.4), were tested under different sliding conditions. Their results indicated the beneficial effects of dimples crucially depended on operating conditions. Friction reduction was obtained at larger loads and larger speeds with lower roughness values. However, with smaller loads and speeds, the beneficial effect of using dimples was found negligible.

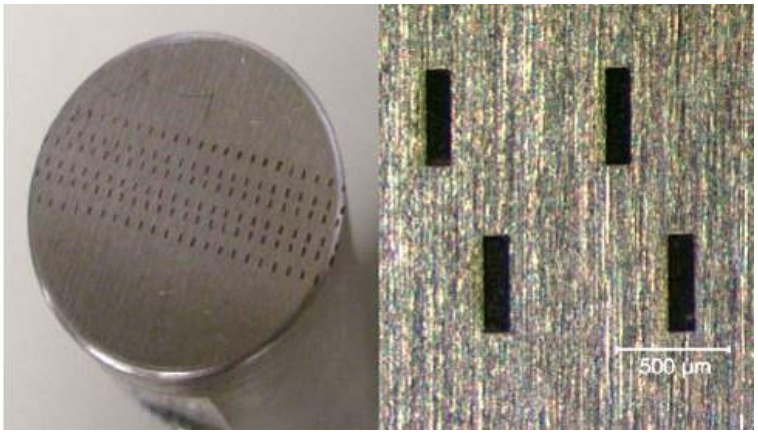

Fig.2.4 Rectangular dimples fabricated by laser surface texturing [16]

Yan et al. [89] investigated the significance of dimple textured parameters on frictional performance. The authors conducted the experiments on dimple textured chromium coated samples with area density of 5 to 20%, dimple diameter of 50 to 300 μm and depth of 5 to 20 μm. The authors reported that a dimple diameter of 100-200 μm, area density of 5% and dimple depth of 5-10 μm exhibited a friction reduction of 77.6% when compared with un-textured case. In a similar study, Schneider et al. [90] investigated the effect of textured area density, aspect ratio and dimple packing patterns (distribution) on the tribological properties of steel surfaces. The dimple aspect ratio was varied in a range of 0.02-0.2 and area density was varied from 5% to 30% with cubic, hexagonal and random dimple distribution. The authors reported that an aspect ratio of 0.1 showed more friction reduction regardless of changing dimple diameter or depth. Higher friction reduction was observed at an area density of 10% with hexagonal dimple distribution. Furthermore, a maximum friction reduction of 80% was achieved with textured surfaces than un-textured surfaces. However, Gachot et al. [78] summarized the optimal coverage ratios of dimple texture for friction reduction under different lubrication regimes. The textures with coverage ratio of 10-30% under full film lubrication, 7-12% under mixed

lubrication regime and 5-7% under boundary lubrication regime showed optimal results, whereas in case of textured coating surfaces, higher coverage ratios (40-70%) yielded better performance.

In recent studies, some of the authors pointed out the importance of combined surface texturing and coating deposition. In this regard, Chen et al. [91] performed some pin on disc experiments on die steel substrate to identify the beneficial effects of surface texturing as well as coating deposition. The authors produced triangular-shaped dimples on steel substrate after TiN coating deposition. The authors compared the results of surface texturing, coating deposition and surface texturing with coating deposition in terms of friction coefficient and wear volume. Their results indicated the combination of surface texturing and coating deposition exhibited excellent tribological performance when compared with other two cases. Furthermore, Sedlaček et al. [92] investigated the effects of surface texture geometry and sequence on tribological properties of sliding surfaces. The authors introduced the negative textures in the form of pyramid, cone and dimples before and after deposition of TiAlN coating. The results showed that dimple shaped textures exhibited better tribological performance, while pyramid shape provided worst tribological performance. In addition, if the surface textures were introduced after coating deposition, the friction coefficient is lower regardless of the texture shape.

Moreover, Segu and his colleagues [93, 94] introduced an innovative approach of multi-scale textures by combining different texture shapes (see Fig.2.5). Their idea of combining micro-dimples and ellipses resulted in faster transition between lubrication regimes and also lower values of friction coefficient for conformal contact conditions [93]. Their results indicated that the maximum friction reduction was obtained at an area density of 0.12 and a dimple depth of 5.5 μm. Furthermore, similar effects have been observed in case of non-conformal conditions with multi scale texture combining squares and triangles [94]. In their study, the results of combined dimples and square, dimples and triangle were compared with dimple textured and un-textured surfaces. It has been observed that the friction coefficient of the surfaces with multi scale texturing was lower than dimple textured and un-textured surfaces.

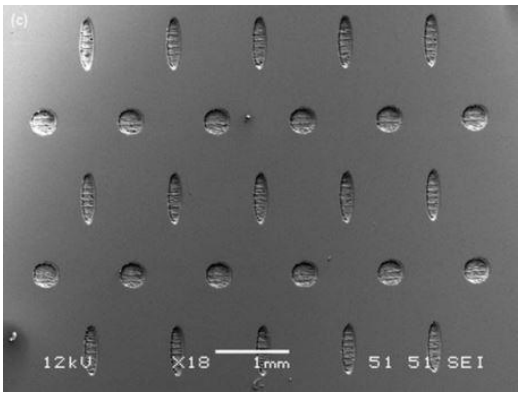

Fig.2.5 SEM image of multi scale texturing of combining dimples and ellipse [93]

In some of the recent studies, positive textures (protrusions) have shown significant impact in reducing friction and wear of the sliding surfaces. Sawant and co-workers [29] investigated the impact of spot textures (protrusions) on the machining performance of High-Speed-Steel (HSS) tools. In their work, the protrusions were fabricated on the rake face of the HSS tool by plasma transferred arc powder deposition method. Their results recommended that spot textured tools were superior in reducing cutting and thrust forces when compared with a non-textured HSS tool. Furthermore, Obikawa and co-workers [30] introduced positive square-shaped textures on the rake face of carbide tools, and this yielded better lubrication conditions in an orthogonal machining operation. In their studies, protrusions were created through spattering, photolithography and etching method.

As for surface texturing in IC engines, Etsion and his research group performed numerous experimental and numerical studies to investigate the effect of negative surface texturing by considering different geometries under different operating conditions. They investigated the impact of surface textures on a flat ring surface under hydrodynamic lubrication and reported some important observations [75]. Based on their studies, there exists an optimum ratio of dimple depth to diameter and area density, which reduced friction and increased the load support of PR-CL contact. Afterward, these results were validated experimentally by performing some reciprocating sliding tests on laser textured dimples [79]. In their study, the authors considered laser textured dimple diameter of 100 μm, depth of 10 μm, and area density of 0.2. They reported a maximum friction reduction of 40% when compared with un-textured case. Zhang et al. [95] conducted experiments with rectangular and circular shape surface textured piston ring surfaces to study the frictional performance near the top and bottom dead centers by

considering real engine conditions. The results indicated that rectangular shaped textures had the lowest average friction coefficient than circular textures and the optimum area density for textured napier ring was found at 15%. Furthermore, in order to investigate the frictional performance of PR-CL contact, Shen and Khonsari [96] designed different piston ring prototypes by varying geometrical parameters of pockets like area ratio, depth, and shape. The experimental results indicated that area density ratio and depth had significant influence, while pocket shape had limited influence on friction reduction.

Extensive work was carried out by Vladescu and his research group [97-99] to explore the impact of micro-dimples on piston ring-cylinder liner (PR-CL) contact under different lubrication regimes. Interestingly, micro-dimples showed beneficial effects under a mixed/boundary lubrication regime. The results indicated friction reduction of 62% [97]. The authors also measured the film thickness and friction force simultaneously by ultrathin film interferometry under transient mixed lubrication conditions. Their results suggested that the presence of surface pockets enhanced the film thickness by 20 nm due to which the friction force was reduced by 41% when compared with un-textured reference case [98]. Afterward, the authors developed a numerical model to validate the experimental results by considering the mixed lubrication conditions of textured PR-CL contact contact [99]. They also conducted some reciprocating tests to identify the optimal geometric parameters of a textured PR-CL contact under different lubrication regimes [100]. In their studies, rectangular-shaped surface pockets of varying depth, width, and density were investigated. They placed the long axis rectangular pockets perpendicular to the sliding direction. Their results suggested that the micro-pockets should be deep, wide, and densely packed for boundary lubrication to have beneficial effects, while shallow, narrow, and sparsely placed micro-pockets were advantages for mixed lubrication.

Surface textures do not always produce beneficial effects, they can also exhibit detrimental effects if the textures are not properly designed. For example, the study conducted by Ryk et al. [79] showed the negative impact of micro-dimpling of surfaces under boundary lubrication. The authors reported that if the dimple depth is not chosen appropriately or the lubricant feed rate is not high enough, the textured surfaces may increases the friction. Their study showed that at high dimple depth and at a low rate lubricant supply, the friction resulting

from textured surfaces was higher than un-textured surfaces. Similarly, Galda and his colleagues [101] reported that micro-dimples had no beneficial effects in terms of friction, wear and seizure resistance. They investigated the effect of spherical and drop-shaped dimples on wear and seizure resistance. The authors provided the most severe conditions of the lubricant by adding dust particles such as SiO_2 and Al_2O_3. Their results concluded that surface textures had no beneficial effect in enhancing the wear and seizure resistance. Another study by Koszela et al. [102] showed similar effects of surface texturing on friction and abrasive wear resistance. They concluded that even when using surface textures, the abrasive particles present at the contact zone cause more plowing friction and thus increased the abrasive wear.

2.2 Influence of surface texture on tribological performance: Numerical studies

Many numerical/theoretical work in the field of surface texturing have focused on the influence of surface texture parameters such as shape, area density/size, distribution as well as operating conditions. Rahmani et al. [103] investigated the optimal geometrical parameters of a parallel slider bearing with square-shaped dimples on tribological performance characteristics including load support, frictional force and friction coefficient. In their analysis, a one-dimensional Reynolds equation was considered under hydrodynamic lubrication regime. They analyzed three parameters, namely number of dimples, length ratio (the ratio of dimple length to distance between two consecutive dimples) and height ratio (the ratio of dimple height to minimum film thickness). The results indicated that increasing the number of dimples didn't affect the tribological performance in terms of load support or friction coefficient. The length ratio and height ratio of 1 and 1.5-1.7 exhibited superior tribological performance. In a similar analysis conducted by the same group [104], three different bottom shapes were considered including rectangular, equilateral triangular and isosceles triangular textures. The performance of rectangular textures was found superior when compared with other shapes in terms of maximum load support as well as minimum friction coefficient. Furthermore, Fowell et al. [36] assessed the influence of textured surfaces with rectangular pockets on the hydrodynamic performance of parallel bearing. They reported the most influential texture parameters on the performance of the bearing. They suggested that the number of textures had little effect, while the texture area density and texture height were crucial parameters in deciding the overall performance (such as

load carrying capacity and friction) of textured surfaces. In addition, sliding speed and lubricant viscosity had no influence on the performance of textured bearing. Their results reported that the textured surfaces enhanced the bearing performance 10% more than un-textured case.

Ji et al. [105] presented a hydrodynamic lubrication model to study the influence of geometric parameters as well as orientation of elliptical textured slider bearing. The authors evaluated the performance of bearing in terms of average hydrodynamic pressure. They suggested elliptical dimples with larger slender ratio (the ratio of length of major axis to length of minor axis) for better hydrodynamic effect. In addition, more hydrodynamic pressure was observed when elliptical dimples were placed parallel to the direction of sliding. Furthermore, Uddin and Liu [106] analysed the tribological performance of a new 'star like' shape of parallel slider surfaces. They observed that the number of apex points of 'star like' shape significantly influence hydrodynamic pressure and friction rather than apex angle and orientation. Furthermore, their results depicted that 'star like' shape of apex points six and texture area density of 0.4 reduced the friction coefficient by 80%, 64.39%, 19.32% and 16.14% when compared to elliptical, chevron, triangular and circular shapes, respectively.

Recently, many researchers studied the combined effects of surface roughness and surface texturing on the frictional performance of sliding surfaces [107-109]. Brunetière and Tournerie [107] studied the behavior of textured mechanical seal surfaces under mixed lubrication regime. The authors solved hydrodynamic Reynolds equation and asperity contact model for hydrodynamic and asperity pressures, respectively. They investigated perfectly smooth surface, rough surface and rough surface with micro-dimples. Their results suggested that a rough surface with surface textures reduced the friction more in hydrodynamic as well as mixed lubrication. This reduction in friction was because of the effects of surface roughness, surface texture and interaction between them [107, 108]. In a similar work, Ma et al. [109] presented a theoretical model to investigate the combined effects of surface texturing and roughness on performance parameters of a parallel sliding contact. The authors modeled the single dimple shaped texture under hydrodynamic as well as mixed lubrication regime by considering different surface roughness values. Their results indicated that the effect of surface roughness on load carrying capacity and friction coefficient is crucial in the case of mixed lubrication, while its effect can be ignored under hydrodynamic lubrication conditions. Furthermore, the increase of surface roughness resulted in increased friction coefficient under mixed lubrication regime.

Furthermore, Siripuram and Stephens [110] addressed the impact of both positive and negative textures under hydrodynamic lubrication regime. They modeled both positive and negative textures by considering different shapes such as square, diamond, circular, triangular and hexagonal. The performance was evaluated in terms of friction coefficient and leakage rate. They reported that texture shape had insignificant impact on friction coefficient; however it had a great impact on leakage rate. The triangular shape shown superior performance whereas square shape shown worst performance in terms of leakage rate. Additionally, the minimum friction coefficients were obtained corresponding to area densities of 0.2 and 0.8 for positive and negative texturing, respectively. Furthermore, Syed and Sarangi [111] presented a hydrodynamic lubrication model to study the performance of sliding contact with positive and negative textures by including the fluid inertia effects. The results indicated that the positive textures exhibited better frictional performance compared to negative textures.

Ronen et al. [75] studied the effect of partially textured piston rings on reduction of friction force. The authors modelled dimple textured ring surfaces under hydrodynamic lubrication regime. It was found that there was 30% of friction force reduction at an optimum texture depth over diameter ratio of 0.14 compared to un-textured piston ring. In a similar work, Kligerman et al. [112] analyzed the textured PR-CL contact to identify the important parameters. The authors modeled the textured ring surface under transient hydrodynamic lubrication regime. Their results indicated that the dimple diameter had no influence on friction force, while the larger area density exhibited better frictional performance. In addition, they reported that the friction force of partial textured ring was lower than that of the full textured ring. Afterward, Liu et.al [113] evaluated the tribological performance of barrel shape compression PR-CL contact with spherical dimples on cylinder liner by varying dimple area density, depth and radius. The authors presented a mixed lubrication model by considering surface roughness of compression ring and cylinder liner. The results indicated that dimple area density and depth had significant effect on tribological performance of PR-CL system whereas dimple radius had negligible effect. Furthermore, the effect of different array modes on tribological properties of PR-CL contact was studied by Yin et al. [114]. The authors considered mixed lubrication model with four array modes, namely; square array, stagger array, stretching and shortening of dimples along liner axis. The results indicated that square array of micro dimples showed better performance in reducing friction compared to other modes. However, in most of the cases

analysis of textured PR-CL system is based on ideal circular cylinder liner bore which is contrary to real engine conditions and overestimates energy savings per engine cycle. Therefore, Usman and Park [115] evaluated the performance of textured PR-CL system by considering non-circular cylinder bore along with asperity contact model. The results indicated that asymmetry PR-CL contact resulted in more frictional power loss when compared to textured circular liner due to leakage of hydrodynamic pressure. However, there are no specific guidelines to select texture parameters such as shape, size and distribution. The texture parameters need to be selected for specific application under a given set of operating conditions [18, 116]. Therefore, optimization of texture parameters could be completely application dependent.

Reviewing the literature, the performance of textured surfaces can quite vary. Some studies of surface texturing have shown considerable reduction in friction coefficient, while others noticed no significant difference between textured and un-textured surfaces [62]. In some cases, surface texturing is beneficial at certain optimal conditions, while other studies report that any kind of surface texturing may be worse than un-textured surface [24]. Some of the authors report that friction reduction due to surface texturing can be achieved only if micro-features are smaller than contact width [117], while others report that friction increases under almost similar conditions [13]. In some studies, the textured surfaces showed increased friction coefficient or wear or did not show beneficial effect at all compared to un-textured surfaces [102, 118]. For example, Kovalchenko et al. [82] observed that laser micro-dimpled surfaces had detrimental effect on tribological performance, when the dimples are deep or the viscosity of the lubricant is high. Whilst some other studies showed surface textures capture the wear debris and remove the wear particles at the contact zone, thereby reducing the wear.

In addition, there is no universal acceptance on issues such as what types of surface texture should be beneficial and under which circumstances. Furthermore, there is no consensus on which texture parameters are the most significant in reducing friction or wear and under what conditions. For example, Kovalnchenko et al. [82] observed that textured surfaces showed beneficial effects under boundary or mixed lubrication regime, while they had no effect in the case of hydrodynamic lubrication. On the contrary, Etsion et al. [84] observed a friction reduction of almost 50% because of surface textures. In another study, Hsu et al. [71] reported that surface texture shape and size had great impact on friction reduction, while Etsion et al. [23]

concluded that texture shape had insignificant effect on friction reduction. Similarly, Hupp [64] and Pettersson [117] stated that textured surfaces of higher area densities exhibited lower friction coefficients under hydrodynamic as well as mixed lubrication conditions, whereas Wang et al. [39, 65] reported smaller area densities as optimum for lower friction coefficients. In most of the studies, trial and error approach was adopted due to lack of systematic approach related to optimization procedures. In fact this trial and error method is the only option in cases of boundary or mixed lubrication regime, where there is a lack of theoretical modelling of textured surfaces. However, there are enough theoretical models for textured surfaces in the case of hydrodynamic lubrication.

2.3 Research gap

The study of literature shows that the fundamental concept and function of surface texturing is still in infancy despite recent improvements in fabrication techniques and computational algorithms. This lack of understanding motivated many researchers to study the various aspects related to surface textures such as the effect of various geometric parameters of surface texture, operational parameters as well as the physical mechanisms behind the friction and wear reduction. In addition, most of the previous works focused on the negative textures to ensure beneficial effects on tribological behaviors under different operating scenarios. Therefore, it is worthwhile to study the influence of positive texturing on the lubrication and tribological behaviors of sliding contact. It is also observed that most of the studies focused mainly on modelling textured surfaces in pure hydrodynamic lubrication condition and less on mixed lubrication. This is because of the complexity of the frictional process involving fluid and asperity interactions. Therefore, it is meaningful to include asperity interaction effects while modelling textured surfaces to predict more accurately the tribological characteristics.

2.4 Research problem

Many researchers have successfully introduced surface textures and attained remarkable benefits in various applications. However, the fundamental concept and function of surface texturing is still lacking despite its recent improvements. Therefore, a thorough investigation of various aspects related to surface texturing is needed to make this process more efficient and easy to implement. The present research work addresses the combined experimental and numerical investigation of positive surface texture on the tribological behavior of parallel sliding contact.

2.5 Research hypothesis

It is believed that positive surface texturing improves the tribological behavior of interacting sliding pairs. It is expected that the input variables texture area density, height and texture shape would show a prominent effect on the output parameters such as friction coefficient through numerical simulation by modified Reynolds equation and asperity contact model. Based on the literature, the material chosen for surface texturing is AISI 1020 steel against EN 31 un-textured disc. In the present research work, tribological behavior is evaluated in terms of measurable output parameters such as friction coefficient, wear rate, hydrodynamic load support and minimum film thickness. These output parameters depends on input variables like texture area density, aspect ratio, lubricant viscosity, texture depth/height, number of textures, texture size, texture shape, applied load, sliding velocity and surface roughness of mating surfaces.

2.6 Objectives of the present work

Keeping in view the above-mentioned aspects, the objectives of the present work can be summarized as follows:

- Development of positive surface textures.
- Experimental investigation of the tribological performance of developed positive textured sliding contact.
- Development of theoretical model to study the effect of positive textures on the tribological performance of parallel sliding contact.
- Optimization of positive texture parameters such as shape, area density, and height on the tribological performance of parallel sliding contact through the developed theoretical model.

The approach of achieving above-mentioned objectives can be seen in Fig.2.6.

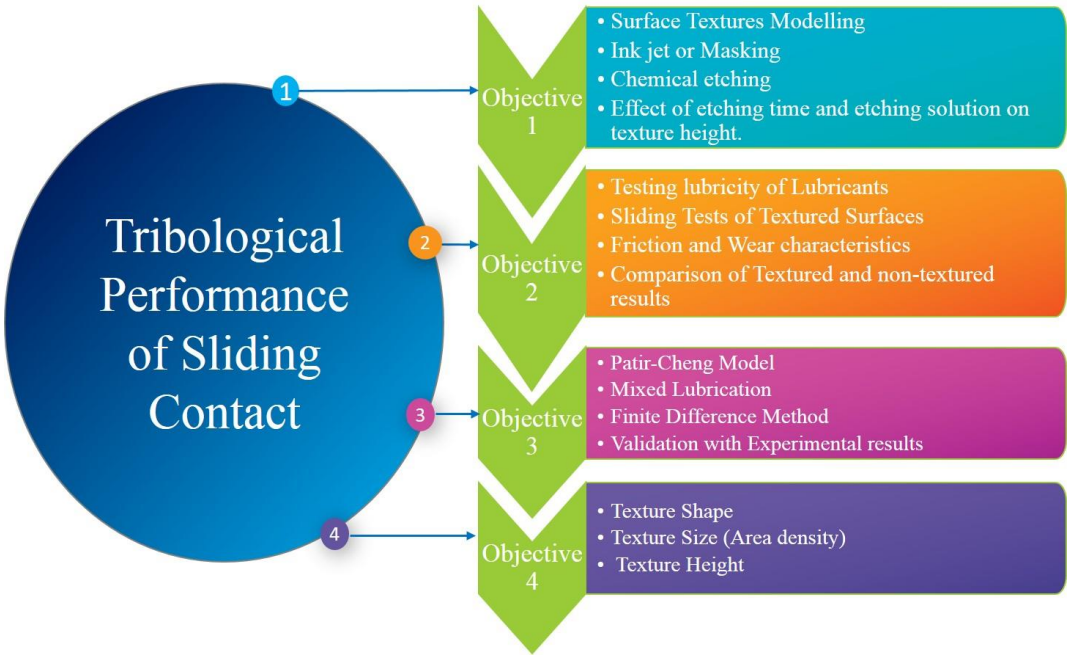

Fig.2.6 Flow of overall research plan

2.7 Summary

In this chapter, the literature review on the experimental and numerical studies of surface texture in investigating tribological performance of different sliding contacts has been presented. The objectives of the present research work based on the research gaps identified are outlined. After framing the research objectives, the development of surface textures are discussed in chapter 3.

Chapter 3

Development of surface textures

The studies mentioned in the literature hold that surface textures make a significant contribution in improving the tribological performance of sliding surfaces. Most of the previous studies focused on negative textures. However, the effect of positive textures has to be addressed in evaluating the tribological behavior of interacting surfaces. This chapter addresses the development of positive textures by varying texture area density and height. A chemical etching method has been chosen to fabricate positive textures due to its simplicity and potency to produce the required geometry [119]. The effect of etching concentration and etching time for the desired texture height is also addressed.

3.1 Fabrication methods

Numerous methods are available for fabricating surface textures on different materials by varying different texture geometric parameters including texture shape, size and distribution. In general, surface texture fabrication methods can be classified into three groups such as etching methods, micro-machining/forming techniques and energy beam/electric discharge methods as shown in Fig.3.1.

3.1.1 Etching methods

Electro-polishing method has been used by Nakatsuji and Mori [120] to fabricate micro-dimples on medium carbon steel. In this process, the authors utilized sulphuric and phosphoric acids for electrolytic reactions to create micro-dimples. Reactive ion etching method was used by Xiaolei and Kato [121] to make micro-pits of depths 2-13 µm, diameters 50-650 µm and area densities 2.8% to 22.5% on silicon carbide (SiC) surfaces. In this method, the diameter/size and texture pattern crucially depends on the masking, while texture depth depends on etching time. Afterwards, Zhang and Meng [122] utilized a photolithography technique and photochemical machining process to create different micro-feature shapes. The authors developed micro-pools of circular (diameter of 20 µm) and triangular (hypotenuse of 50-300 µm) shapes on ASTM

1020 steel surfaces. In this method, a patterned photoresist film was prepared by using photolithography which was followed by dipping in chemical etchant solution to create micro-features on steel surfaces. The etchant solution was prepared by a mixture of HNO_3:H_3PO_4: H_2O.

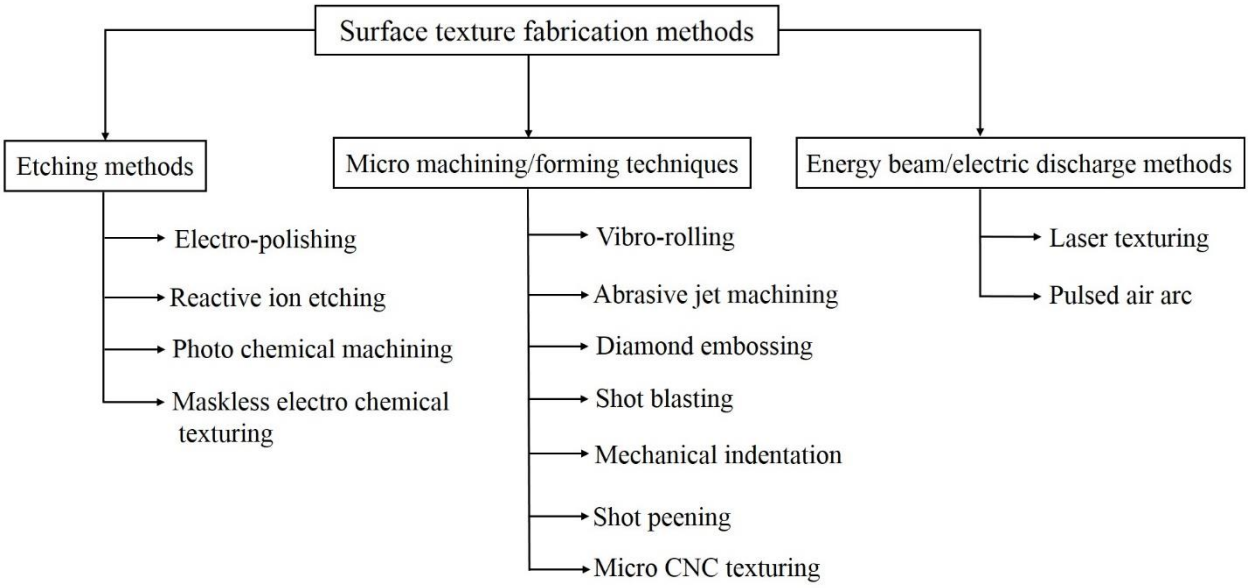

Fig.3.1 Classification of surface texture fabrication methods

Furthermore, a mask-less electro chemical texturing process was used by Parreira et al. [123] to produce microstructures on electricity conducting materials such as carbon steels. The authors used AISI 430 steel as a cathodic tool and NaCl solution as electrolyte to create micro-features of various shapes. They produced micro-grooves, micro-dots and chevron shapes of sizes 400-800 µm and depths 20-80 µm. In a similar work, Xuan et al. [124] used masking followed by electrochemical machining. The authors utilized a photoresist of thickness 50 µm as a mask, with patterned micro-grooves produced by photolithography. They developed micro-grooves of sizes 148.5-258.6 µm and depths 17.6-58 µm on phosphor bronze anodic surfaces with $NaNO_3$ as the electrolyte solution. The material restriction is the main drawback of the electrochemical texturing method since it is limited to electricity conducting materials [123]. Moreover, modified photolithography was introduced by Kortikar [125] to fabricate both positive and negative textures on the surface of any random cross-section and orientation.

3.1.2 Micro machining/forming techniques

Vibro-rolling method was used to produce micro-grooves of different patterns on metallic surfaces, particularly on precision tools [24, 126]. In the vibro-rolling method, the diamond tool with pre-rolling against the specimen causes plastic deformation and creates micro-grooves of the required pattern. Among various techniques, abrasive jet machining is a promising technique [13, 127, 128]. In abrasive jet machining, a jet of high-velocity air mixed with fine abrasive particles is directed towards the target surfaces to create micro-features. The micro-dimples of sizes 40, 80 and 120 µm, area densities of 7.5%, 15% and 30% and depth of 5 µm were fabricated on the silicon nitride surfaces by abrasive jet machining [13]. The main drawback of abrasive jet machining is that taperness occurs with increase of dimple depth [129]. A novel approach based on the use of diamond embossing technique was developed by Pettersson and Jacobson [130] to create micro-scale textures on flat and curved metallic surfaces. This method involves anisotropic etching of patterned silicon wafer surface and a CVD deposition of the diamond film followed by application of load with the help of hardness tester. The authors developed sharp pyramid shape textures and rooftop shape textures with a length of 100 µm and spacing of 80 µm between textures. In this method, post-processing such as polishing is necessary to remove the burrs around the micro-dimples. Furthermore, Nakano et al. [131] utilized photolithography followed by shot blasting to generate micro-grooves and mico-dimples of width/diameter 60 µm and a depth of 6-10 µm on cast iron surfaces. Initially, the texture patterns were prepared by photolithography, followed by a shot blasting process. In the shot blasting process, air with abrasive particles, was used to remove the unmasked portions. Large areas can be textured irrespective of the materials' chemical reactivity using shot blasting process.

Moreover, vibro-mechanical texturing was used by Greco et al. [132] to fabricate elliptical shaped-dimples on cylindrical-shaped work pieces. The authors used a vibrating single-point cutting tool to produce elliptical dimples of sizes 50-550 µm along with axial and circumferential directions and depths of 2-50 µm on aluminum and steel surfaces. Any material which can be turned on lathe machine can be textured using vibro-mechanical texturing method. This method is limited to cylindrical work pieces only, which can be processed on a lathe machine. On the other hand, a mechanical Vickers indenter was used to create micro-dimples of different sizes on steel surfaces using mechanical indentation technique [133]. In this method, a diamond indenter

was utilized to create hemispherical dimples of diameter 65 µm and depth 0.2-1.45 µm on AISI52100 steel. The dimple depth can be controlled by the load applied to the diamond indenter. This method is a time-consuming process because it requires plastic deformation of the material and also post-processing methods such as polishing, to remove the material surrounded by micro-dimples. Furthermore, shot peening method has been utilized by Vrbka et al. [134] to create random peaks and valleys on AISI 52100 steel surfaces. In this method, hard particles combined with high velocity causes plastic deformation of surfaces and changes surface topography as well as mechanical properties of the surfaces. The authors used glass breeds of diameter 0.07-0.11 µm as abrasive particles to create an average roughness of 0.14-0.17 µm on the target surfaces. An innovative method of CNC texturing was used by Cho and Park [135] to produce micro-holes on the surfaces of polymers. They fabricated cylindrical micro-holes of diameter and depth of 125 µm with an area density of 5%-30% on the surfaces of polyoxymethylene. This method is well suited for texturing of polymeric surfaces since high energy beam methods fail to create textures due to melting of polymer surfaces.

3.1.3 Energy beam/electric discharge methods

High energy beam method such as pulsed air arc treatment has been used by Moshkovith et al. [136] to generate micro-dimples on the surfaces of SAE 5020 steel. In this method, a pulsed air arc of high voltage was used between the thin electrode and specimen to get micro-features on the substrate. The authors developed hemispherical dimples of diameter<20 µm. When compared to all other techniques, surface texturing through laser ablation is a popular method and has many advantages in terms of flexibility, high accuracy and resolution. Many authors used laser ablation to fabricate different geometrical micro-features on a wide range of engineering materials such as metals, polymers, ceramics, crystalline structures and glass [24, 117, 137-140]. The authors produced hemispherical dimples of diameter>100 µm and depth<10 µm on the surfaces of bearing steel GCr15, 100C6 steel, nickel alloy 400 and spring steel 1095. Although laser surface texturing is an accurate and popular method, it can only produce negative textures such as dimples of spherical and conical shapes [24].

3.2 Development of positive textures by chemical etching process

Chemical etching process has been chosen to fabricate positive textures due to its simplicity and potency to produce the required geometry [119]. In chemical etching process, the surface is

exposed to chemical and allows the material to get etched wherever required, and the remaining portion kept under the masking material. In the chemical etching process, masking is one of the critical stages, depending on which the desired shape can be achieved. The masking process used in the earlier literature is costly and time-consuming. Therefore, in the present work, new material of masking is proposed, i.e. using carbon black as masking material which has been applied on the substrate by the application of heat and pressure. This masked specimen is used in the chemical etching process. A detailed procedure of producing the surface textures on the substrate is explored below with the help of Fig.3.2.

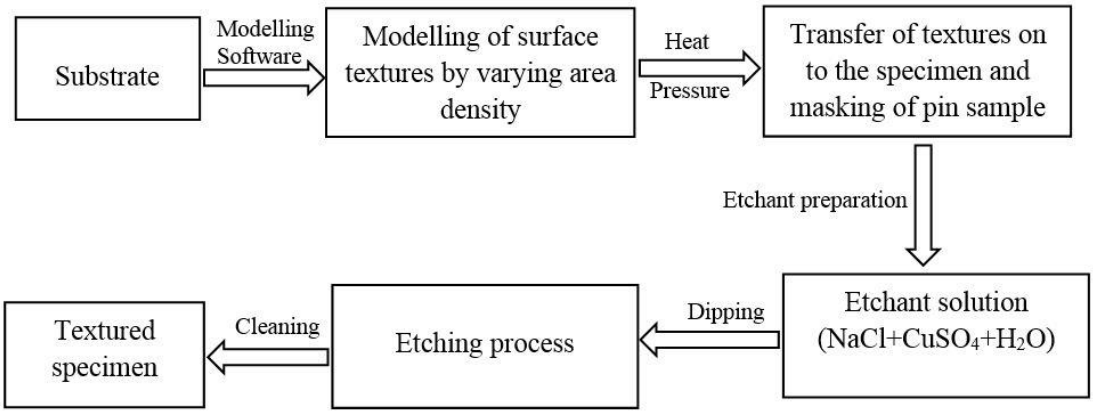

Fig.3.2 Development of surface textures

Firstly, the pin surface (AISI 1020) is polished and cleaned with acetone to remove dirt particles. The square-shaped textures (chosen because of simple shape) are created using CREO-software by varying area density from 0.1-0.5, as shown in Fig.3.3 (a). Then, these textures are transferred on to the photo paper by using carbon black material with the help of laser printer and further on to the pin surface by applying heat and pressure for 4-5 minutes with the help of clothing iron. The transferred textures on to the surface from photo paper are shown in Fig.3.3 (b). The carbon black material can resist the action of chemicals, i.e., it acts as a masking material. The etching solution is prepared by mixing sodium chloride (powder form), copper sulphate (powder form) and hot distilled water in a specific ratio by weight. Then the solution is stirred for proper mixing with the help of magnetic stirrer, and the solution becomes blue-colored, as shown in Fig.3.3 (c). Afterwards, all the other sides of the pin surface are covered with a tape in order to avoid unwanted chemical reactions, as shown in Fig.3.3 (d). Then the masked substrate is kept face down in the solution for etching so that the etched metal falls and

goes away from the substrate, as shown in Fig.3.3 (e). The indication for the etching process is that the solution changes its color to deep green, and the bubbles are formed around the substrate. After the etching process, the specimen is washed with water to remove acid, and the masking material is removed by cleaning it with acetone. The images of the textured specimen after the etching process can be seen in Fig.3.3 (f). The SEM image of developed square-shaped textures is shown in Fig.3.4.

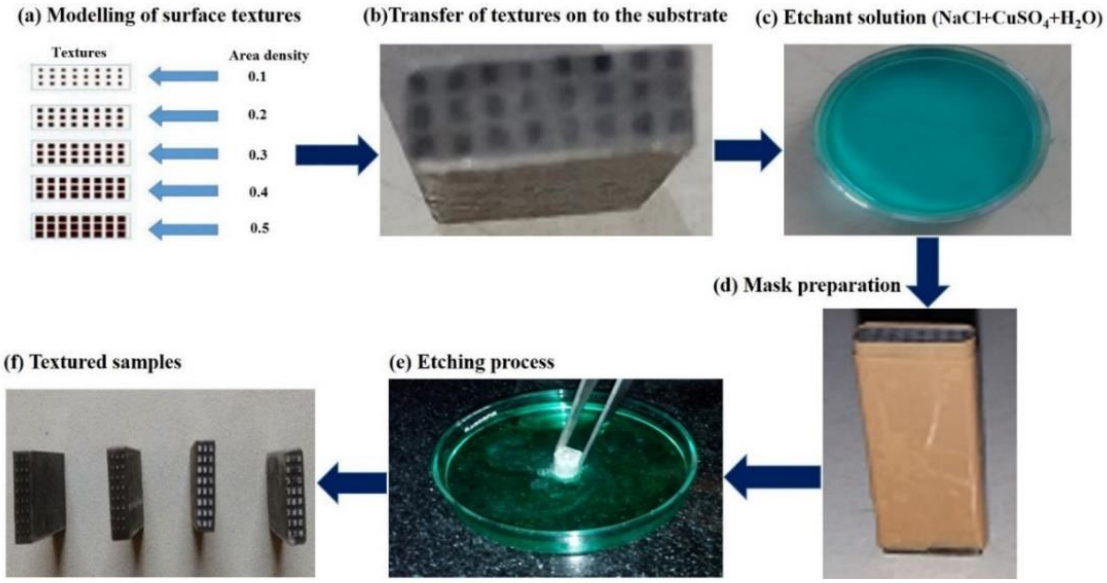

Fig.3.3 Steps involved in fabrication of surface textures by chemical etching process

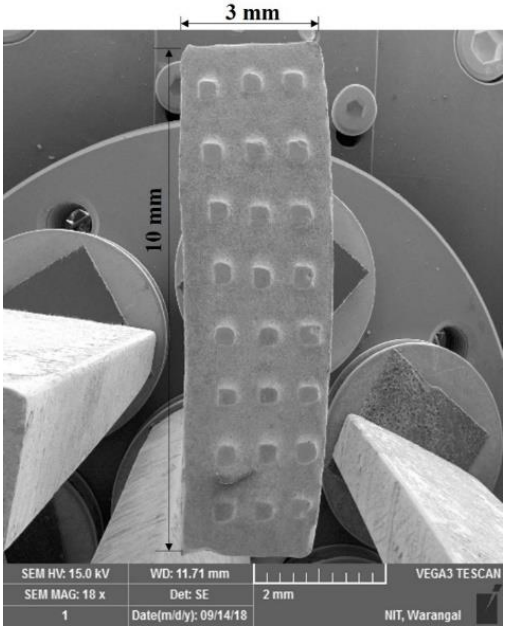

Fig.3.4 SEM image of developed square-shaped textures

3.3. Texture size and height measurements

After the fabrication of surface textures, the dimensions such as texture height and size are measured with the help of a 3-D microscope. The microscope image of square-shaped textures on the pin surface in 3-D and 2-D view is shown in Fig.3.5.

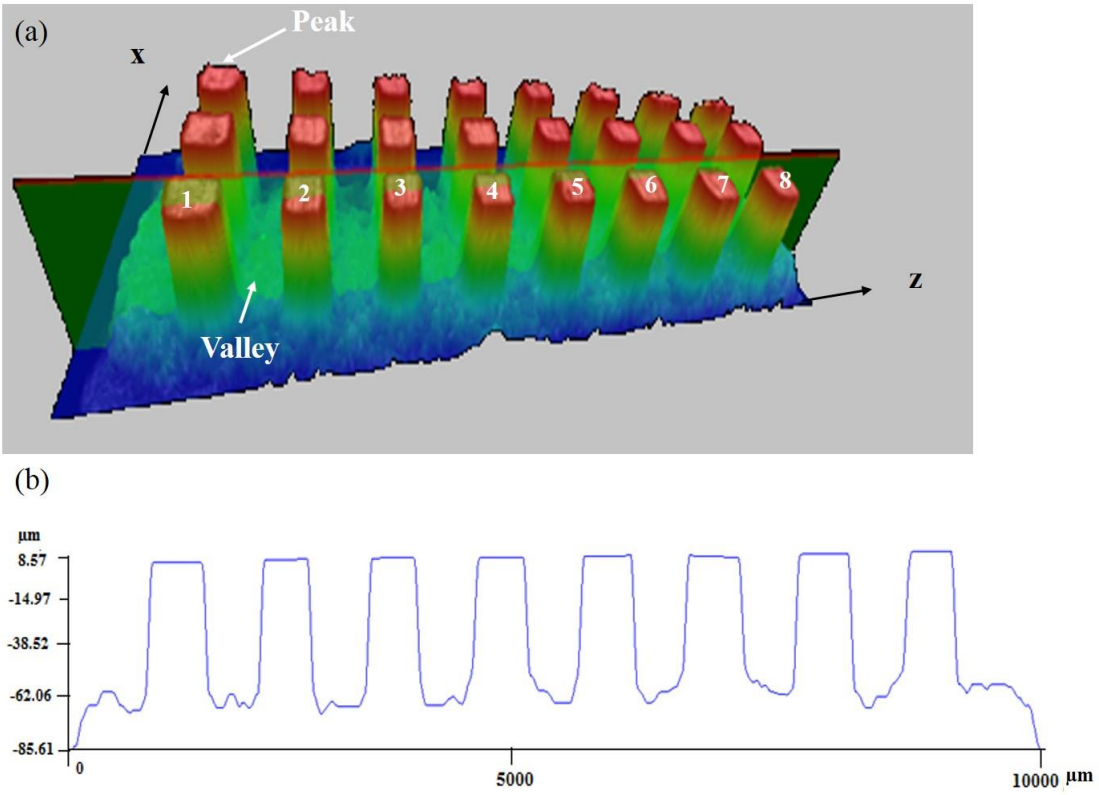

Fig.3.5 3-D microscope image of distribution of textures

In the present work, the square-shaped textures are fabricated by varying texture area density and height. All the surfaces of the samples have the same number of textures (taken as 24) but different sizes and pitches in order to obtain different area densities. The area density (S_p) is defined as the ratio of the total area occupied by textures to the total surface area of the sample as follows:

$$S_p = \frac{a^2 \times N}{l \times b} \tag{3.1}$$

From equation (3.1), the size of square-shaped texture can be calculated as follows:

$$a = \sqrt{\frac{S_p \times l \times b}{N}} \tag{3.2}$$

Where, S_p= area density, a = side length of the square-shaped texture, N = number of textures, l = length of sample surface (10 mm), b = width of the sample surface (3 mm).

In the present work, an etchant concentration ($NaCl+CuSO_4+H_2O$) and etching time of 1:1:5 and 16±1 minutes respectively, are used to produce surface textures of various area densities which are shown in Fig.3.6. The parameters shown in Fig. 3.6 for different area densities are summarized in Table 3.1. The symbols d_1 and d_2 are horizontal and vertical distance between the two consecutive textures, respectively.

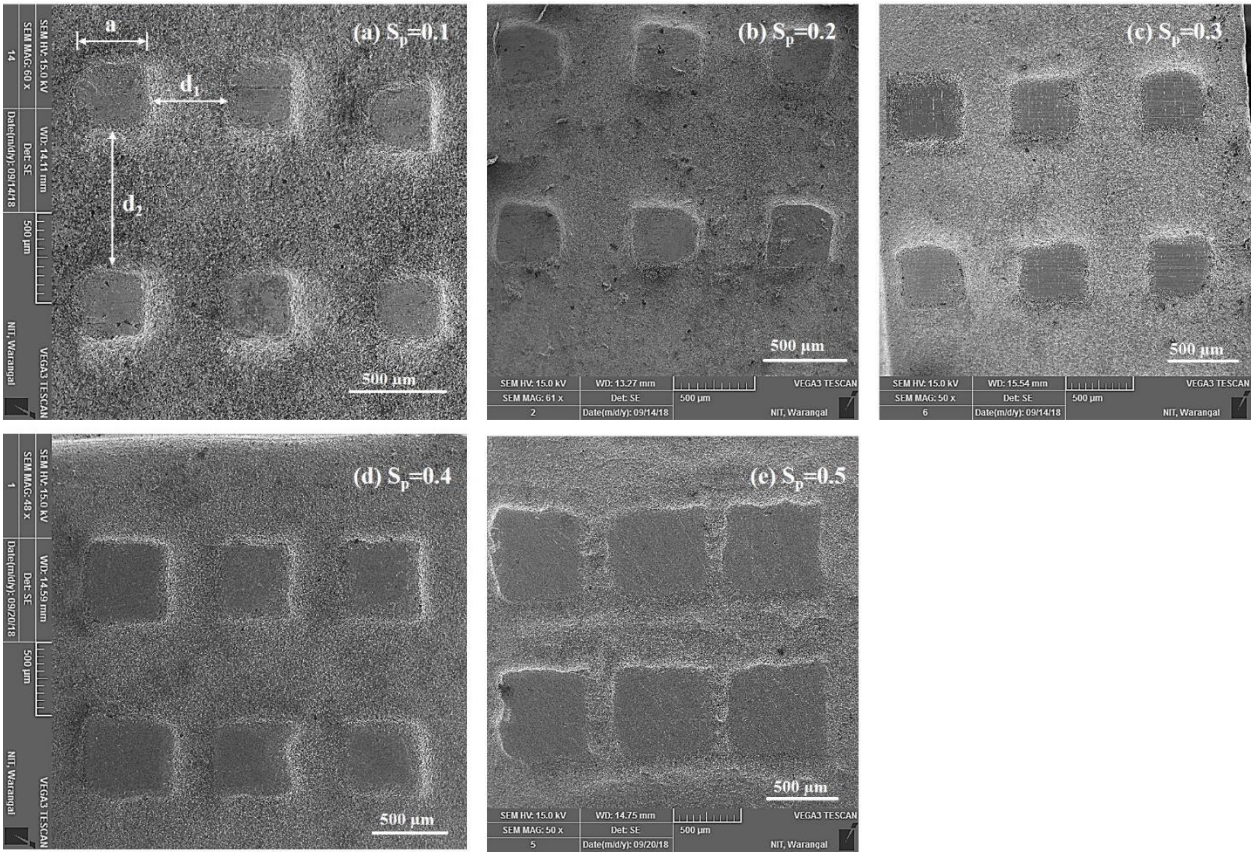

Fig.3.6 SEM image of textured arrays for various area densities

Table 3.1 Parameters of textured array

Parameter	S_p **= 0.1**	S_p **= 0.2**	S_p **= 0.3**	S_p **= 0.4**	S_p **= 0.5**
a (µm)	350	500	600	700	800
d_1 (µm)	950	800	670	560	450
d_2 (µm)	700	500	350	200	100

After the development of textured surfaces with varying area density, the height of surface textures is measured using a 3-D microscope. In order to measure the texture height, the peak and valley heights at different points (can be seen in Fig.3.5 (a)) are utilized. The height difference between peak and valleys is measured as the height of the corresponding texture. All the texture heights are measured three times at each location, and the average value is taken as the actual height of the texture. The measured mean texture height values with standard deviations at different location points are presented in Table 3.2, and the corresponding average texture height value is obtained as 70 µm.

Table 3.2 Texture height measurement results

Location point	1	2	3	4	5	6	7	8
Mean texture height (µm)	70.54± 1.04	69.17± 1.68	72.55± 1.26	69.05± 0.47	69.11± 1.8	67.99± 2.04	68.91± 0.93	71.52± 1.69

3.4 Effect of etching time and etchant concentration on texture height

Texture height can be controlled by varying etching time and etchant concentration. In the present work, the square-shaped textures are developed by varying texture height in the range of 10-100 µm, in a step size of 30 µm. In order to study the influence of etching time and etchant concentration, each experiment is conducted three times, and the mean etching time is evaluated for the desired texture height. The experiments are conducted by varying etching time for different texture heights at a constant etchant concentration. The results of texture height values for different etching times at the etchant concentration of 1:1:5 are shown in Fig.3.7. For lower texture heights, the etching time is lower while more etching time is required for higher texture heights.

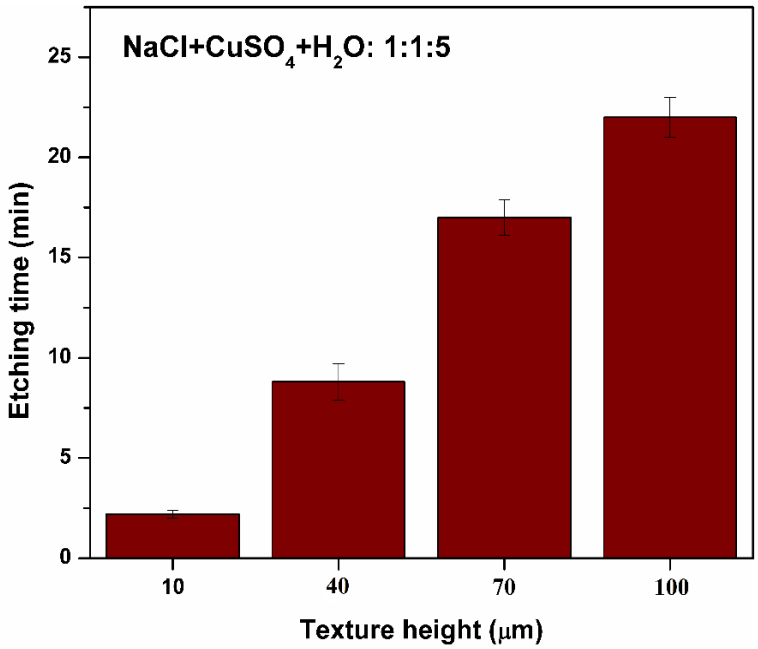

Fig.3.7 The influence of etchant concentration on texture height

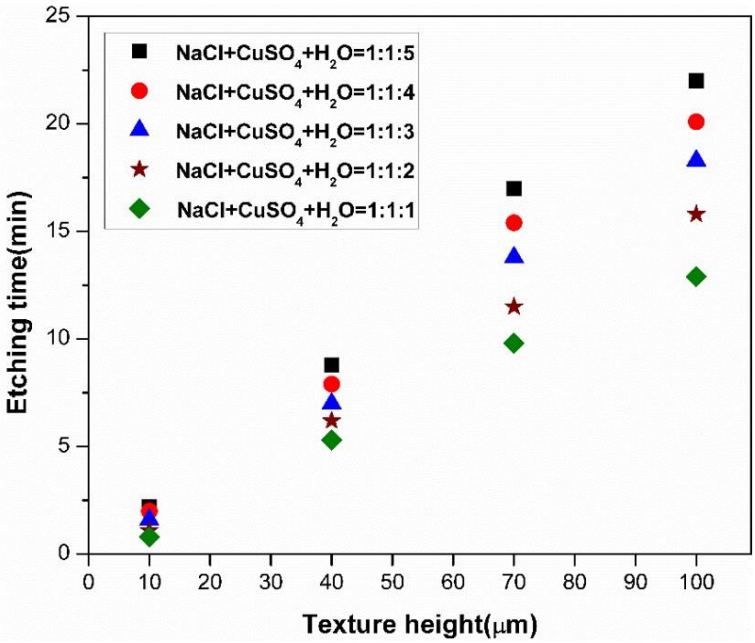

Fig.3.8 The influence of etchant concentration on texture height

Afterwards, the effect of etching concentration for the desired texture height is explained with the help of Fig.3.8. The etchant concentration is varied by changing the weight of distilled water. Figure 3.8 shows, the concentrated solutions took less average etching time than the diluted solution to obtain the desired texture height. The difference between etching times for

different etchant concentration is minimum for lower texture heights, while it is maximum for higher texture heights. The experimental results indicated that the diluted solutions are better to obtain lower values of texture heights, whereas concentrated solutions are recommended for higher texture heights. The control over texture height is difficult in the case of higher etchant concentration, particularly for lower texture heights. Also, the lower etching times may accelerate the possibilities of errors, especially for lower texture heights. Therefore, diluted solutions are recommended to obtain lower texture heights by avoiding unnecessary deviations in texture height values.

3.5 Summary

In this chapter, square-shaped positive surface textures have been developed on the sample surface using carbon black as masking material followed by a chemical etching process, which is simple and economical. The effect of etching time and etchant concentration for the desired texture height is discussed. The preliminary studies presented here are helpful for better understanding of the development process of surface textures. The studies presented in this chapter also provide a basis for further research on the fabrication of surface textures with different aspects such as texture shape, size and height. After the fabrication of surface textures, the experimental analysis of textured surfaces on tribological performance parameters such as friction and wear are discussed in chapter 4.

Chapter 4

Friction and wear studies of positive textured sliding contact: Experimental studies

After the development of square-shaped positive textures as discussed in the previous chapter, the present chapter addresses the impact of this developed textured surfaces on friction and wear behavior of parallel sliding contact. This chapter provides the information on the selection of appropriate lubricant to lubricate the parallel sliding contact followed by tribological sliding experiments to characterize the friction and wear behavior of textured surfaces. In addition, the worn surface morphologies of textured surfaces are discussed.

4.1 Selection of lubricant

It is well known that proper lubrication is one of the key factors to improve the tribological behavior of interacting sliding surfaces. Lubricant is a widely used element between the interacting surfaces in various mechanical components, which are in relative motion. The lubricant oil reflects the performance of the engine through its properties, and also the condition of lubricant oil affect the overall engine performance. The main function of a lubricant is to reduce friction and wear of the interacting surfaces by avoiding metal to metal contact. In addition, it can also reduce corrosion, temperature, contamination and vibrations between the sliding surfaces. Proper lubrication enhances the working life as well as fuel efficiency of the engine. The tribological properties such as friction and wear of engine components can significantly affect the engine performance. If the friction and wear of the components increases, the working life of the engine decreases [141]. The relationship between engine performance and engine lubricant is an important diagnostic tool to decide the overall efficiency of the engine. Therefore, in order to select the appropriate lubricant, different lubricants are tested for better lubricity. In the present work, three lubricants, namely SAE20W-50, SAE15W-40, and SAE10W-30 were selected, which are commercially available lubricants for automobiles. The selected lubricants are synthetic in nature and the viscosity of these lubricant does not change much during the test period. All the selected lubricants are supplied by Castrol India Limited and

the same brand has been used during all the tests. These are tested on four-ball tester for a better understanding of their frictional and wear properties.

The friction and wear tests are conducted on a four-ball tester (Ducom made, model: TR-30L-IAS) according to a standard test procedure of ASTM D4172. The schematic view of the four-ball tester assembly is shown in Fig.4.1. The four-ball tester assembly consists of four steel balls out of which three balls remains stationary, while the fourth ball rotates against these three balls (see Fig. 4.1).

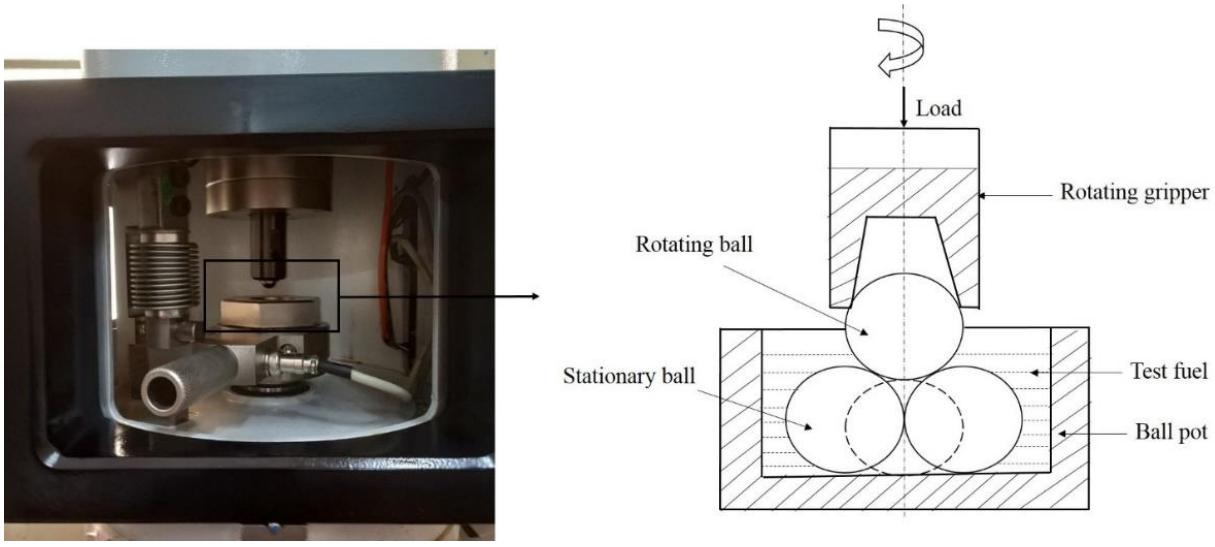

Fig.4.1 Four ball tester assembly

Before each test, the four steel balls are cleaned with acetone and wiped dry with a tissue. Three steel balls are placed in a ball pot and tightened to a torque of a minimum 67 Nm using a torque wrench in order to avoid relative motion between them. Then 10 ml of test lubricant is poured into the ball pot and ensured that the lubricant fills all the voids in the ball pot. This ball pot is placed beneath the spindle to which the fourth ball is fixed through collet chuck, and this ball rotates against three balls which are placed in the ball pot. The operating conditions of four-ball tester are shown in Table 4.1. Each test is conducted for 1 hour, and new steel balls are used for each test. After each test, the frictional torque can be measured with the help of a torque sensor for corresponding applied normal load. Afterwards, the friction coefficient is calculated by Eq. (4.1).

$$Friction\ coefficient = \frac{T\sqrt{6}}{3W_1 r} \quad (4.1)$$

Where, T is the frictional torque in Kg-mm, W_1 is the applied load in Kg and r (3.67 mm) is the center distance between the contacting lower ball surfaces to the axis of rotation.

Table 4.1 Operating conditions of four ball tester

Parameter	**Condition**
Experimental conditions (ASTM D4172)	
Load	15 Kg
Speed	600, 900, 1200, 1500 rpm
Test duration	1 hr.
Testing ball conditions	
Ball material	AISI E-52100
Ball diameter	12.7 mm
Ball hardness	62 HRC
Ball roughness	0.1 µm

After the completion of each test on the four-ball tester, the wear scar diameter of three stationary balls which are in ball pot is measured with the help of an image acquisition system, as shown in Fig.4.2. It consists of a camera to capture the image of wear scar and a compound lens to capture the image at pre-defined focal length to measure the wear scar diameter. The wear scar can be viewed on the PC with the help of SCARVIEW software, and the wear scar is measured using the ellipse tool. The focal length can be adjusted to get a clear image, and this image is captured by the camera which would be transferred and stored in PC.

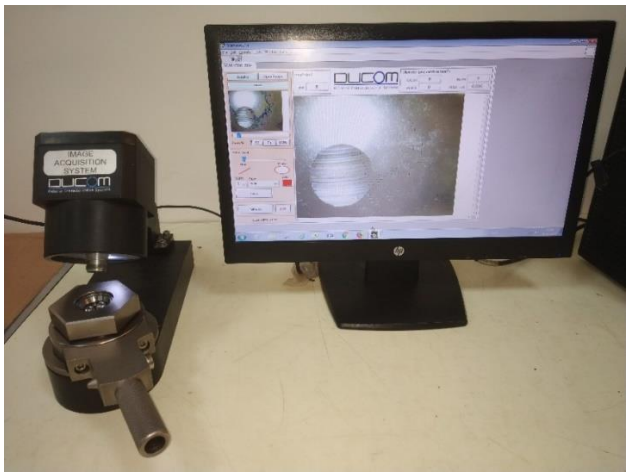

Fig.4.2 Wear scar captured by image acquisition system

The variation of frictional torque for different test lubricants is depicted in Fig.4.3. The tests are conducted at an applied load and rotating speed of 15 kg and 1200 rpm, respectively. Among the tested lubricants, SAE10W-30 shows maximum frictional torque while SAE15W-40 exhibits minimum frictional torque (see Fig. 4.3).

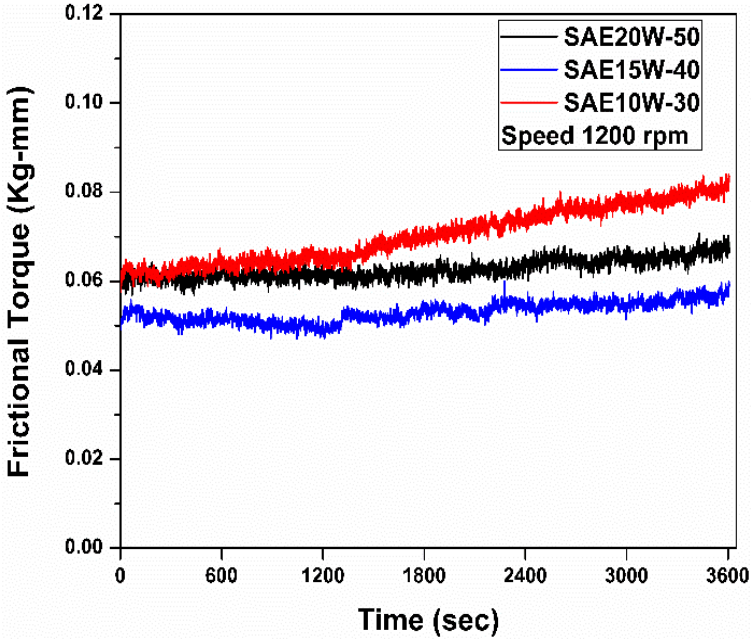

Fig.4.3 Frictional torque vs time for different lubricants

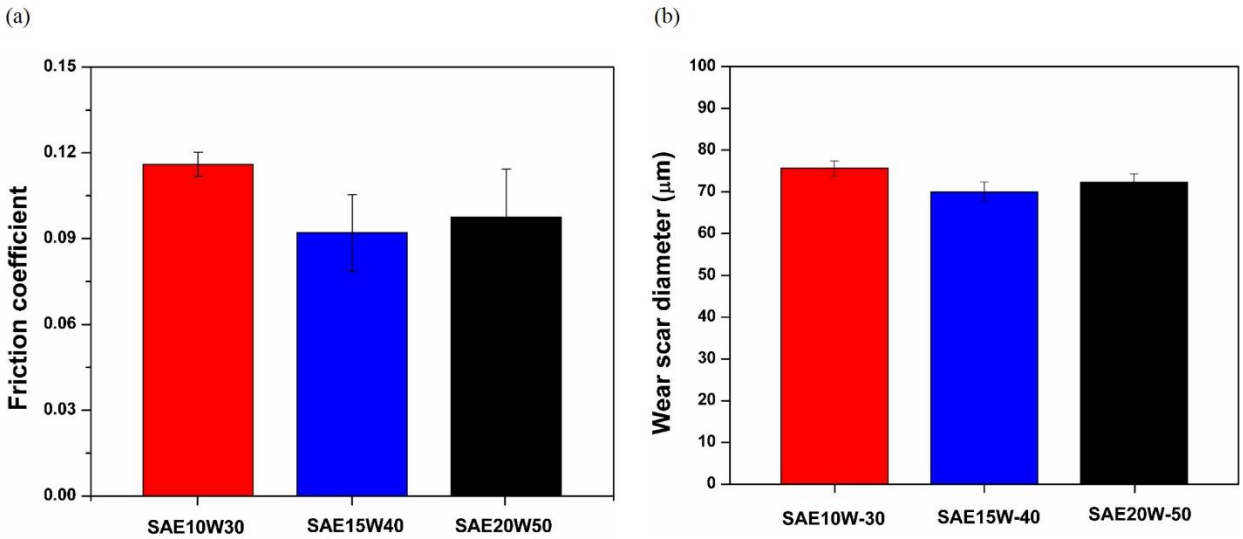

Fig.4.4 Friction coefficient and wear scar diameter of different lubricants

Figure 4.4 shows the measured mean friction coefficient and wear scar diameter of different tested lubricants at an applied load of 15 kg and speed of 1200 rpm. It is observed that the mean

friction coefficient of SAE20W-50, SAE15W-40 and SAE10W-30 lubricants are 0.097, 0.092 and 0.116, respectively (see Fig.4.4 (a)). The mean wear scar diameter for SAE20W-50, SAE15W-40 and SAE10W-30 lubricants are 72 µm, 68 µm and 78 µm, respectively (as can be seen in Fig.4.4 (b)). The test results revealed that lubricant SAE15W-40 exhibits excellent frictional and wear resistance when compared with other lubricants. This friction and wear reduction with SAE15W-40 lubricant may be due to lower frictional torque when compared with other lubricants, which can be observed in Fig.4.3.

Furthermore, the frictional and wear performance of lubricants is also tested by varying rotational speed. Figure 4.5 shows the friction coefficient and wear scar diameter of tested lubricants at an applied load of 15 kg. The friction coefficient and wear scar diameter are increased with the rotating speed for all the lubricants tested (see Fig.4.5 (a) & (b)). This may be due to the fact that for higher speeds, the lubricant moves away from the contact zone and allows the direct contact of the surfaces, which increases the friction coefficient and wear scar diameter. However, lubricant SAE15W-40 exhibits superior frictional and wear performance among other lubricants considered in the study. Based on the above experimental results, SAE15W-40 is selected to lubricate the parallel sliding contact in further analysis. Table 4.2 shows the properties of selected lubricant.

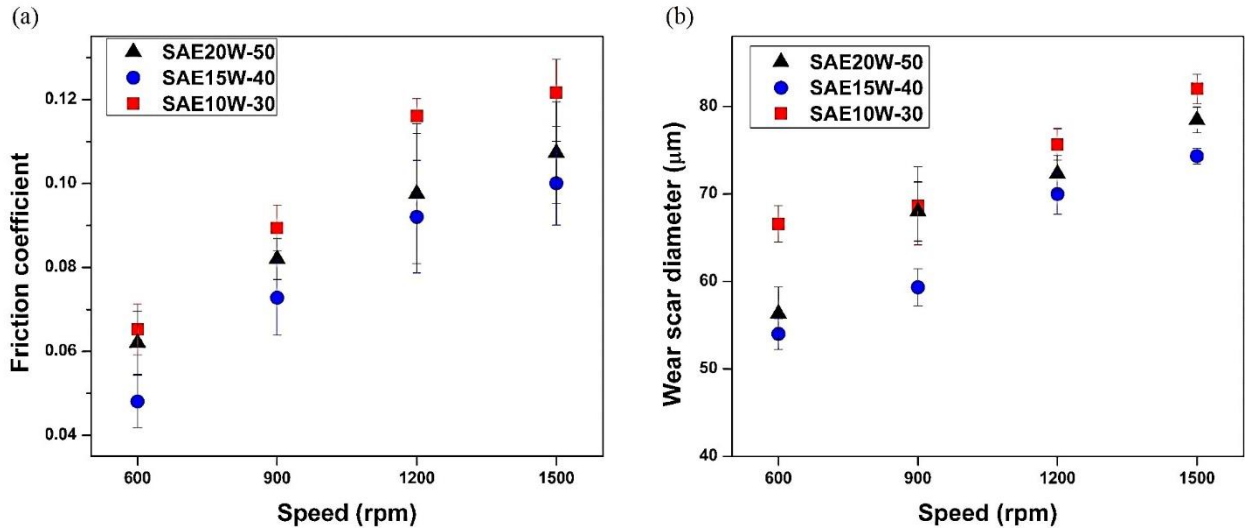

Fig.4.5 Tribological performance of various lubricants for varying speeds

Table 4.2 Properties of selected lubricant

Lubricant	Density (gm/cm^3)	Flash point (^{0}C)	Dynamic viscosity at 30^{0}C (Pas)
SAE15W-40	0.8725	232	0.121

4.2 Experimental investigation on the tribological performance of positive textured sliding contact

In general, the sliding contacts operate in a different lubrication regime by changing the fluid film thickness. At lower speeds or contact reversals (such as PR-CL contact near dead centers), insufficient lubrication conditions occur at the conjunction due to lack of relative motion between the interacting surfaces, resulting in poor tribological behavior. This causes mechanical interaction of asperities of mating surfaces and leads to a boundary or mixed lubrication regime. Sliding contacts operating in mixed or boundary lubrication regime generate more frictional losses than hydrodynamic lubrication regime. These conditions are quite common at PR-CL contact near dead centers and piston reversals, where surface texturing may provide greater benefits to improve tribological conditions. Therefore, in the present work, a fundamental study on the influence of surface texturing is carried out under laboratory conditions to achieve the beneficial effects in terms of friction and wear reduction. The experiments are conducted with the selected lubricant for the developed textured surfaces in order to investigate the tribological performance of the sliding contact.

4.2.1 Apparatus

Pin on disc friction and wear test rig (Magnum make, model: TE-165-SPOD) was used to conduct the experiments by providing the lubricant between the mating surfaces. The pin on disc test rig mainly comprises a testing unit, a display unit, and a controller unit (see Fig. 4.6). The testing unit includes a lever to apply the normal load on the pin (stationary strip) against the disc (moving plate), a pin holder to hold the pin firmly, and an oil reservoir for continuous supply of the lubricant. The LVDT sensors are placed at the end of the lever to measure the friction force and coefficient of friction of stationary pin, which is coupled to the display unit. The controller unit controls the speed of the motor. The experiments are conducted between the textured stationary pin and un-textured moving disc as shown in Fig.4.7.

Fig.4.6 Pin on disc friction and wear test rig set up

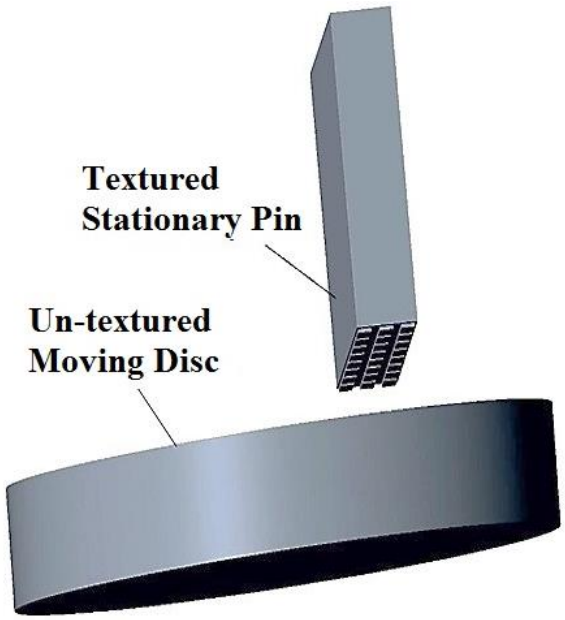

Fig.4.7 A schematic view of textured pin and un-textured disc

4.2.2 Specimen

In the present work, a small fraction of flat strip (pin) is chosen against rotating disc by considering conformal (parallel surfaces) contact between them. The strip is made from AISI 1020 steel of length of 28 mm having a cross-section of 10 mm x 3 mm and the counter face material (disc) is prepared from EN31 steel with a diameter of 165 mm and a thickness of 8 mm.

The materials were procured from Apollo metal industries, Hyderabad in heat treated condition, which were used in experimentation. In the present work, texture height produced on the pin surface was in several microns. Therefore, the texture heights produced by etching process may not destroy the heat treated layer much. Furthermore, the average surface roughness of pin and disc materials were maintained at 0.417±0.048 µm and 0.351±0.004 respectively, which was measured by surface roughness tester (Handy surf). The properties of the materials used in the present work are provided in Table 4.3.

Table 4.3 Material properties

Specimen	Material	Modulus of Elasticity	Yield strength	Hardness
Fixed Strip (Pin)	AISI 1020	200 GPa	295 MPa	130 HB
Moving disc	EN 31	215 GPa	450 MPa	63 HRC

4.2.3 Experimental conditions

The parameters that have been varied in the present work are texture area density, height and normal load by keeping sliding speed constant. The experimental conditions are adopted from the conditions of PR-CL sliding contact near the dead centers. In a real engine condition, severe friction and wear occur near the top and bottom dead centers of PR-CL sliding pair. Generally, the mixed lubrication regime is a predominant mechanism in these regions due to the presence of thin oil films, which causes adverse effects on friction and wear. Therefore, the experiments were designed to be closer to such realistic conditions. In a typical real engine, the nominal contact pressure near dead centers is in a range of 0.1 MPa-0.5 MPa [79]. The lower value of contact pressure corresponds to the ring's elasticity, and the higher value corresponds to average additional gas pressure in one complete operating cycle. In the present work, three values of contact pressures have been considered for the present analysis, i.e., 0.16 MPa, 0.33 MPa, and 0.5 MPa and its corresponding normal loads for the considered area of pin surface are obtained as 5 N, 10 N and 15 N respectively. The average angular velocity near the top and bottom dead centers would be below 500 rpm in a real engine condition [95]. In the present work, to avoid the boundary lubrication conditions at lower velocities, the angular velocity has been chosen closer to 500 rpm, i.e. 400 rpm, and the corresponding sliding velocity is obtained as 1.67 m/s, based on a track radius of 40 mm. Area density has been considered from 0.1 to 0.5 in a step size of 0.1.

The texture height varied in a range of 10-100 μm in a step size of 30 μm. The experimental conditions are presented in Table 4.4.

Table 4.4 Experimental conditions

Test parameter	Value
Normal load (N)	5,10,15
Area density	0.1,0.2,0.3,0.4,0.5
Texture height (μm)	10, 40, 70, 100
Track radius (mm)	40

All the experiments are performed at a room temperature of 30^0C for a sliding distance, d_s of 1200 m at each load-speed combination. From the literature, it has been observed that in order to provide sufficient lubrication condition at the contact zone, an oil drop has been supplied at a time interval of 15 seconds [142] and 30 seconds [79]. In the present work, continuous supply of lubricant is provided with an oil drop of weight 0.01 gm at a time interval of 5 seconds (12 drops per minute) at the inlet zone of sliding contact.

4.2.4 Friction and wear rate calculations

In the present work, the sliding tests are conducted on a pin on disc apparatus to study the influence of positive texturing on friction and wear properties of parallel sliding surfaces. All the tests are performed in two sets; the first set consisted of un-textured surfaces, and the second set of square-shaped textured surfaces.

Before starting each experiment, pin and disc surfaces are cleaned with acetone to remove oil and dirt particles and then dried. After each test, friction coefficient and wear rate (the ratio of wear volume per unit sliding distance) of pin sample are calculated by using Eqs. (4.2) and (4.3), respectively. The average friction coefficient is utilized to evaluate the friction properties, whereas average wear rate is used to evaluate the wear properties.

$$Friction\ coefficient = \frac{F}{W_1} \tag{4.2}$$

$$Wear\ rate\ (mm^3/m) = \frac{W_i - W_f}{\rho d_s} \tag{4.3}$$

Where, F = Frictional force in N, W_1= Applied normal load in N, W_i = Weight of the pin sample before the experiment in gm, W_f = Weight of the pin sample after the experiment in gm, ρ = Density of the pin material in gm/mm^3, d_s = Sliding distance in m.

4.3 Results and discussion

The experiments have been conducted on square-shape textured and un-textured surfaces under lubricated sliding conditions. However, in order to visualize the effect of a lubricated sliding condition, the results of dry sliding condition for plain surface (un-textured) are also included. In the experiments, the square-shaped texture with a size of 500 µm and a texture height of 70 µm are utilized to investigate the beneficial effects of surface textures. After each test, the friction coefficient and wear rate are calculated by using Eqs. (4.2) & (4.3). In the lubricated condition, the textured and un-textured samples are represented by (T+O) and (O), respectively.

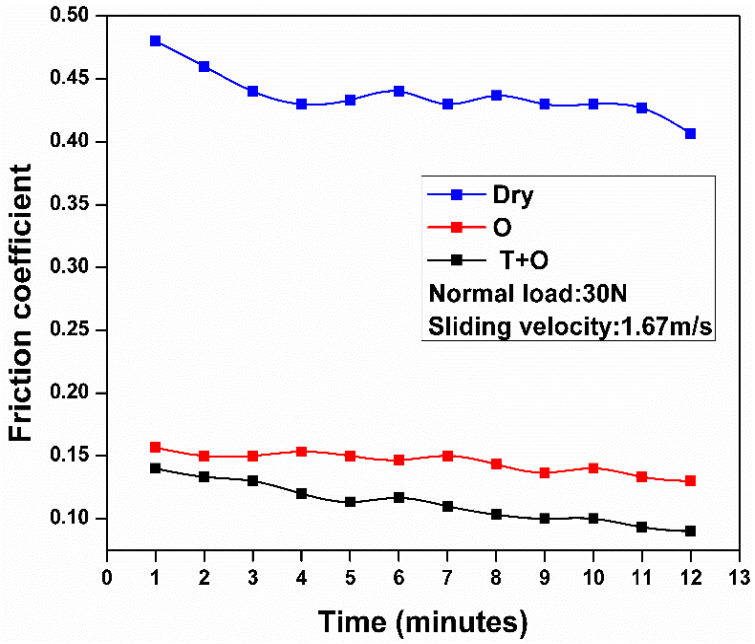

Fig.4.8 Friction coefficient vs time at a normal load of 30 N and sliding velocity of 1.67 m/s

The result of friction coefficient for different contact conditions is described in Fig 4.8. A drastic decrease of friction coefficient is identified under the lubricated condition compared to the

dry sliding state, which is obvious due to the presence of the lubricant. Under lubricated conditions, the textured surface exhibited more beneficial effects in reducing the friction coefficient as compared to the un-textured surface (see Fig.4.8). This friction reduction may be due to an additional hydrodynamic lift generated by textures between the interacting surfaces, which is not present in the case of un-textured surfaces.

Figure 4.9 shows the results of wear rate under dry and lubricated sliding conditions. It is observed that the pin sample experienced severe wear rate under dry condition when compared with lubricated condition. However, a further reduction in wear rate has been observed with the presence of the surface textures compared to un-textured lubricated surfaces. This is probably due to the ability of surface texturing, which offers a lower area of contact between the interacting surfaces and capturing the wear debris in the space between the textures, thereby reducing the wear rate.

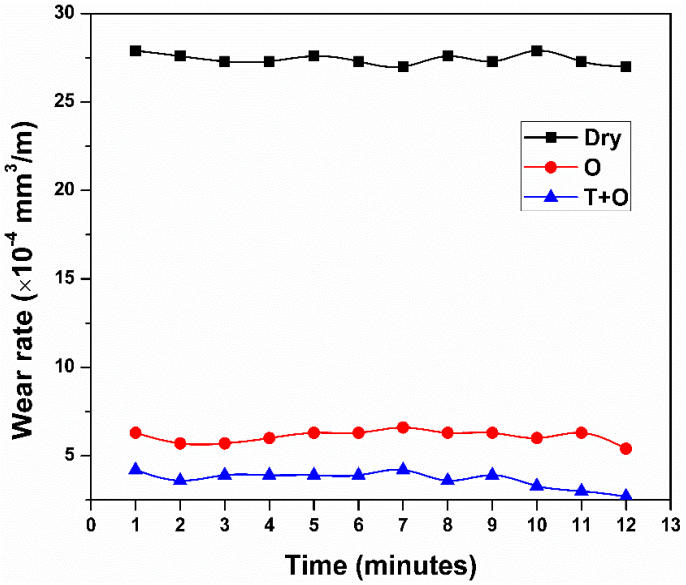

Fig.4.9 Wear rate vs time at a normal load of 30 N and sliding velocity of 1.67 m/s

The wear reduction with textured surfaces is further confirmed by worn surface analysis which is shown in Fig.4.10. It can be seen in Fig.4.10 (a) that the deep grooves and scratches are an indication of severe abrasive wear under dry condition. Similarly, the narrow wear scars from Fig.4.10 (b) & (c) would be evident for mild abrasive wear in lubricated conditions. Moreover, it is observed from Fig. 4.10 (c) that the textures are not damaged severely and there is no further indication of severe wear tracks or deep grooves when compared with un-textured surfaces.

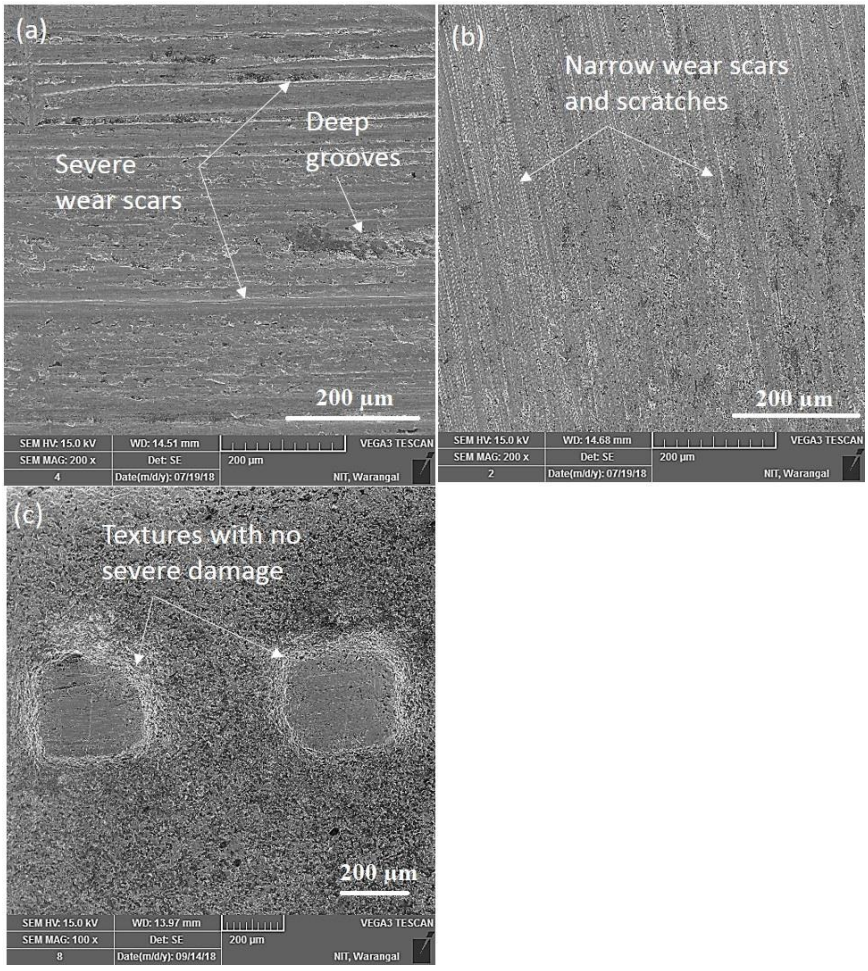

Fig.4.10 SEM images of pin surface under (a) dry condition, (b) lubricated condition without textures (c) lubricated condition with textures

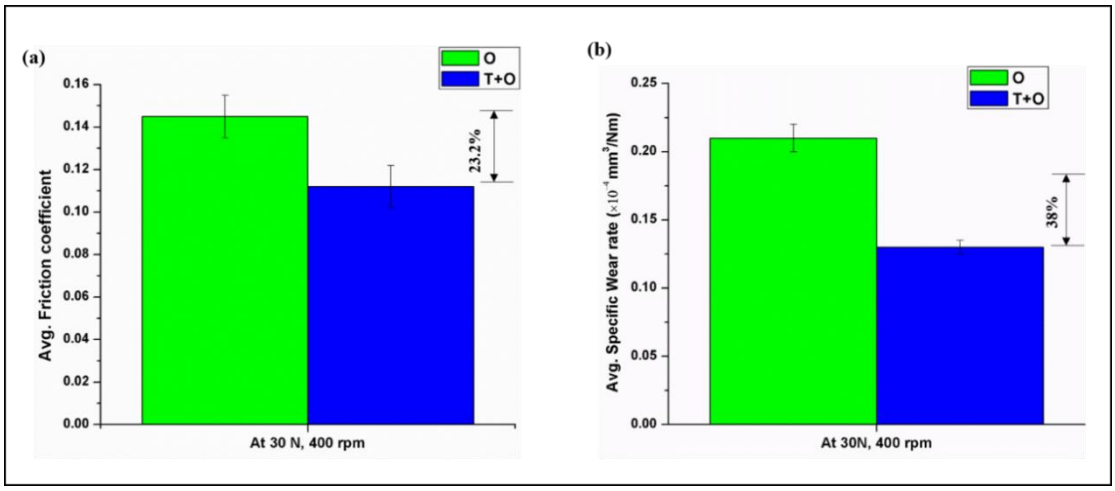

Fig.4.11 Average friction coefficient and wear rate results

Furthermore, Fig.4.11 shows the mean friction coefficient and wear rate of textured and un-textured surfaces under lubricated conditions. The results confirm that textured surfaces significantly reduces the mean friction coefficient and wear rate compared to an un-textured lubricated case (see Fig.4.11 (a) & (b)). A maximum reduction of 23.2 % in the friction coefficient and 38% of wear rate was observed with textured surfaces.

As observed, textured surfaces exhibited beneficial effects in terms of friction and wear reduction of the sliding contact. Therefore, the effect of geometric parameters of square-shaped positive textures such as area density and texture height on the tribological performance of parallel sliding contact was investigated.

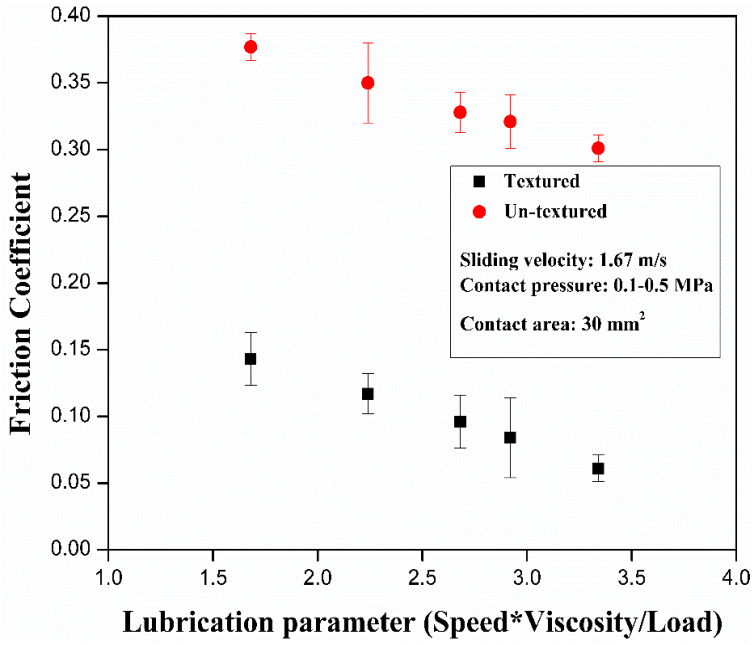

Fig.4.12 Stribeck curves for textured and un-textured surfaces

Before a detailed discussion on the influence of geometric parameters is offered, Stribeck curves were drawn to assess the lubrication regimes at different operating conditions. Stribeck curves were plotted showing friction coefficient as a function of lubrication parameter (the ratio of sliding speed to nominal contact pressure with constant viscosity) for both textured and un-textured surfaces (as can be seen in Fig.4.12). From Fig.4.12, it can be observed that the decrease in friction coefficient resulted in increase of lubrication parameter for both textured and un-

textured surfaces. The tested pin samples followed similar trends to previous studies [82, 143] which indicated that the contact is operating in mixed lubrication regime.

Stribeck curves confirm that the operating regime is in mixed lubrication regime for both textured and un-textured surfaces. Later, the experiments were conducted to study the influence of texture area density and texture height on the friction and wear behavior of sliding contacts.

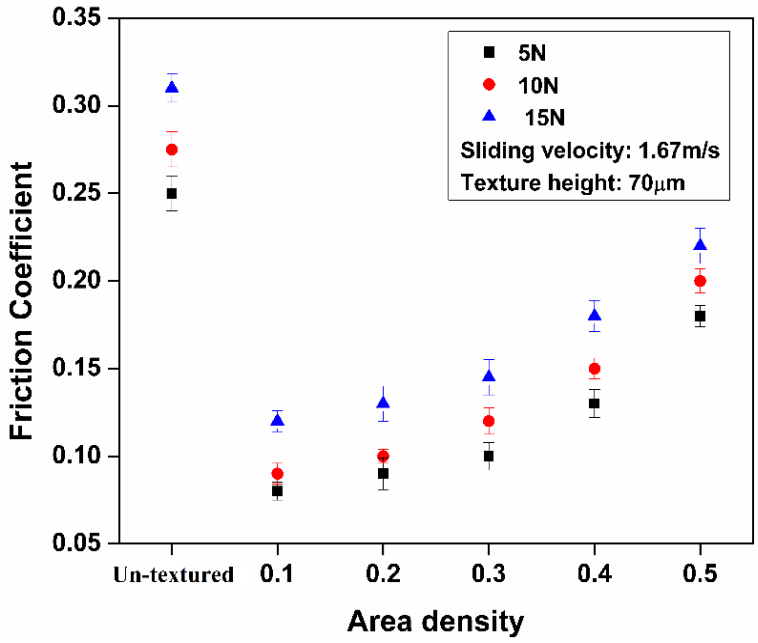

Fig.4.13 Influence of square-shaped texture area density on friction coefficient

The effect of texture area density on friction coefficient at a texture height of 70 µm for different loads is shown in Fig.4.13. The surface becomes smooth, i.e., un-textured when the area density is considered to be zero. It can be observed from Fig.4.13 that all textured surfaces exhibit better friction performance compared to un-textured surfaces. It can also be observed that the average friction coefficient increased with the increase of normal load for both textured and un-textured surfaces. This is probably due to the fact that the increase of normal load causes high asperity interactions at the conjunction of sliding surfaces, thereby resulting in higher values of average friction coefficient. A significant reduction in average friction coefficient is observed with lower values of area density. Furthermore, at a normal load of 5 N and an area density of 0.1, a maximum reduction of average friction coefficient is found to be 67.64% and 54.8% compared to un-textured surfaces and a textured surface of area density of 0.5 respectively. This

friction reduction can be better explained by hydrodynamic lift caused by pressure build-up due to extra oil supply at the contact zone generated by surface textures. The hydrodynamic lift is lower in case of higher area density of textures because of undesired edge effects which may limit the hydrodynamic lift [144].

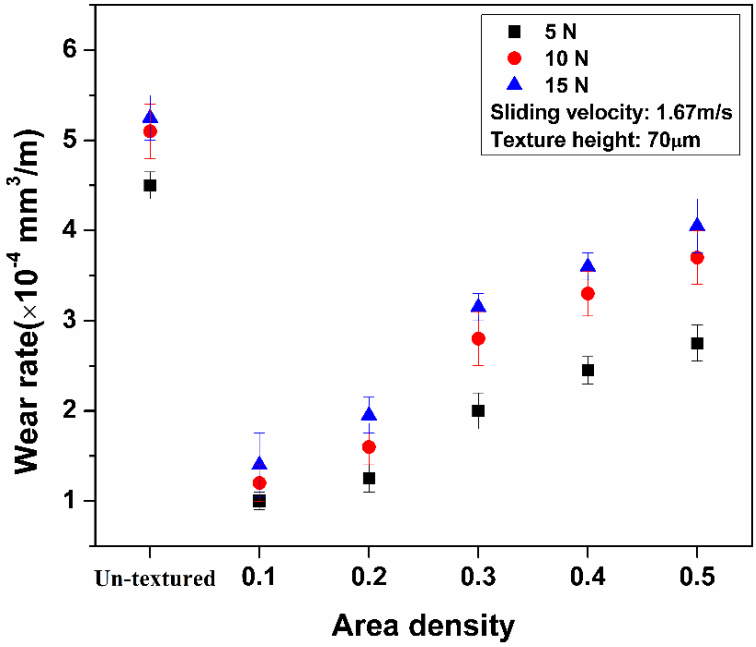

Fig.4.14 Influence of square-shaped texture area density on wear rate

The behavior of wear rate with area density is shown in Fig.4.14. It is found that an increasing trend of wear rate is observed with increase of normal load for both textured and un-textured surfaces. It can also be observed that the textured surfaces exhibit better performance compared to un-textured surfaces. Furthermore, at an area density of 0.1 and a normal load of 5 N, a maximum reduction of wear rate is found to be 81.6% and 69.3% compared to un-textured surfaces and a textured surface of area density of 0.5, respectively. This reduction in wear rate is better explained by wear debris entrapment. The surfaces with lower area density provide more space for the entrapment of wear debris compared to higher area density. Due to this, ploughing action between rubbing surfaces is reduced and thereby reduces the wear rate.

The SEM images for worn surfaces of smooth (un-textured) and textured specimens with area density of 0.1 and 0.5 are shown in Fig.4.15 (a), (b) & (c) respectively, after a sliding distance of 1200 m with normal load and sliding velocity of 5 N and 1.67 m/s respectively.

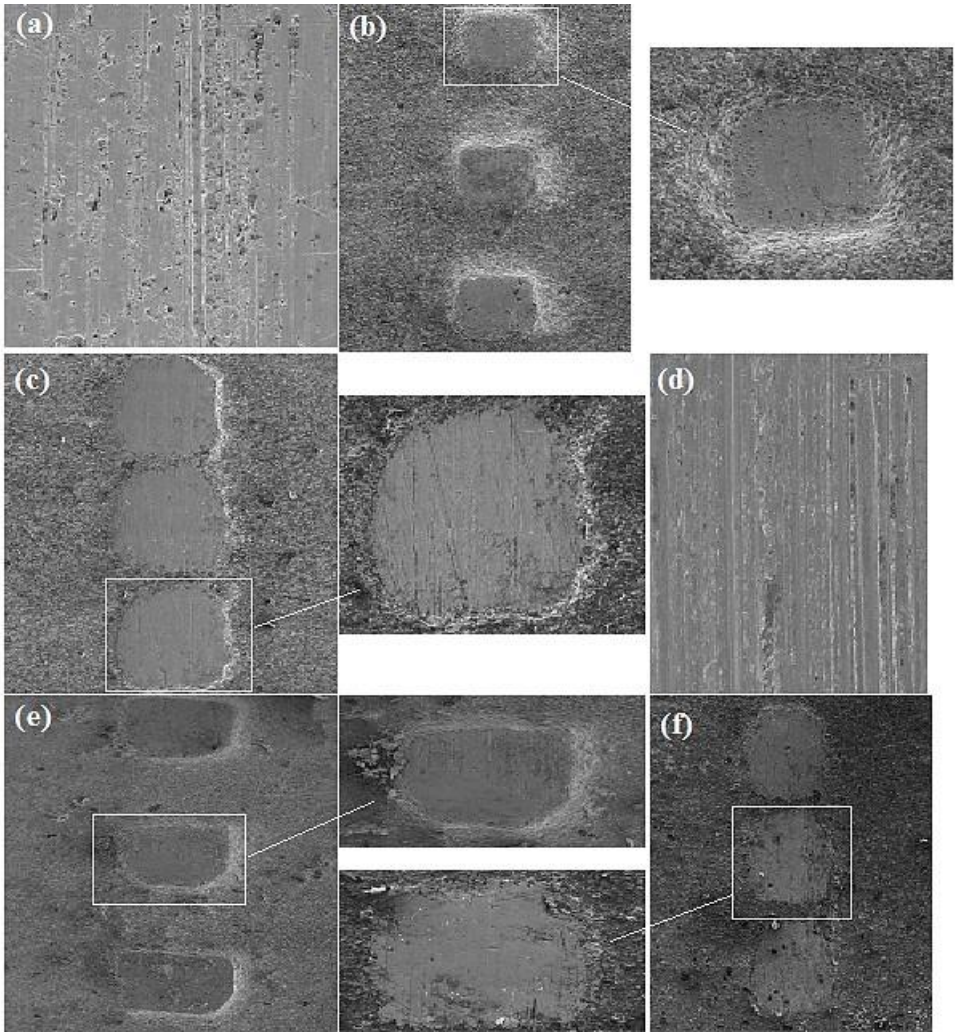

Fig.4.15 SEM images of worn surfaces with: (a) S_p = 0 (un-textured), 5N; (b) S_p = 0.1, 5N; (c) S_p = 0.5, 5N; (d) S_p = 0 (un-textured), 15N; (e) S_p = 0.1, 15N; (f) S_p = 0.5, 15N

It can be observed that deep grooves and scratches on un-textured surface in sliding direction are an indication for abrasive wear (see Fig.4.15 (a)). In case of textured surfaces (see Fig.4.15 (b) & (c)), no indication of severe wear scars or deep grooves is evident compared to un-textured surface. It can be noticed that when the friction coefficient is in a range of 0.05-0.15, then the type of wear regime is termed as mild wear. While, the wear regime termed as severe when the friction coefficient is in a range of 0.15-2.0 [145]. Textures with lower area density (0.1) exhibit milder wear compared to higher area density (0.5) (see Fig.4.13). Furthermore, the enlarged view of the worn surface of texture with lower area density indicated that the texture is not as severely damaged as the texture with higher area density. This may be due to the fact that the wear debris

is captured in the space between the textures of lower area density. This effective function of capturing wear debris causes a decrease of abrasive wear [88, 146, 147]. In the case of higher area density, the edges of texture experienced higher wear compared to lower area density, and it may be due to undesired high-stress concentrations developed at the edges. Similar effects were observed at higher normal load (15N) but with higher magnification of wear scars and depth of penetration (see Fig.4.15 (d), (e) & (f)). From worn surfaces of pin samples, it is reported that lower area densities would be better to improve the tribological properties of parallel sliding contact.

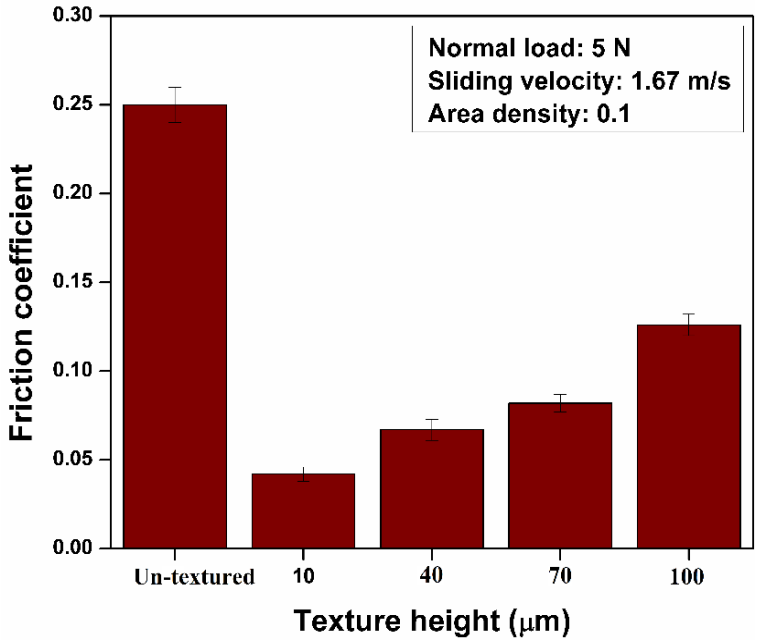

Fig.4.16 Impact of square-shaped texture height on friction coefficient

The impact of texture height on friction coefficient at an area density and normal load of 0.1 and 5 N, respectively is given in Fig.4.16. The textured surfaces exhibit superior performance in friction reduction than un-textured surfaces. The maximum friction reduction is achieved with textured surfaces, and corresponds to a texture height of 10 μm when compared with un-textured surfaces. As for the texture height concern, lower texture height values show better frictional performance than higher texture heights. The friction coefficient value is measured as 0.042 for a texture height of 10 μm, while friction coefficient value of 0.126 is obtained when the texture height is increased to 100 μm. Furthermore, a maximum reduction of 85.4% in friction coefficient is observed with textured surfaces at a height of 10 μm compared to un-textured

surfaces. This may be due to lower asperity interactions occur in the case of lower texture heights that may reduce the friction coefficient.

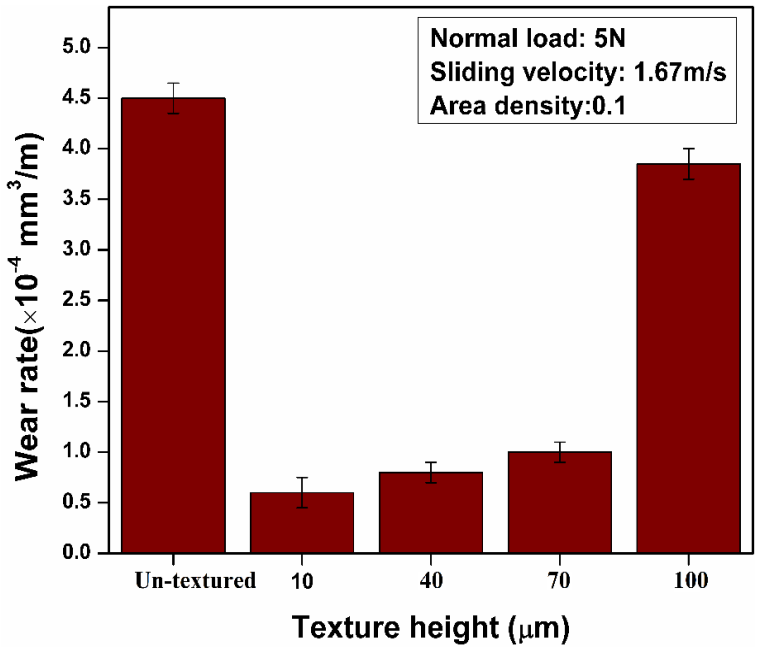

Fig.4.17 Impact of square shaped texture height on wear rate

The influence of texture height on wear rate is also presented in Fig.4.17. It is observed that textured surfaces exhibit better wear performance than un-textured surfaces. The maximum reduction of 88.9 % is achieved with textured surfaces of 10 μm texture height than un-textured surfaces. Moreover, the increase in texture height resulted in increased wear rate. This may be due to the development of additional stress concentrations in the case of higher texture heights that may increase the wear rate more than lower texture heights. In addition, the increase in wear rate between the texture heights of 70 and 100 μm is not gradual. This may be due to more domination of undesired stress concentration effects at a texture hight of 100 μm when compared to a texture height of 70 μm, which resulted in a sudden increase of wear rate between texture heights of 70 and 100 μm. Furthermore, the worn surfaces of textured samples also reveal that the lower texture heights are superior in reducing wear rate when compared with higher texture heights. As can be seen from Fig.4.18, the textured surfaces at a texture height of 100 μm are severely damaged than at a texture height of 10 μm. It is also observed that wear debris present in the case of higher texture heights (see Fig.4.18), which may accelerate the wear process, due to which the wear rate is more in the case of higher texture heights when compared with lower

texture heights. From the worn surface analysis, it is reported that lower texture heights would be recommended for improved tribological properties of parallel sliding contact.

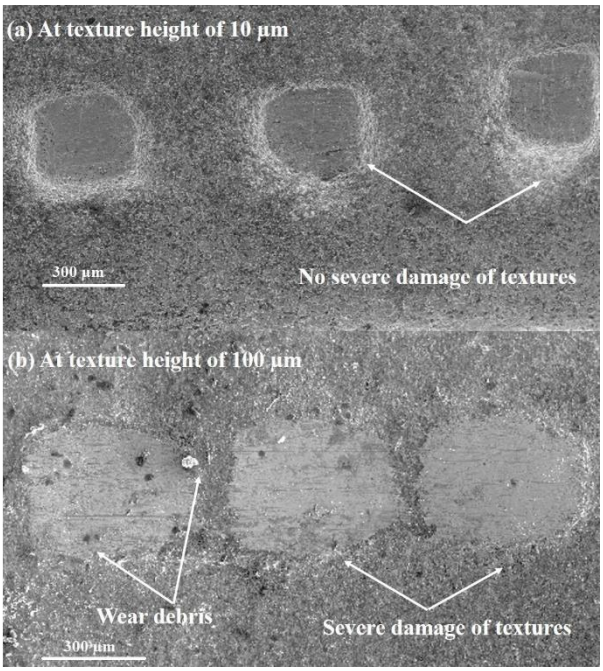

Fig.4.18 SEM images of worn surfaces at different texture heights

4.4 Summary

In this chapter, an experimental study was carried out in order to understand the effect of square-shaped positive surface texture on the tribological performance of parallel sliding contact. An improved tribological behavior is observed in textured surfaces when compared with un-textured surfaces. It is observed from the Stribeck curves that the contact is operating in mixed lubrication regime for both textured and un-textured surfaces. The maximum reduction of 67.64% in friction reduction and 81.6% in wear rate is obtained with a texture area density of 0.1 at a texture height of 70 µm as compared to un-textured case. On the other hand, the lower texture heights exhibit better friction and wear resistance. At a texture height of 10 µm, the maximum reduction in friction coefficient and wear rate is observed as 85.4% and 88.9% respectively, when compared with un-textured surfaces. The effect of texture shape may also effect the tribological properties; however, conducting experiments for different texture shapes is costly and time-consuming. In this regard, a theoretical model is developed in chapter 5 which can be used to study the influence of various textural aspects such as shape, area density and height.

Chapter 5

Numerical modelling of textured sliding contact under mixed lubrication regime

This chapter provides a theory relating to the numerical modelling of mixed lubrication in textured parallel sliding contact. The modified Reynolds equation (Patir-Cheng flow model) and asperity contact model (Greenwood-Tripp model) are solved for hydrodynamic and asperity pressures, respectively. The effect of surface roughness on fluid flow is taken into account by considering fluid correction factors under mixed lubrication. The numerical simulations are performed by employing the finite difference method with Gauss-Seidel iteration scheme. The numerical simulation results are validated with previously available results and also with the experimental results of square-shaped positive textures which were obtained in the previous chapter.

5.1 Mathematical formulation

In general, a lubricated sliding contact operates under different regimes of lubrication such as hydrodynamic, mixed, and boundary lubrication. The lubricant enters the clearance between the interacting sliding surfaces through micro-wedge effect and supports the total applied load and this type of lubrication regime can be named hydrodynamic lubrication. However, in situations such as lower speeds or higher loads, lubricant starvation occurs. At these conditions, the asperities of the surfaces interact with each other and interrupt the fluid film. This asperity interaction generates certain pressure. This asperity pressure in addition to hydrodynamic pressure supports the total applied load and the type of lubrication regime can be called as mixed lubrication regime. A modified Reynolds equation is used to evaluate the average hydrodynamic pressure, while the asperity contact model is used to determine the asperity pressure. The models used in the present work are discussed in the following sections.

5.1.1 Derivation of modified Reynolds equation

The modified Reynolds equation is derived by solving the classical Reynolds equation for rough bearing with randomly distributed roughness through flow simulation [148, 149].

The local film thickness can be defined as follows (see Fig.5.1);

$$h_T = h + \delta_1 + \delta_2 \tag{5.1}$$

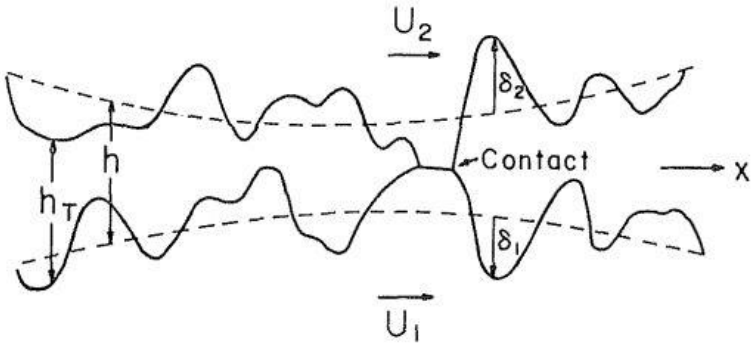

Fig.5.1 Film thickness function [148]

Here h_T is local film thickness, δ_1, δ_2 are random roughness of amplitudes measured from the mean values. By assuming Gaussian distribution of asperity heights with mean is equal to '0', the combined roughness has a variance of $\sigma = \sqrt{\sigma_1^2 + \sigma_2^2}$ with standard deviations of σ_1 and σ_2.

The isothermal, isoviscous, incompressible generalized Reynolds equation and the local flows are given as [148]:

$$\frac{\partial}{\partial x}\left(\frac{h_T^3}{12\mu}\frac{\partial p}{\partial x}\right) + \frac{\partial}{\partial z}\left(\frac{h_T^3}{12\mu}\frac{\partial p}{\partial z}\right) = \frac{U_1 + U_2}{2}\frac{\partial h_T}{\partial x} + \frac{\partial h_T}{\partial t} \tag{5.2}$$

$$q_x = -\frac{h_T^3}{12\mu}\frac{\partial p}{\partial x} + \frac{U_1 + U_2}{2}h_T \tag{5.3}$$

$$q_z = -\frac{h_T^3}{12\mu}\frac{\partial p}{\partial z} \tag{5.4}$$

Here, p is local fluid film pressure, q_x, q_z are local flows in x and z-directions respectively, which are random functions.

In order to derive modified Reynolds equation, the expected flows for rough bearing has been analyzed. Consider a small control volume of area $\Delta x \times \Delta z$ as given in Fig.5.2.

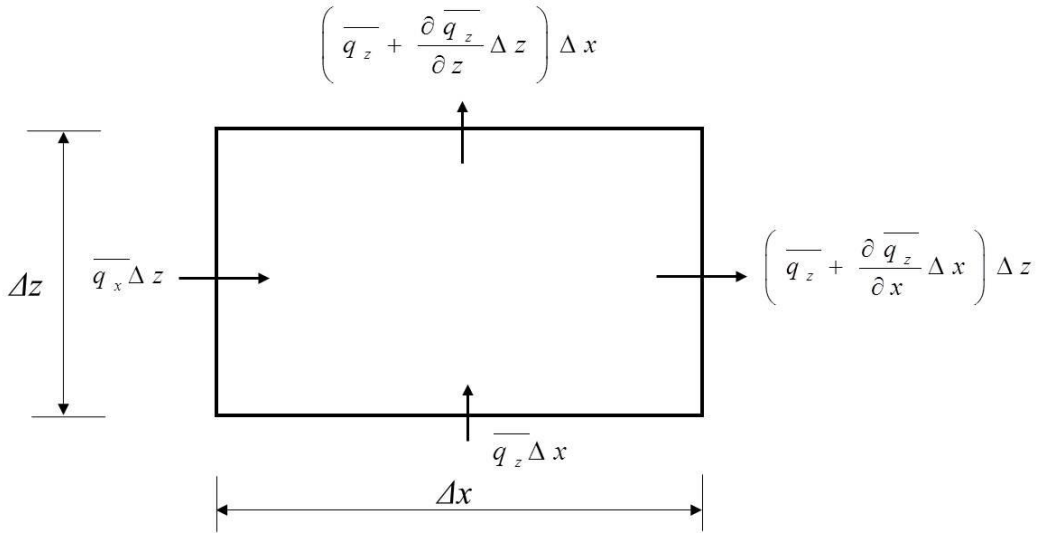

Fig.5.2 Control volume for mean flow [148]

Considering mean expected flows entering the control volume in *x* and *z*- directions as:

$$\overline{q_x} = \frac{1}{\Delta z}\int_z^{z+\Delta z} q_x dz = \frac{1}{\Delta z}\int_z^{z+\Delta z}\left(-\frac{h_T^3}{12\mu}\frac{\partial p}{\partial x} + \frac{U_1+U_2}{2}h_T\right)dz \tag{5.5}$$

$$\overline{q_z} = \frac{1}{\Delta x}\int_x^{x+\Delta x} q_z dx = \frac{1}{\Delta x}\int_x^{x+\Delta x}\left(-\frac{h_T^3}{12\mu}\frac{\partial p}{\partial z}\right)dx \tag{5.6}$$

Now, defining pressure flow factors and shear factor such that the mean expected flow in *x* and *z*-directions are as flows:

$$\overline{q_x} = -\phi_x \frac{h^3}{12\mu}\frac{\partial \overline{p}}{\partial x} + \left(\frac{U_1+U_2}{2}\right)\overline{h_T} + \frac{U_1-U_2}{2}\sigma\phi_s \tag{5.7}$$

$$\overline{q_z} = -\phi_z \frac{h^3}{12\mu}\frac{\partial \overline{p}}{\partial x} \tag{5.8}$$

Where, $\overline{p}$ is mean hydrodynamic pressure, $\overline{h_T}$ is mean gap, $\overline{q_x}$ and $\overline{q_z}$ are mean expected flows in *x*, *z*-directions respectively, ϕ_x, ϕ_z are pressure flow factors that compare the flow in rough bearing to smooth bearing, ϕ_s is additional flow transport due to sliding in a rough bearing.

The first term of the R.H.S of Eq. (5.7) represent mean flow due to mean pressure gradient in *x*- direction. The second term represents the flow transport due to entrainment velocity, while the third term represents additional flow transport due to sliding in a rough bearing with the combined effect of both roughness and sliding in rough bearing. The third term is not present in the generalized Reynolds equation, which is for smooth surfaces.

By performing mean flow balance on control volume;

$$\left(\overline{q_x}+\frac{\partial\overline{q_x}}{\partial x}\Delta x\right)dz-\overline{q_x}dz+\left(\overline{q_z}+\frac{\partial\overline{q_z}}{\partial z}\Delta z\right)dx-\overline{q_z}dx+\Delta x\Delta z\frac{\partial\overline{h_T}}{\partial t}=0 \tag{5.9}$$

$$\frac{\partial\overline{q_x}}{\partial x}+\frac{\partial\overline{q_z}}{\partial z}=-\frac{\partial\overline{h_T}}{\partial t} \tag{5.10}$$

Substitute $\overline{q_x}$ and $\overline{q_z}$ (i.e., Eqs. (5.7) & (5.8)) in Eq. (5.10) to get average Reynolds equation, which is given as follows:

$$\frac{\partial}{\partial x}\left(\phi_x\frac{h^3}{12\mu}\frac{\partial\overline{p}}{\partial x}\right)+\frac{\partial}{\partial z}\left(\phi_z\frac{h^3}{12\mu}\frac{\partial\overline{p}}{\partial z}\right)=\left(\frac{U_1+U_2}{2}\right)\frac{\partial\overline{h_T}}{\partial x}+\frac{U_1-U_2}{2}\sigma\frac{\partial\phi_s}{\partial x}+\frac{\partial\overline{h_T}}{\partial t} \tag{5.11}$$

Wu et al. [150] and Meng et al. [151] defined a contact factor such that $\phi_c=\frac{\partial\overline{h_T}}{\partial h}$ and it is also noted that for the lower value of $ø_c$, the probability of surface contact is higher and vice-versa. After substituting $ø_c$ in Eq. (5.11), it becomes:

$$\frac{\partial}{\partial x}\left(\phi_x\frac{h^3}{12\mu}\frac{\partial\overline{p}}{\partial x}\right)+\frac{\partial}{\partial x}\left(\phi_z\frac{h^3}{12\mu}\frac{\partial\overline{p}}{\partial z}\right)=\phi_c\left(\frac{U_1+U_2}{2}\right)\frac{\partial h}{\partial x}+\frac{U_1-U_2}{2}\sigma\frac{\partial\phi_s}{\partial x}+\phi_c\frac{\partial h}{\partial x} \tag{5.12}$$

$$\frac{\partial}{\partial x}\left(\phi_x\frac{h^3}{\mu}\frac{\partial\overline{p}}{\partial x}\right)+\frac{\partial}{\partial x}\left(\phi_z\frac{h^3}{\mu}\frac{\partial\overline{p}}{\partial z}\right)=6U\phi_c\frac{\partial h}{\partial x}+6\sigma\frac{\partial\phi_s}{\partial x}+12\phi_c\frac{\partial h}{\partial x}$$

(5.13)

From Eq. (5.13), the roughness effects on lubricant flow can be attributed to four factors $ø_x$, $ø_z$, $ø_s$ and $ø_c$. All these factors except $ø_c$ depends on oil film thickness ratio ($H=h/\sigma$) and surface pattern parameter, γ (the length to width ratio of asperities), while $ø_c$ depends on oil film thickness ratio only.

When $H\to\infty$, then ϕ_x, $\phi_z\to 1$ & $\phi_s\to 0$, then Eq. (5.13) can be reduced to generalized Reynolds equation for smooth surfaces.

By assuming isotropic roughness patterns i.e. γ=1, these flow factors are approximated by Patir and Cheng [148, 149] as follows:

$$\phi_x = \phi_z = 1 - 0.9e^{-0.56H} \tag{5.14}$$

$$\phi_s = \begin{cases} 1.899H^{0.98}e^{-0.92H+0.05H^2} & H \le 5 \\ 1.126e^{-0.25H} & H > 5 \end{cases} \tag{5.15}$$

$$\phi_c = \begin{cases} e^{-0.6912+0.782H-0.304H^2+0.0401H^3} & 0 \le H < 3 \\ 1 & H \ge 3 \end{cases} \tag{5.16}$$

Similar to the mean flow factors, the shear stress factors are defined such that the mean expected hydrodynamic shear stress is given as:

$$\bar{\tau} = \frac{\mu U}{h}(\phi_f + \phi_{fs}) + \phi_{fp}\frac{h}{2}\frac{\partial \bar{p}}{\partial x} \tag{5.17}$$

Where, the term ϕ_f arises from averaging the sliding velocity component of the shear stress. The term ϕ_{fp} is correlation factor for mean pressure flow component of the shear stress. The term ϕ_{fs} arises from the combined effect of roughness and sliding.

For isotropic roughness surfaces, these are approximated as follows [148, 149]:

$$\phi_{fp} = 1 - 1.40e^{-0.66H} \tag{5.18}$$

$$\phi_{fs} = \begin{cases} 11.1H^{2.31}e^{-2.38H+0.11H^2} & 0.5 < H < 7 \\ 0 & H > 7 \end{cases} \tag{5.19}$$

$$\phi_f = \begin{cases} \frac{35}{32}z_1\left\{(1-z_1^2)^3\ln\frac{z_1+1}{\epsilon^*} + \frac{1}{60}\left[-55 + z_1(132 + z_1(345 + z_1(-160 + z_1(-405 + z_1(60 + 147z_1)))))\right]\right\} & H \le 3 \\ \frac{35}{32}z_1\left\{(1-z_1^2)^3\ln\frac{z_1+1}{z_1-1} + \frac{z_1}{15}\left[66 + z_1^2(30z_1^2 - 80)\right]\right\} & H > 3 \end{cases} \tag{5.20}$$

Here, $z_1=h/3$, $\epsilon^* = \epsilon/3\sigma$ and $\epsilon=\sigma/100$

5.1.2 Asperity contact model for rough surfaces

In the mixed lubrication regime, the total load is carried by both lubricant and asperities. The asperities of rough contact surfaces interact mechanically with each other, thereby developing asperity contact pressures. These pressures can collectively contribute to the total load support of the system. In the present work, these contact pressures are calculated by adopting the well-known Greenwood-Tripp asperity contact model [152] as follows:

$$p_{asp} = K' E' F_{2.5}(H) \tag{5.21}$$

$$K' = \frac{16\sqrt{2}}{15}\pi(\eta\beta\sigma)^2\sqrt{\frac{\sigma}{\beta}} \tag{5.22}$$

$$E' = \frac{1}{\frac{1-\nu^2_1}{E_1} + \frac{1-\nu^2_2}{E_2}} \tag{5.23}$$

Where η is the asperity density, β is the asperity mean radius of curvature, E_1,ν_1, E_2, ν_2 are the modulus of elasticity and Poisson's ratio of stationary and moving surfaces respectively, and the integral function $F_{2.5}$ (H) represents the randomly distributed asperity heights. By assuming Gaussian distribution of asperity heights, the function $F_{2.5}$ (H) can be approximated as follows [153, 154]:

$$F_{2.5}(H) = \begin{cases} A'(4-H)^{Z'} & H < 4 \\ 0 & H \geq 4 \end{cases} \tag{5.24}$$

The parameters A'= 4.4068×10^{-5}, Z'=6.804 and K'=1.198×10^{-4} have been adopted from the studies of Akalin and Newaz [153] and Hu et al. [154].

The modified Reynolds model utilized in the present work assumes the fluid as Newtonian, iso-viscous, iso-thermal, fluid inertia and squeeze effect neglected and no-slip condition prevails. The asperity model considered in the present work neglects the effect of elastic deformation of the surfaces and asperities. In addition, the models presented here assumed a constant values of mean surface roughness, asperity density and asperity mean radius of curvature.

In general, the transition from one lubrication regime to another lubrication regime occurs by changing the load, velocity or viscosity, which further leads to a change in film

thickness. Theoretically, lubrication regimes can be classified based on the oil film ratio h/σ, as shown in Fig.5.3. If the oil film thickness ratio $H \geq 4$, then the frictional pair operates in pure hydrodynamic lubrication regime, where the total load is carried by the lubricant. For oil film thickness ratio of $1 < H > 4$, the contact operates in mixed lubrication regime, where the total load is carried by both lubricant and asperity contacts. Similarly, if oil film thickness ratio $H \leq 1$, then the friction pair operates in boundary lubrication regime, where the asperity contacts carry the total load. Therefore, the asperities interaction is possible only when the oil film thickness ratio, H is less than 4.

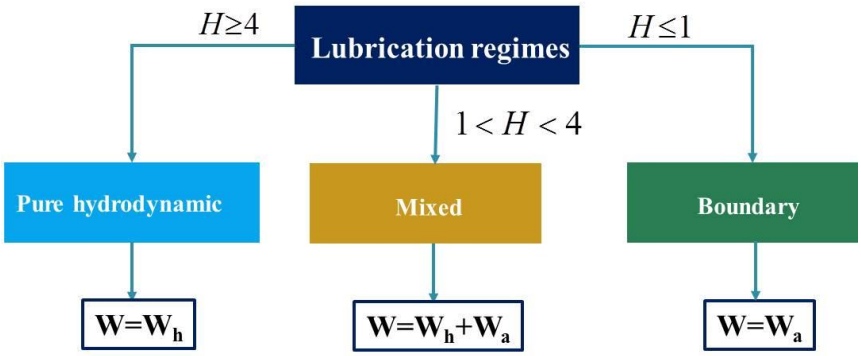

Fig.5.3 Classification of lubrication regimes

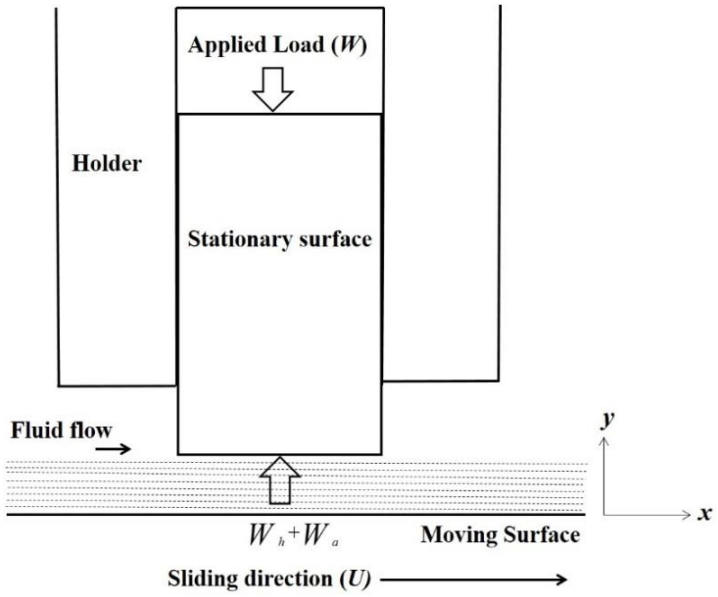

Fig.5.4 Contact configuration of parallel sliding contact

In the present work, the stationary surface is loaded by assuming the conditions near the dead centers in PR-CL sliding contact. At these conditions, mixed lubrication is predominating with no localized surface deformation [153, 155]. In the mixed lubrication regime, the total load (W) is supported by the hydrodynamic load (W_h) as well as asperity load (W_a) as shown in Fig.5.4. The modified Reynolds equation (Patir-Cheng flow model) and asperity contact model (Greenwood-Tripp model) are solved for hydrodynamic and asperity pressures, respectively.

5.1.3 Film thickness equation

Texture geometry should be well defined in order to study the effect of texture forms under different lubricating conditions. In order to obtain the beneficial effects of surface texturing, surface textures in the form of protrusions are introduced on the stationary surface of axial width b with square shape. The computational domain, along with the geometry of the features considered in the present study, is shown in Fig.5.5. The computational domain is modelled by placing each individual feature (i.e., an axisymmetric shape with base $2r_p$ and height h_t) at the center of an imaginary unit cell of size $B \times B$. The symbol h_0 represents the minimum oil film thickness.

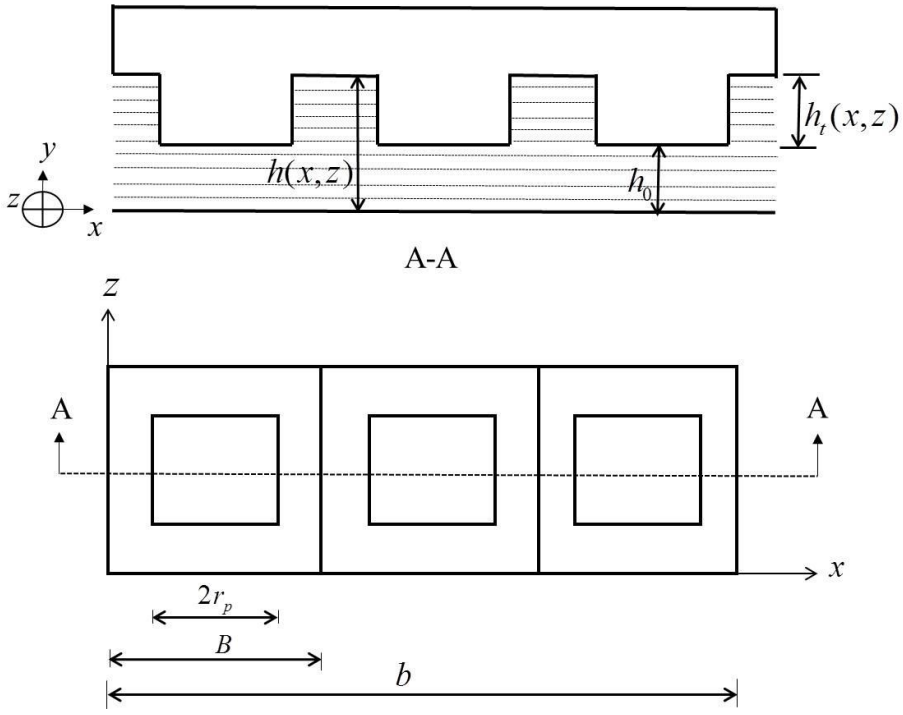

Fig.5.5 Computational domain considered for mathematical modeling

From Fig.5.5, the equation for mean oil film thickness is given as:

$$h(x,z)=\begin{cases} h_0 & \text{above texture} \\ h_0 + h_t(x,z) & \text{elsewhere} \end{cases} \tag{5.25}$$

The area density of texture S_p is the ratio of the area occupied by texture (A_t) and the area of the unit cell (A_u) which is given as:

$$S_p = \frac{A_t}{A_u} \tag{5.26}$$

$$r_p = \sqrt{\frac{S_p B^2}{4}} \tag{5.27}$$

It is worthwhile to mention that when altering the texture area density, the size of texture $2r_p$ changes while the unit cell size B remains constant (see Eq. (5.27)).

5.1.4 Boundary conditions

The ambient pressures are considered at both inlet and outlet boundaries across the sliding direction i.e., z-direction. In order to consider the texture interaction effects, the periodic boundary conditions are assumed in the sliding direction i.e., x-direction. The cavitation effects are taken into account by considering Reynolds cavitation condition, which implies that pressure at each node and pressure gradient with respect to the direction normal to boundary is zero. Although the Reynolds boundary condition does not include the mass conservation of fluid flow, it is much easier to implement it in the numerical simulations. In recent studies, several authors have successfully implemented this condition in investigating the textured sliding contacts [38, 156-158]. Therefore, Reynolds boundary model is adopted in the present study. The mathematical equations of the boundary conditions are shown in Fig.5.6.

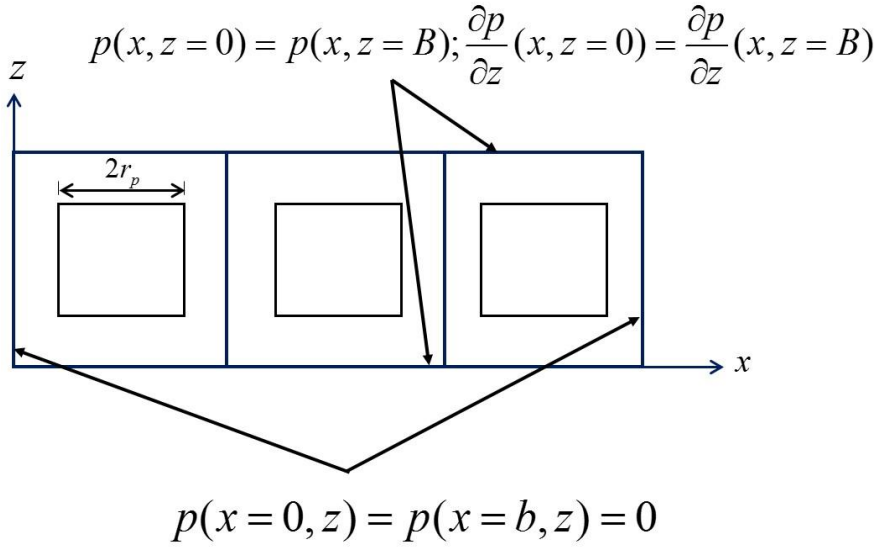

Fig.5.6 Boundary conditions used in the present analysis

5.1.5 Load support and friction equations

The total load support, W of the contact system, is the sum of the load carried by the fluid film (W_h) and the load carried by the asperities due to mechanical interactions (W_a), thus the total load support is given as:

$$W = W_h + W_a \tag{5.28}$$

Herein W_h and W_a can be calculated by the given equations:

$$W_h = \int_0^b \int_0^B p\,dx\,dz \tag{5.29}$$

$$W_a = \int_0^b \int_0^B p_{asp}\,dx\,dz \tag{5.30}$$

Friction coefficient (f) of the sliding pair can be calculated using the equation:

$$f = \frac{F}{W} \tag{5.31}$$

Where F is the total friction force, which is a combination of dissipative forces due to hydrodynamic and asperity interaction effects. The hydrodynamic friction force can be calculated from viscous shear stress generated in the fluid film. The asperity friction force on the other hand is obtained from simple Coulomb's law. The hydrodynamic friction force (F_h), the

asperity friction force (F_a) and total friction force (F) acting on the textured surface are calculated as:

$$F_h = \int_0^b \int_0^B \bar{\tau}\, dxdz \tag{5.32}$$

$$F_a = \int_0^b \int_0^B (C_f\, p_{asp}) dxdz \tag{5.33}$$

$$F = F_h + F_a \tag{5.34}$$

Where C_f is the boundary friction coefficient which is adopted as 0.12 in the present study based on the previous works [157-159].

5.2 Numerical solution

The modified Reynolds equation (5.13) is solved by using finite difference method. The set of algebraic equations are derived by finite difference method through the discretization of modified Reynolds equation. The discretized terms and detailed numerical solution procedure are provided in Appendix. The derived sets of algebraic equations are solved using point successive under relaxation method with Gauss- Seidel iterative scheme while satisfying appropriate boundary conditions. A mesh size of 150×100 (nx×nz) and pressure convergence of 10^{-5} is adopted based on the mesh convergence test, which is discussed in section 5.2.

The convergence criteria chosen for the generated fluid film pressure is:

$$\sum_{i}^{nx} \sum_{j}^{nz} \frac{\left|\overline{p_n}(i,j) - p_o(i,j)\right|}{p_n(i,j)} \leq 1\times10^{-5} \tag{5.35}$$

Where the subscripts n and o denote new and old iterations.

After calculating the fluid film pressure, the asperity pressure is determined using Eq. (5.21). Afterward, the fluid film pressure and asperity pressure are utilized to determine the total load support (W) given in Eq. (5.28). The convergence criteria chosen for the load balance is:

$$\frac{\left|W_1 - W\right|}{W_1} \leq 1\times10^{-3} \tag{5.36}$$

Where W_1 is the total load applied on the stationary surface. If the above criterion is not met, then the minimum fluid film thickness is adjusted as:

$$h_0^n = h_0^o + (W_1 - W)\,\mathrm{Rel} \tag{5.37}$$

In the present analysis, a relaxation factor Rel=0.1 is used. Once the load is balanced, the hydrodynamic pressure and asperity pressure determined at each node are used to calculate the friction coefficient using Eq. (5.31). The flow chart for the approach of numerical simulation to calculate the friction coefficient of the textured sliding contact is shown in Fig.5.7.

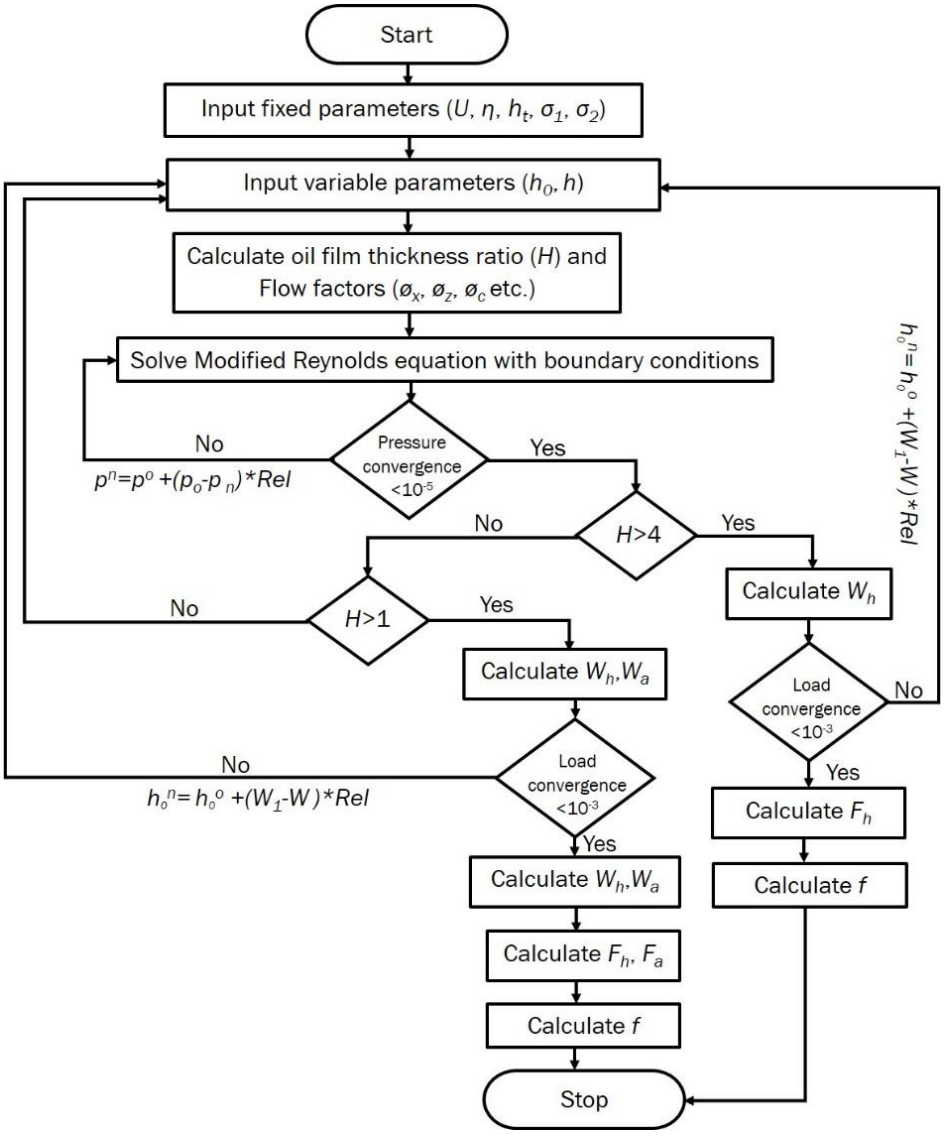

Fig. 5.7 Flow chart of numerical simulation approach

5.3 Grid convergence test

Before discussing the effect of the surface texture on the tribological characteristics of parallel sliding contact, a grid convergence test is performed to ensure that the result is independent of mesh size and pressure convergence value. Simulations are performed by considering a single square-shaped texture which is placed at the center of the unit cell having a texture area density and height of 0.1 and 10 µm, respectively. The grid points are varied in *x* and *z*-directions, respectively. Figure 5.8 shows the load support varying with mesh size for different pressure convergence values under pure hydrodynamic lubrication condition. As shown in Fig.5.8 (a), the load support is not deviating much, corresponds to *nx*=150 for a pressure convergence value of 10^{-5}. Similarly, the result of load support is close enough to accuracy value for *nz*=100 (see Fig.5.8 (b)). Therefore, a mesh size of 150×100/unit cell and convergence value of 10^{-5} are employed in the present study. The current mesh size yields results close enough to the accuracy desired.

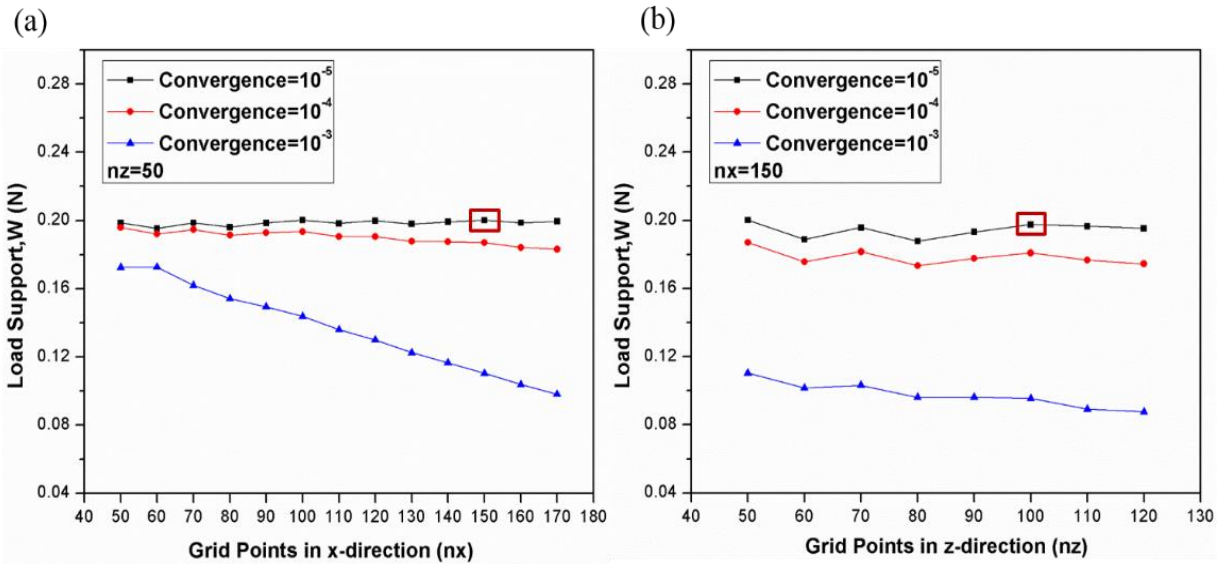

Fig.5.8 Grid convergence test results when different meshes are adopted

5.4 Validation of the present model

In order to validate the present model, a comparison of numerical results with Gu et al. [157] has been performed. The parameters considered for validation are presented in Table 5.1. Figure 5.9 represents the percentage of hydrodynamic load support for an un-textured piston ring surface under mixed lubrication regime. In the study by Gu et al. [157], the simulations were performed

with different crown heights by considering a one-dimensional average flow model with fully flooded inlet conditions. Based on their study, the hydrodynamic load support percentage of PR-CL sliding contact was more for higher crown heights when compared with lower crown height values. As can be seen from Fig.5.9, the present model is in good agreement with the model presented by Gu et al. [157].

Table 5.1 Parameters considered for the model validation

Parameter	**Value**
Elastic modulus of liner surface, E_1	120 GPa
Elastic modulus of ring surface, E_2	250 GPa
Minimum film thickness, h_0	1 µm
Composite roughness, σ	0.63 µm
Dynamic viscosity of fluid, μ	0.01 Pas
Sliding velocity, U	8 m/s
Height of the ring crown	0.01-8 µm

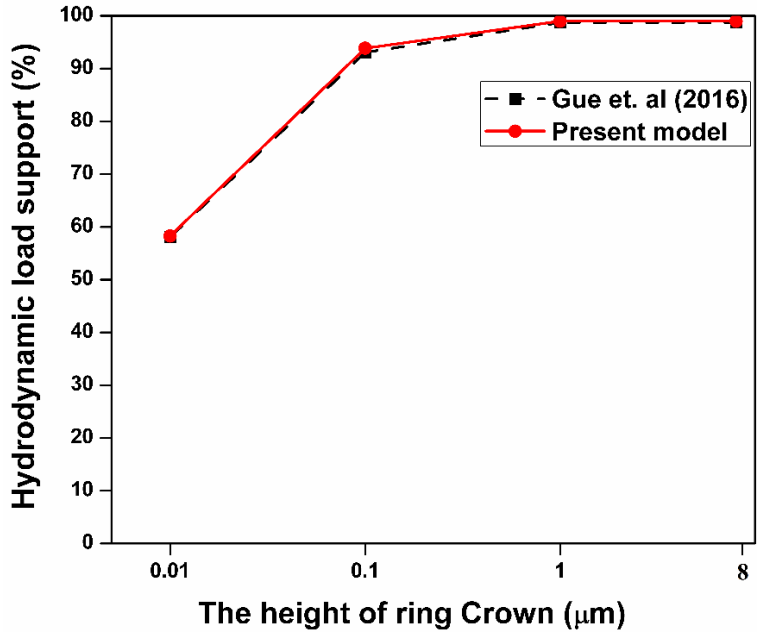

Fig.5.9 Validation of developed numerical model

5.5 Comparison between experimental and numerical results

In the present work, a theoretical model is developed to study the influence of positive texturing of parallel sliding contact. The numerical simulation results are compared with experimental results of square-shaped positive textures through the theoretical model developed. In the present analysis, a small fraction of textured surface is considered, shown in Fig.5.10. The present analysis considered the number of textures in the sliding direction as 3. The load acting on the considered fraction of textured surface is obtained as 0.5 N, corresponding to an experimental load of 5 N on the whole surface. The average roughness of the stationary surface (σ_1) and moving surface (σ_2) surfaces are measured as 0.417 µm and 0.351 µm, respectively. Therefore, the composite roughness ($\sigma = \sqrt{\sigma_1^2 + \sigma_2^2}$) is obtained as 0.546 µm. The parameters used in both numerical and experimental analysis are presented in Table 5.2.

Table 5.2 Parameters considered in experimental and numerical analysis

Parameter	**Value**
Elastic modulus of liner surface, E_1	215 GPa
Elastic modulus of ring surface, E_2	200 GPa
Poisson's ratio of liner surface,ν_1	0.3
Poisson's ratio of ring surface,ν_2	0.3
Composite roughness, σ	0.546 µm
Dynamic viscosity of fluid μ	0.121 Pa s
Sliding velocity, U	1.67 m/s
Axial width of the textured surface, b	3 mm
Area density of texture, S_p	0.1-0.5
Height of texture, h_t	10 µm
Normal load (experimental)	5 N
Normal load (numerical)	0.5 N

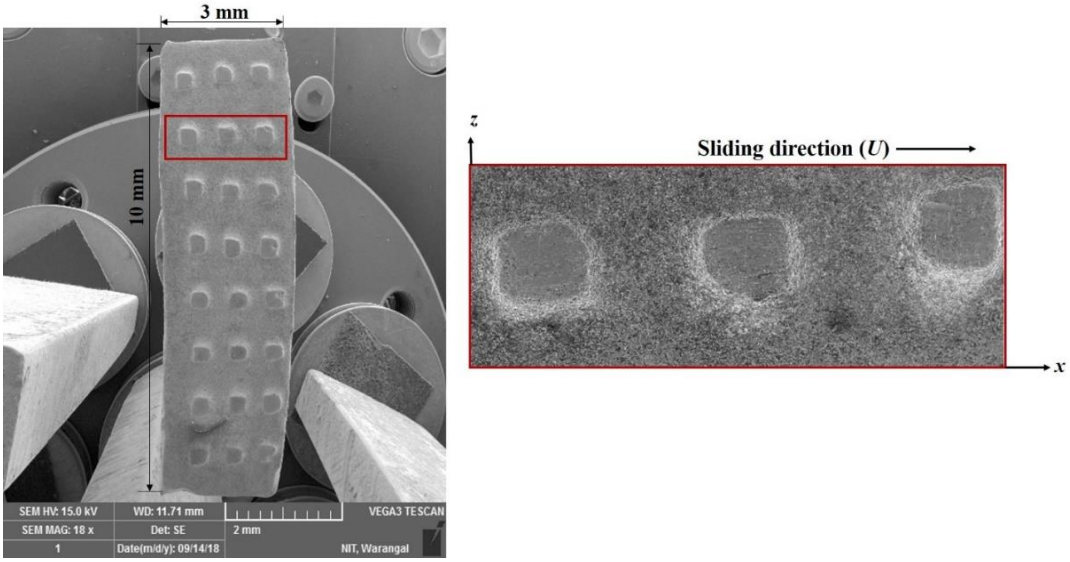

Fig.5.10 Textured surface considered for mathematical modelling

Simulations are performed by varying area density from 0.1 to 0.5 at a texture height of 10 µm, as shown in Fig.5.11. A similar trend of friction coefficient is observed in both experimental and numerical studies with the increase of area density. This result indicates that simulation results are qualitatively in agreement with experimental results for square-shaped textures. However, the deviation between the results, particularly at higher area densities, may be due to experimental and numerical errors.

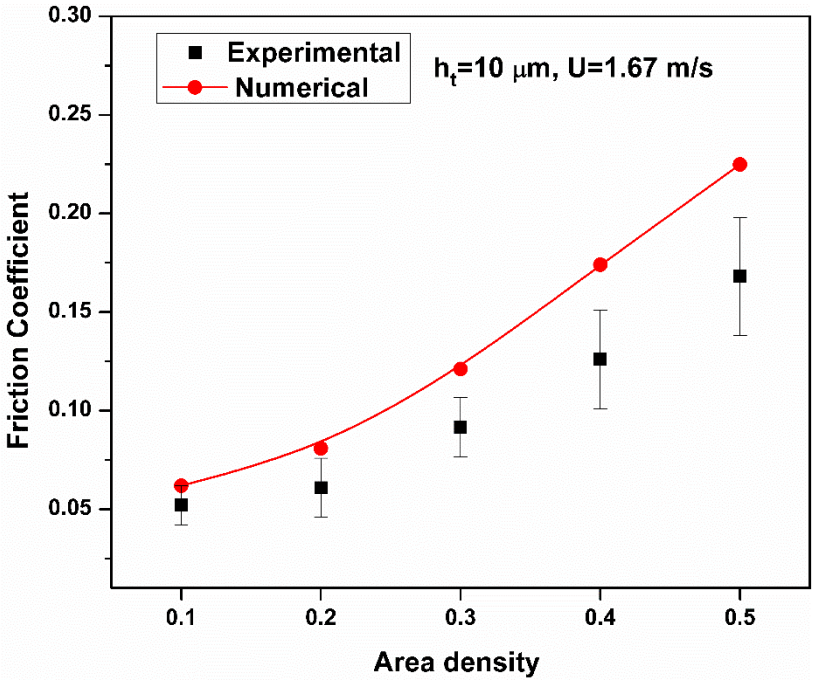

Fig.5.11 Comparison between experimental and numerical simulation results

5.6 Summary

In this chapter, a theoretical model has been developed for textured parallel sliding contact under a mixed lubrication regime. Well-known models such as Patir-Cheng model and Greenwood-Tripp model are solved for hydrodynamic pressure and asperity pressure, respectively. The effect of surface roughness on fluid flow is considered by taking into account corrective flow factors. The model developed is validated with simulation results in previously available literature. The numerical results are also compared with the experimental results of square shaped textures. The result indicates that the simulation results are qualitatively in agreement with experimental results. In the next chapter, the numerical model thus developed is used to investigate the effect of various aspects of surface texture such as texture shape, area density and height on the tribological performance of parallel sliding contact.

Chapter 6

Investigation of surface textured geometric parameters on tribological performance of parallel sliding contact

The numerical model developed in the previous chapter is utilized in the present chapter to optimize the geometric parameters of the surface texture for better tribological performance. This chapter emphasizes the impact of various texture geometric parameters such as texture shape, area density, and texture height on tribological performance parameters such as friction coefficient, hydrodynamic load support percentage and minimum film thickness. In addition, the effect of sliding velocity on tribological performance parameters for different texture shapes is discussed. The range of geometric parameters considered in the present numerical solution and the influence of texture shape, area density and texture height are explained in the following sub-sections.

6.1 Textured geometric parameters

Performing the experiments by varying different texture shapes with different area density and texture height is time consuming and costly. Within mind, a theoretical model is developed in order to perceive economic gain. Theory relating to the numerical modelling of mixed lubrication in textured parallel sliding contact by considering the effect of surface roughness on fluid flow, was developed in the previous chapter. In this chapter, the impact of various texture parameters on tribological performance is explored. The tribological performance is evaluated in terms of friction coefficient, hydrodynamic load support percentage, and minimum film thickness. It is desired to obtain lower values of friction coefficient and higher values of hydrodynamic load support percentage as well as minimum film thickness. In mixed lubrication regime, although the total load is supported by the lubricant and asperity contacts, it is beneficial to obtain more hydrodynamic load support than asperity load support in order to achieve better tribological performance. In the present analysis, hydrodynamic load support percentage is evaluated to characterize the hydrodynamic load support of textured sliding contact. The material

parameters, operating parameters and texture parameters considered in the numerical simulations are presented in Table 6.1.

Table 6.1 Parameters considered in numerical simulations

Parameter	**Value**
Material parameters	
Elastic modulus of moving plate, E_1	215 GPa
Elastic modulus of stationary strip, E_2	200 GPa
Poisson's ratio of moving plate, v_1	0.3
Poisson's ratio of stationary strip, v_2	0.3
Composite roughness, σ	0.546 µm
Texture parameters	
Area density, S_p	0.5-0.95
Texture height, h_t	2.5-20 µm
Operating parameters	
Dynamic viscosity of fluid μ	0.121 Pa s
Axial width of the textured surface, b	3 mm
Sliding velocity, U	0.1-2 m/s
Numerical load, W	0.5 N

In the present analysis, different texture shapes such as square, triangular, circular and elliptical are considered (see Fig.6.1). As various texture shapes are considered, half of the base length (r_p) can be different for different configurations which are calculated by equations given in Table 6.2. Herein, the possible range of area density (S_p) for various texture shapes is also presented. Accordingly, the textured surface is modelled for different texture shapes by varying area density.

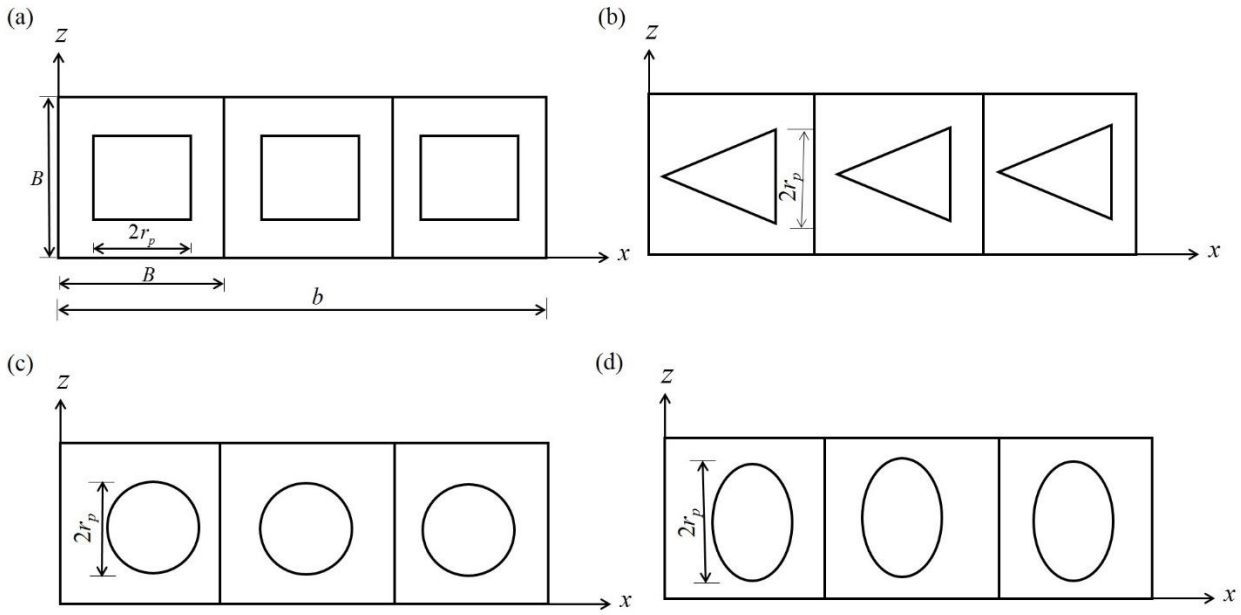

Fig.6.1 Modelled configurations with different texture shapes (a: square, b: triangular, c: circular, d: elliptical)

Table 6.2 Area density calculations for different texture shapes

Texture shape	A_t	A_u	r_p	Range of area density, S_p
1. Square 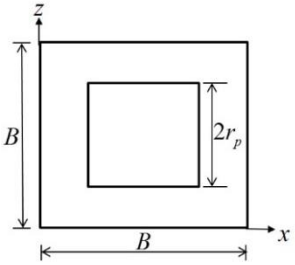	$(2r_p)^2$	B^2	$\sqrt{\frac{S_p B^2}{4}}$	0.01-0.95
2. Triangular 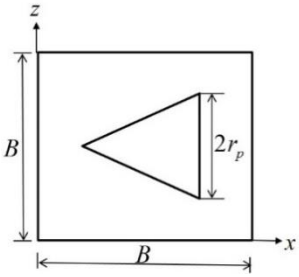	$\frac{\sqrt{3}}{4}(2r_p)^2$	B^2	$\sqrt{\frac{S_p B^2}{\sqrt{3}}}$	0.01-0.3

3. Circular 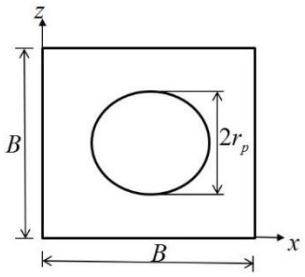	πr_p^2	B^2	$\sqrt{\frac{S_p B^2}{\pi}}$	0.01-0.75
4. Ellipse 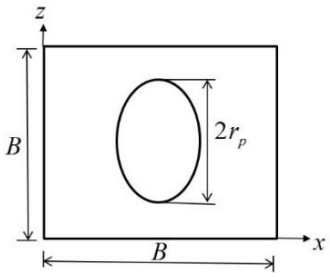	$2\pi r_p^2$	B^2	$\sqrt{\frac{S_p B^2}{2\pi}}$	0.01-0.35

Texture height is a crucial factor while designing textured surfaces. In the present analysis, the texture height is varied in a range of 2.5 μm-20 μm for all texture shapes. The increase of texture height beyond 20 μm may increase the asperity interactions more, which may produce detrimental hydrodynamic effects at the conjunction and therefore the chances of occurring boundary lubrication regime is more. The texture parameters along with operating conditions considered in the present analysis are presented in Table 6.1.

6.2 Influence of texture area density on tribological performance

The effect of texture area density for different texture shapes on friction coefficient at a constant texture height of 10 μm is presented in Fig.6.2. As can be seen from Fig.6.2, the friction coefficient is decreases initially as the area density increases from 0.05 to 0.1 for all texture shapes, and a further increase of area density increased friction coefficient. The experimental results of friction coefficient also showed a similar trend with the increase of area density (see Fig. 4.12). Furthermore, there exists an optimum area density that minimizes the friction coefficient. The optimum area density is found to be 0.1, for all texture shapes. Moreover, among the considered texture shapes, elliptical shape is most significant in reducing friction coefficient whereas circular shape generates high values of friction coefficient. Furthermore, at an area density of 0.1, the maximum percentage reduction in friction coefficient by elliptical textures

with respect to other shapes, i.e., circular, square and triangular are 26.5%, 19.1%, and 12.5%, respectively.

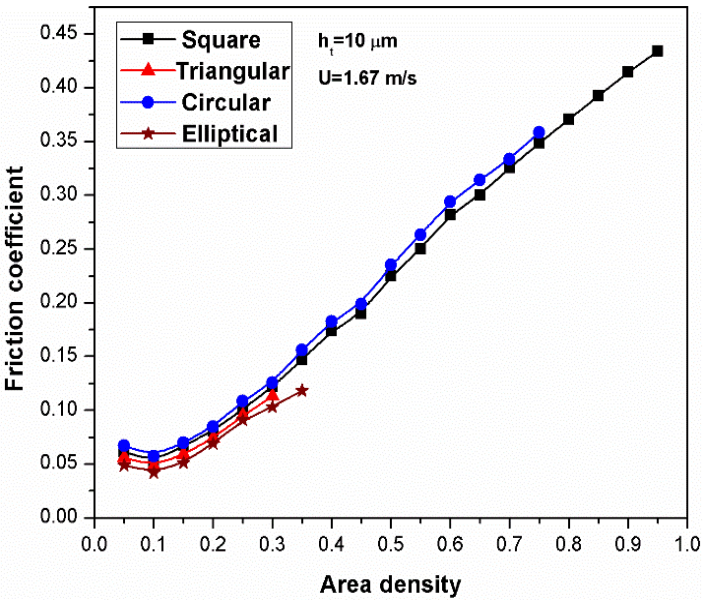

Fig.6.2 Influence of area density on friction coefficient

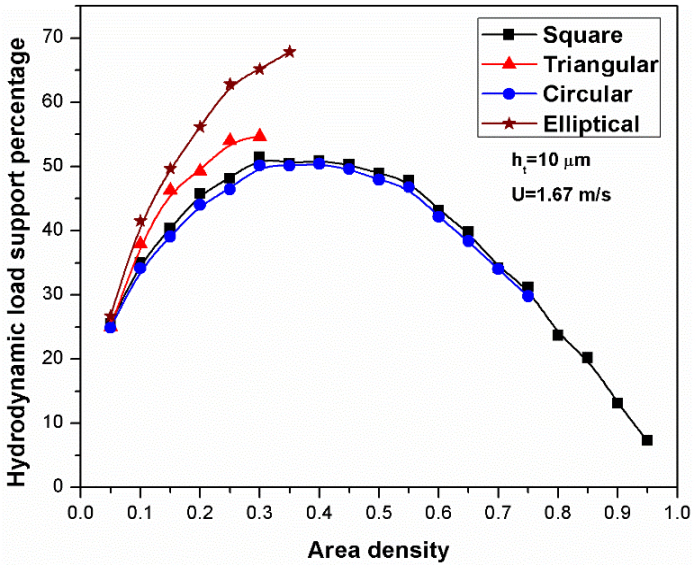

Fig.6.3 Influence of area density on hydrodynamic load support percentage

The impact of area density on hydrodynamic load support percentage is shown in Fig.6.3. As can be seen from Fig.6.3, the hydrodynamic load percentage increases with area densities in

the range of 0.05-0.45, any further increase in area density resulted in decrease of hydrodynamic load support percentage because of the domination of asperity interactions at higher area densities. It seems that among all the texture shapes, elliptical textures generate maximum hydrodynamic load support percentage. Because the pressure developed in elliptical textures occupy more area under the curve as shown in Fig 6.4 (d), due to which hydrodynamic load support percentage is maximum when compared to other texture shapes (as can be seen in Fig.6.4). It confirms that elliptical textures are superior in generating hydrodynamic pressure, thereby increasing the ability to support the total load.

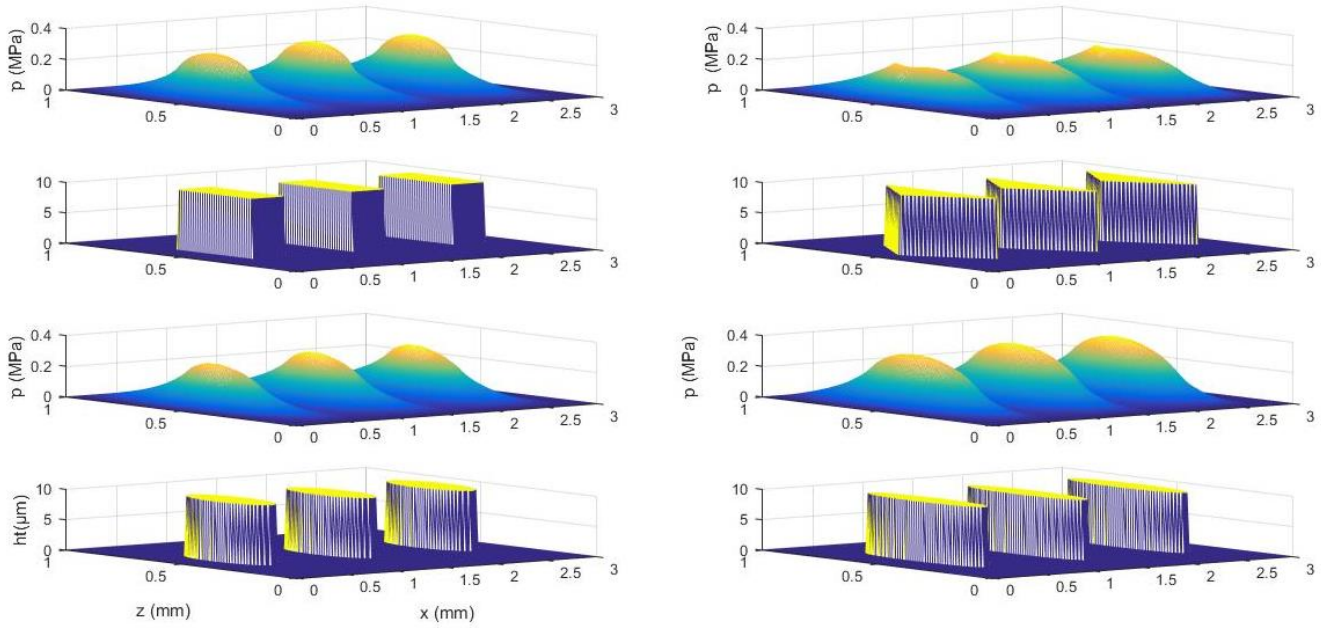

Fig.6.4 Hydrodynamic pressure distribution at S_p=0.1, h_t=10 μm and U=1.67 m/s: (a) square, (b) triangular, (c) circular, (d) elliptical

Figure 6.5 depicts the influence of area density on minimum film thickness for various texture shapes. As can be seen, the minimum film thickness increases initially with the increase of area density from 0.05-0.5, and a further increase of area density does not affect minimum film thickness. Moreover, elliptical shape exhibits superior performance in increasing minimum film thickness compared to other shapes.

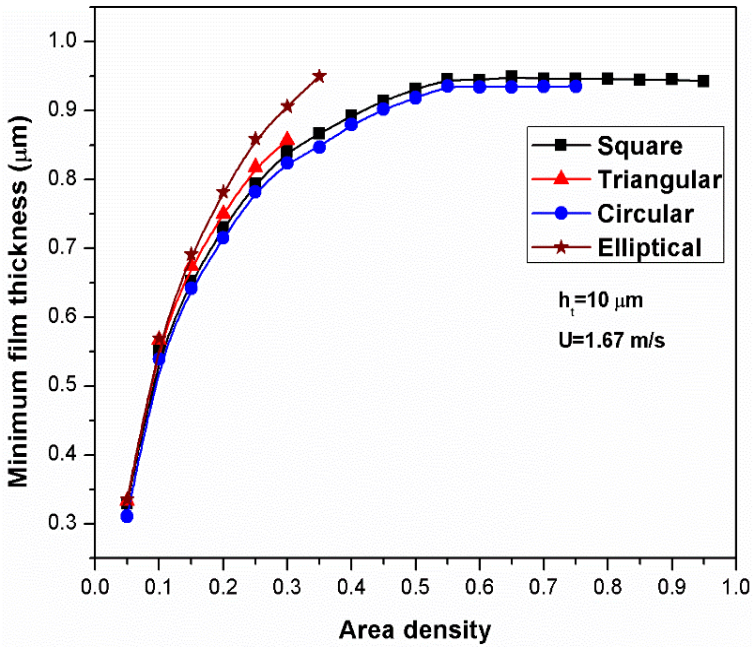

Fig.6.5 Influence of area density on minimum film thickness

6.3 Influence of texture height on tribological performance

The impact of texture height on tribological performance parameters for various texture shapes is explored with the help of Fig.6.6. It can be seen from Fig.6.6 that significant changes in friction coefficient are observed as the texture height changes from 2.5 μm to 20 μm in a step size of 2.5 μm. The increase of texture height from 2.5 to 5 μm results in a decrease of friction coefficient for all textured surfaces of different shapes. A further increase in texture height resulted in increased friction coefficient. The results confirm that lower texture heights proved superior in reducing friction coefficient, in particular for an optimum value of 5 μm, where all texture shapes show the minimum friction coefficient. In agreement with previous results [100], the shallower textures show beneficial effects in reducing the friction coefficient. The numerical results presented here are also in line with the experimental results, where larger values of texture heights generated more friction coefficients (see Fig. 4.15). This is because smaller texture heights generate additional hydrodynamic pressures compared to considerably larger texture heights for all texture shapes. Moreover, it is observed that at a texture height of 5 μm, the elliptical textures decreased the friction by 18.3%, 13%, and 4.7% when compared with circular, square and triangular textures respectively.

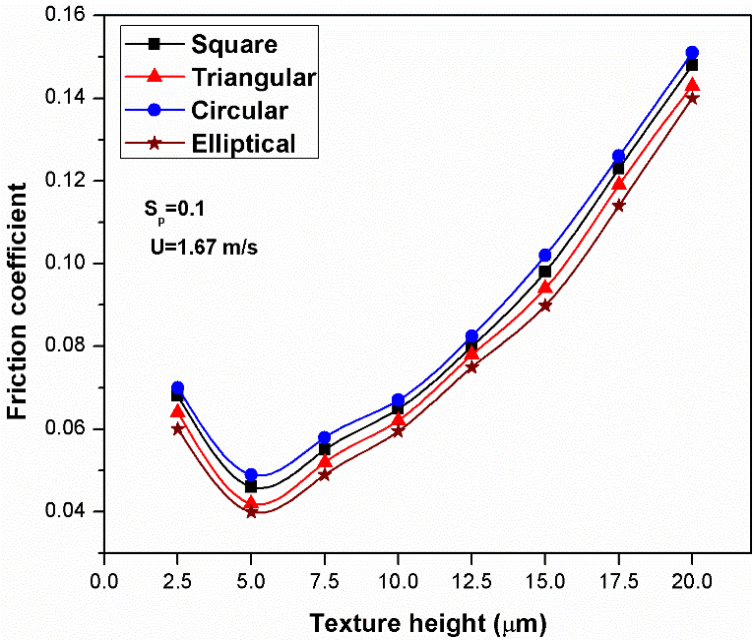

Fig.6.6 Influence of texture height on friction coefficient

Figure 6.7 shows the hydrodynamic load support percentage as a function of texture height for various texture shapes. It is observed that increase of texture height reduces the hydrodynamic load support percentage for all texture shapes. The higher texture heights shows more domination of asperities interaction than lower texture heights. As can be seen in Fig.6.8, the elliptical texture shape at lower texture height (h_t=5 μm) generates more hydrodynamic pressure than higher texture height (h_t=20 μm). Moreover, similar results of hydrodynamic pressure are observed for all the remaining texture shapes with variation of magnitudes. As for the texture shape's concern, the elliptical shape exhibit superior hydrodynamic load carrying performance, while circular shape generate lowest hydrodynamic load carrying performance when compared with other texture shapes.

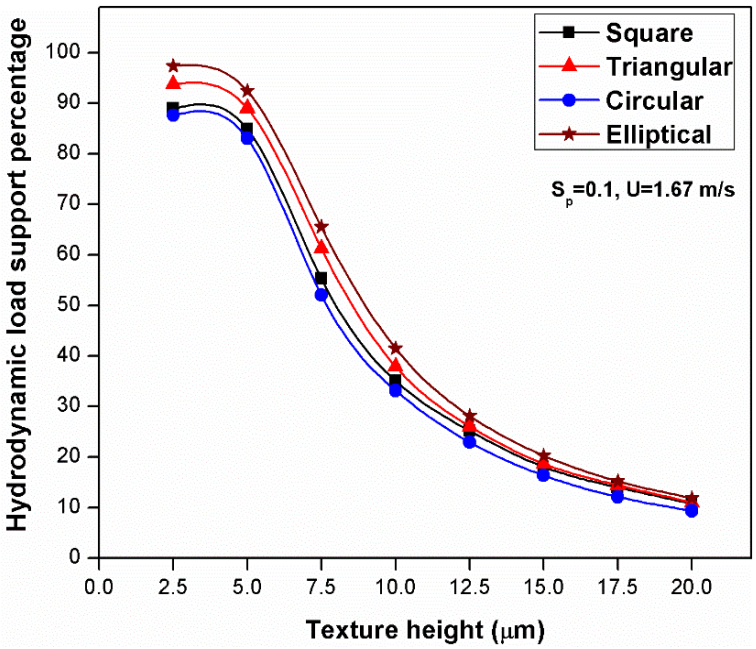

Fig.6.7 Influence of texture height on hydrodynamic load support percentage

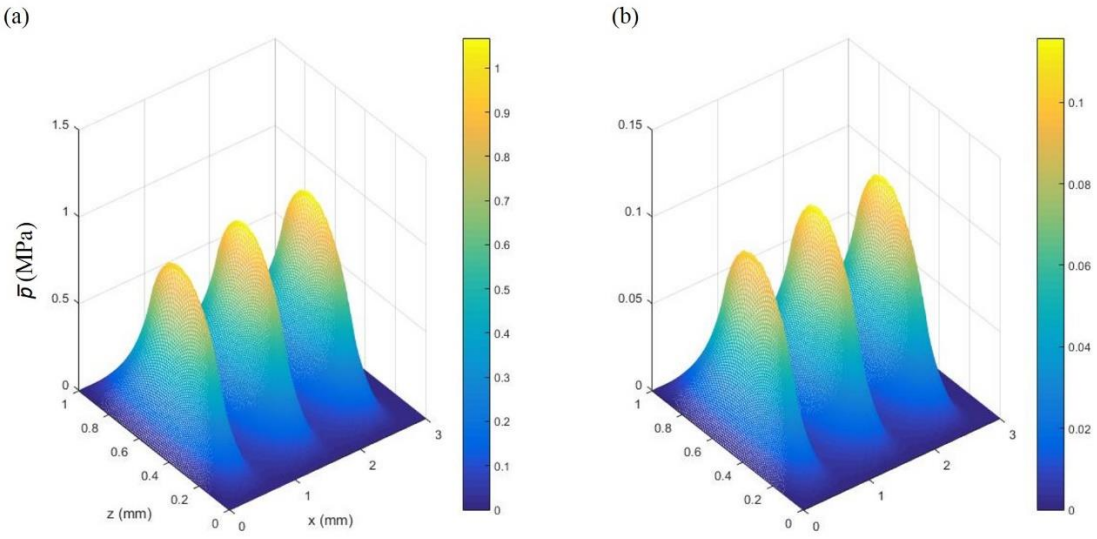

Fig.6.8 Hydrodynamic pressure profiles for elliptical shape at S_p=0.1, U=1.67 m/s: (a) h_t=5 µm, (b) h_t=20 µm

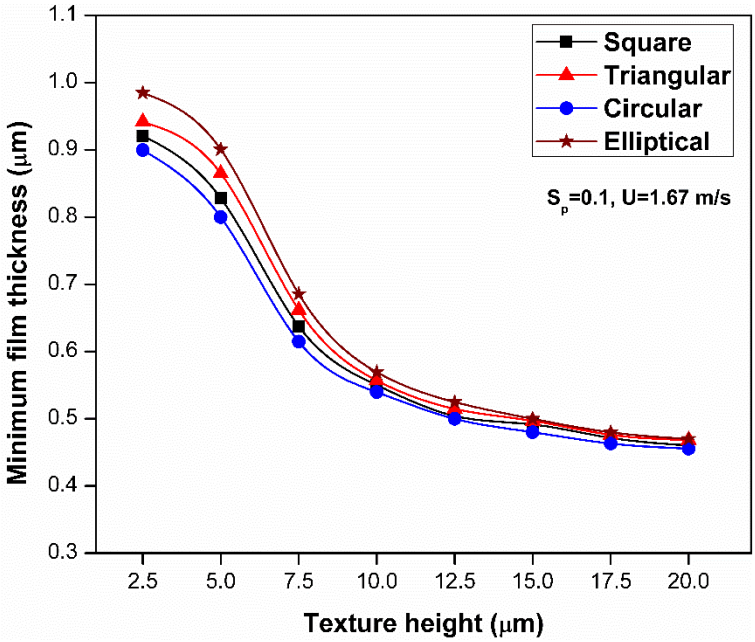

Fig.6.9 Influence of texture height on minimum film thickness

Figure 6.9 depicts the impact of texture height on minimum film thickness for different texture shapes. It is observed that considerably lower texture heights are better in generating minimum film thickness than higher texture heights. Among all texture shapes, the minimum film thickness is more for elliptical shape, while the circular shape exhibit minimum at all texture heights. However, at higher texture heights the effect of texture shape on minimum film thickness is limited compared to lower texture heights. Because, the variation in percentage of hydrodynamic load support is lower for higher texture heights as depicted in Fig.6.7.

6.4 Influence of sliding velocity on tribological performance

The variation of friction coefficient as a function of sliding velocity for various texture shapes is shown in Fig.6.10. The result exhibits that increase of sliding velocity from 0.1 to 0.5 m/s decreased the friction coefficient and a further increase of sliding velocity resulted in increased friction coefficient for all texture shapes. From the obtained results, it is observed asperity pressure is more predominated due to which higher friction coefficient is generated for sliding velocities less than 0.5 m/s. In addition, a sudden drop in the friction coefficient when the sliding velocity increased from 0.1 m/s to 0.5 m/s is due to generation of additional hydrodynamic load support percentage at a sliding velocity 0.5 m/s when compared with a sliding velocity of 0.1

m/s, as shown in Fig.6.11. Furthermore, for sliding velocities greater than 0.5 m/s, the hydrodynamic pressure is more predominant and increased the friction coefficient gradually when the sliding velocity varied in a range of 0.5-2 m/s. This may be due to additional viscous shear forces which raised the friction coefficient more in the case higher sliding velocities than lower velocities. For all the considered texture shapes, the maximum friction reduction is achieved for a sliding velocity of 0.5 m/s. As for texture shape's concern, elliptical shape exhibits superior friction reduction, while circular shape generates higher friction coefficient values among all considered shapes. Furthermore, it is observed that at a sliding velocity of 0.5 m/s, the elliptical shape of textures reduced the friction coefficient by 26.8%, 19.8%, and 12% compared to circular, square and triangular shapes, respectively.

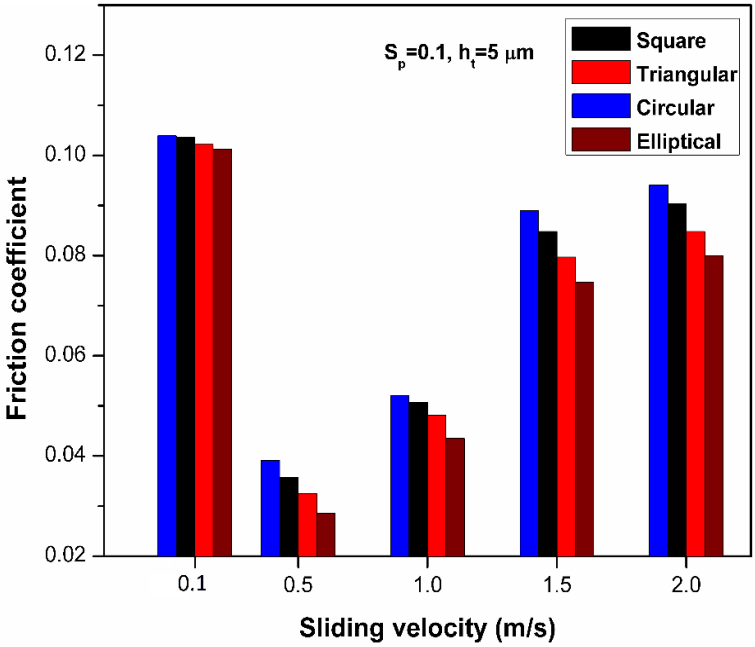

Fig.6.10 Friction coefficient as a function of sliding velocity for different texture shapes

The variation of hydrodynamic load support percentage with sliding velocity for different texture shapes is shown in Fig 6.11. The result depicts that increase of sliding velocity increases the hydrodynamic load support percentage for all texture shapes. Furthermore, at lower velocities the hydrodynamic load support is lower due to more interaction of asperities between the sliding surfaces. However, higher velocities show superiority in generating hydrodynamic load support percentage than lower velocities. The hydrodynamic pressure profiles for elliptical textured shape are depicted in Fig.6.12. As can be seen, at higher velocity (U=2 m/s), the area under the

curve is more than the lower velocity (U=0.5 m/s). A similar trend of results are obtained for all other texture shapes with the variation of sliding velocity. Moreover, elliptical textures exhibit better hydrodynamic load carrying performance than all other considered texture shapes.

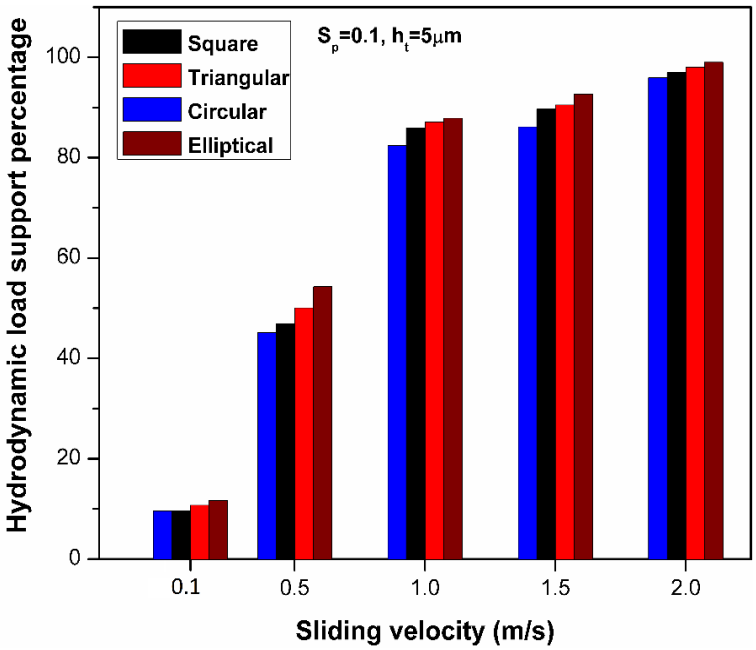

Fig.6.11 Hydrodynamic load support percentage vs sliding velocity

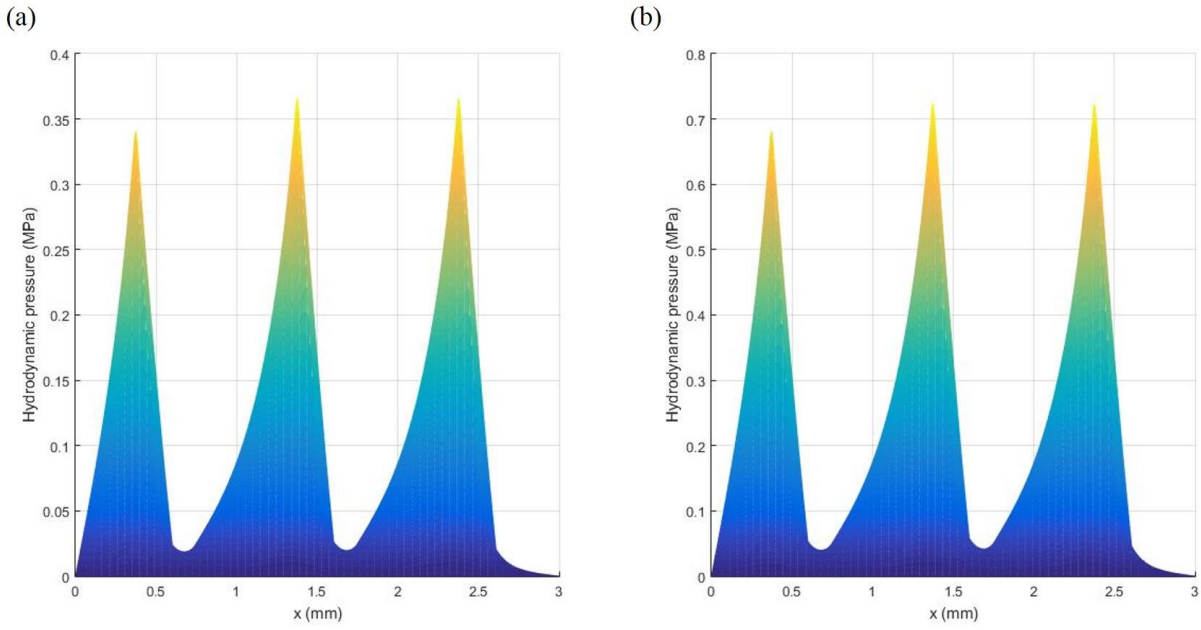

Fig.6.12 Hydrodynamic pressure profiles for elliptical shape at S_p=0.1, h_t=5 µm: (a) U=0.5 m/s, (b) U=2 m/s

The impact of sliding velocity on minimum film thickness for different texture shapes is depicted in Fig.6.13. It can be seen that higher velocities exhibit greater values of minimum film thickness than lower velocities. Furthermore, elliptical textures showed better performance in generating additional minimum film thickness, while circular textures generate lowest minimum film thickness among considered shapes. However, at lower velocities, the beneficial effect of texture shape is limited than at higher velocities.

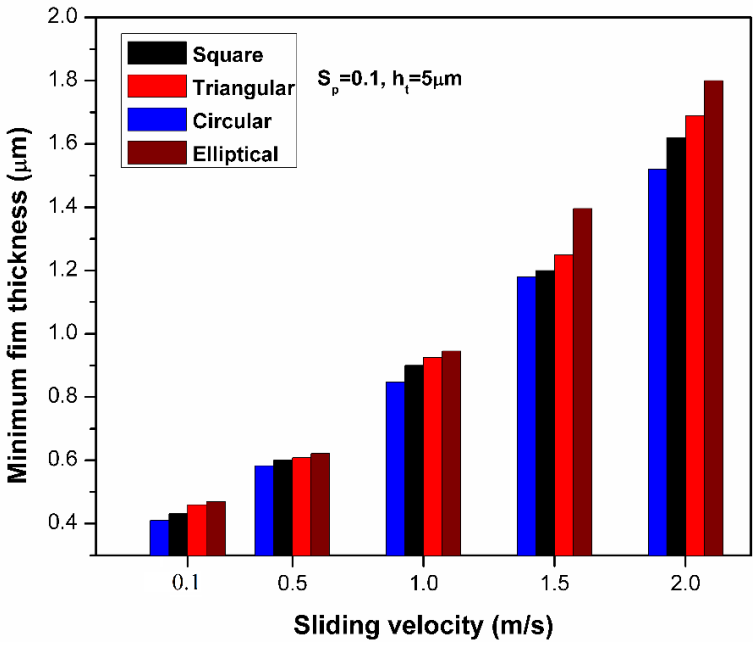

Fig.6.13 Minimum film thickness vs sliding velocity

The numerical simulations reveal that optimum results are obtained for elliptical shape at an area density of 0.1, texture height of 5 μm, and a sliding velocity of 0.5 m/s. The simulations are also performed for un-textured surfaces at these optimal conditions and compared with the results of textured surfaces. The friction coefficient results of both textured and un-textured surfaces are shown in Fig. 6.14. The textured surfaces reduced the friction coefficient by 87% compared with the un-textured case.

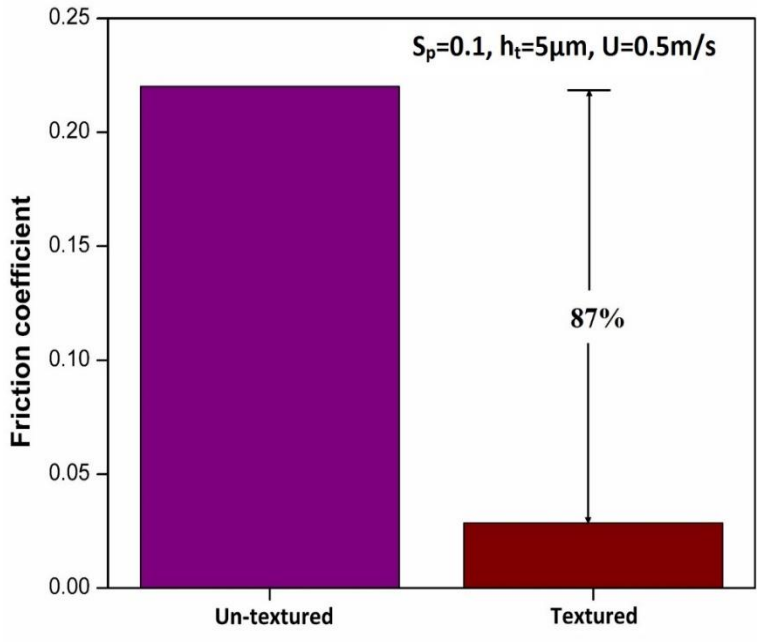

Fig.6.14 Comparison of un-textured and textured surfaces

6.5 Summary

In this chapter, the effect of various texture geometric parameters was investigated for the improvement in tribological performance of the parallel sliding contact. The texture area density of 0.1 and texture height of 5 µm exhibit better tribological behavior for all considered texture shapes. It is observed that for all the textured surfaces, the sliding velocity of 0.5 m/s shows excellent frictional resistance. Furthermore, texture shape is crucial in improving the tribological performance of the sliding contact. In this regard, the elliptical texture shape has shown better improvement in tribological performance of parallel sliding contact compared with other texture shapes. Moreover, the elliptical textured surfaces reduced the friction coefficient to a maximum of 87% compared to un-textured surface.

Chapter 7

Conclusions and future scope

The present dissertation focused on the experimental and numerical investigation on the effect of positive surface textures on tribological behavior of parallel sliding contact. Chemical etching method was chosen to fabricate square-shaped positive textures of varying texture area density and height. After the fabrication of surface texture, different lubricants were tested in order to select the appropriate lubricant. Furthermore, the textured surfaces are tested for frictional and wear performance between the parallel sliding surfaces with continuous supply of the selected lubricant.

Performing the experiments with different texture shapes for different texture area density and height is time consuming and costly. In this context, a theoretical model was developed to investigate the effects of texture shape, area density and height on tribological performance parameters. In modeling, the modified Reynolds equation (Patir-Cheng flow model) and asperity contact model (Greenwood-Tripp model) were solved for hydrodynamic and asperity pressures, respectively. The developed numerical model was quantitatively validated with previously available result and qualitatively with the present experimental results. Later, the numerical analysis was extended to study the effect of various texture aspects such as shape, area density and height on the tribological performance of parallel sliding contact.

7.1 Conclusions

From the experimental and numerical studies performed, the conclusions of the present work can be summarized as follows:

- A new masking material such as carbon black was successfully used for the fabrication of surface textures by using chemical etching process. Despite previous etching methods, the method proposed in the present work is simple and well suited for laboratory experiments.

- The experimental results for square-shaped textures exhibited minimum friction coefficient and wear rate at an area density and a texture height of 0.1 and 10 μm, respectively.
- The maximum reduction in friction coefficient and wear rate was observed to be 85.4% and 88.9%, respectively when compared with un-textured surface.
- The numerical simulation results depicted lower value of friction coefficient at an area density of 0.1 and a texture height of 5 μm for all the considered texture shapes.
- Sliding velocity showed a prominent effect on tribological performance of the textured parallel sliding contact. Among all the considered sliding velocities, the sliding velocity of 0.5 m/s exhibited better tribological performance parameters for all texture shapes.
- Texture shape has shown significant impact on the tribological performance of parallel sliding contact. In this regard, elliptical shape of texture exhibited superior anti frictional performance as compared to other shapes.
- At an area density of 0.1, texture height of 5 μm, sliding velocity of 0.5 m/s and elliptical shape of texture exhibited maximum friction reduction of 87% compared to un-textured case.

On the whole, reduction in friction and wear can be achieved by introducing positive surface textures on the interacting parallel sliding surfaces. The improvement in lubrication performance can be attained by varying various aspects of surface texture such as shape, area density and height. In future, this makes surface texturing vital and prominent technique to use in industrial applications. In addition, the present work will provide a basis for better understanding of lubrication in textured parallel sliding surfaces.

7.2 Future scope

Based on the present work, the following recommendations have been made for future scope of the work in the research area.

- Fabrication of minimum size of texture in the present method is 350 μm. In future, the study can be further extended to produce lower texture sizes than 350 μm by modifying the present method.

- Numerical studies can also be extended by considering different aspects of surface textures such as varying texture distribution and orientation.
- The developed theoretical model can be modified further by incorporating different aspects like fluid inertia effect, squeeze effect, temperature effect and non-Newtonian fluid effect.

References

[1] Vilhena, L.M., Podgornik, B., Vižintin, J. and Možina, J., 2011. Influence of texturing parameters and contact conditions on tribological behaviour of laser textured surfaces. Meccanica, 46(3), pp.567-575.

[2] Wang, J., Zhou, J., Zhu, S.S. and Zhang, J.S., 2017. Friction properties of groove texture on Cr12MoV surface. Journal of Central South University, 24(2), pp.303-310.

[3] Jiang, S.W., Jiang, B., Li, Y., Li, Y.R., Yin, G.F. and Zheng, C.Q., 2004. Friction and wear study of diamond-like carbon gradient coatings on Ti6Al4V substrate prepared by plasma source ion implant-ion beam enhanced deposition. Applied Surface Science, 236(1-4), pp.285-291.

[4] Martins, R.C., Moura, P.S. and Seabra, J.O., 2006. MoS2/Ti low-friction coating for gears. Tribology International, 39(12), pp.1686-1697.

[5] Garrido, A.H., González, R., Cadenas, M. and Battez, A.H., 2011. Tribological behavior of laser-textured NiCrBSi coatings. Wear, 271(5-6), pp.925-933.

[6] He, D., Zheng, S., Pu, J., Zhang, G. and Hu, L., 2015. Improving tribological properties of titanium alloys by combining laser surface texturing and diamond-like carbon film. Tribology international, 82, pp.20-27.

[7] Hu, T., Zhang, Y. and Hu, L., 2012. Tribological investigation of MoS2 coatings deposited on the laser textured surface. Wear, 278, pp.77-82.

[8] Ye, Y., Wang, C., Chen, H., Wang, Y., Zhao, W. and Mu, Y., 2017. Micro/Nanotexture Design for Improving Tribological Properties of Cr/GLC Films in Seawater. Tribology Transactions, 60(1), pp.95-105.

[9] Zeng, Q., Qin, Y., Chang, W. and Luo, X., 2018. Correlating and evaluating the functionality-related properties with surface texture parameters and specific characteristics of machined components. International Journal of Mechanical Sciences, 149, pp.62-72.

[10] Podgornik, B., Vilhena, L.M., Sedlaček, M., Rek, Z. and Žun, I., 2012. Effectiveness and design of surface texturing for different lubrication regimes. Meccanica, 47(7), pp.1613-1622.

[11] Rashwan, O., 2013. Micro Surface Texturing for Friction Control. PhD thesis, University of Windsor.

[12] Wahl, R., Schneider, J. and Gumbsch, P., 2012. Influence of the real geometry of the protrusions in micro textured surfaces on frictional behaviour. Tribology letters, 47(3), pp.447-453.

[13] Wakuda, M., Yamauchi, Y., Kanzaki, S. and Yasuda, Y., 2003. Effect of surface texturing on friction reduction between ceramic and steel materials under lubricated sliding contact. Wear, 254(3-4), pp.356-363.

[14] Pettersson, U. and Jacobson, S., 2004. Friction and wear properties of micro textured DLC coated surfaces in boundary lubricated sliding. Tribology letters, 17(3), pp.553-559.

[15] Kortikar, S.N., Stephens, L.S., Hadinata, P.C. and Siripuram, R.B., 2003. Manufacturing of microasperities on thrust surfaces using ultraviolet photolithography. In Proceedings of ASPE Winter Topical Meeting (pp. 148-154). Raleigh, NC.

[16] Meng, F., Davis, T., Cao, J., Wang, Q.J., Hua, D. and Liu, J., 2010. Study on effect of dimples on friction of parallel surfaces under different sliding conditions. Applied surface science, 256(9), pp.2863-2875.

[17] Yu, H., Wang, X. and Zhou, F., 2010. Geometric shape effects of surface texture on the generation of hydrodynamic pressure between conformal contacting surfaces. Tribology Letters, 37(2), pp.123-130.

[18] Gropper, D., Wang, L. and Harvey, T.J., 2016. Hydrodynamic lubrication of textured surfaces: A review of modeling techniques and key findings. Tribology International, 94, pp.509-529.

[19] Hamilton, D.B., Walowit, J.A. and Allen, C.M., 1966. A theory of lubrication by micro irregularities. Transactions of ASME, Journal of Basic Engineering, pp.177-185.

[20] Anno, J.N., Walowit, J.A. and Allen, C.M., 1968. Microasperity lubrication. Journal of Lubrication Technology, 90(2), pp.351-355.

[21] Anno, J.N., Walowit, J.A. and Allen, C.M., 1969. Load support and leakage from microasperity-lubricated face seals. Journal of Lubrication Technology, 91(4), pp.726-731.

[22] Etsion, I. and Burstein, L., 1996. A model for mechanical seals with regular microsurface structure. Tribology Transactions, 39(3), pp.677-683.

[23] Etsion, I., Kligerman, Y. and Halperin, G., 1999. Analytical and experimental investigation of laser-textured mechanical seal faces. Tribology Transactions, 42(3), pp.511-516.

[24] Wong, V., Tian, T., Smedley, G., Moughon, L., Takata, R. and Jocsak, J., 2006. Low-engine-friction technology for advanced natural-gas reciprocating engines. Massachusetts Institute of Technology.

[25] Etsion, I., 2005. State of the art in laser surface texturing. Journal of tribology, 127(1), pp.248-253.

[26] Vermeulen, M. and Scheers, J., 2001. Micro-hydrodynamic effects in EBT textured steel sheet. International Journal of Machine Tools and Manufacture, 41(13-14), pp.1941-1951.

[27] Wagner, K., Völkl, R. and Engel, U., 2008. Tool life enhancement in cold forging by locally optimized surfaces. Journal of Materials Processing Technology, 201(1-3), pp.2-8.

[28] Ike, H., Tsuji, K. and Takase, M., 2002. In situ observation of a rolling interface and modeling of the surface texturing of rolled sheets. Wear, 252(1-2), pp.48-62.

[29] Sawant, M.S., Jain, N.K. and Palani, I.A., 2018. Influence of dimple and spot-texturing of HSS cutting tool on machining of Ti-6Al-4V. Journal of Materials Processing Technology.

[30] Obikawa, T., Kamio, A., Takaoka, H. and Osada, A., 2011. Micro-texture at the coated tool face for high performance cutting. International Journal of Machine Tools and Manufacture, 51(12), pp.966-972.

[31] Etsion, I. and Halperin, G., 2002. A laser surface textured hydrostatic mechanical seal. Tribology Transactions, 45(3), pp.430-434.

[32] Yagi, K., Takedomi, W., Tanaka, H. and Sugimura, J., 2008. Improvement of lubrication performance by micro pit surfaces. Tribology Online, 3(5), pp.285-288.

[33] Wan, Y. and Xiong, D.S., 2008. The effect of laser surface texturing on frictional performance of face seal. Journal of Materials Processing Technology, 197(1-3), pp.96-100.

[34] Yu, X.Q., He, S. and Cai, R.L., 2002. Frictional characteristics of mechanical seals with a laser-textured seal face. Journal of Materials Processing Technology, 129(1-3), pp.463-466.

[35] Brizmer, V., Kligerman, Y. and Etsion, I., 2003. A laser surface textured parallel thrust bearing. Tribology Transactions, 46(3), pp.397-403.

[36] Fowell, M.T., Medina, S., Olver, A.V., Spikes, H.A. and Pegg, I.G., 2012. Parametric study of texturing in convergent bearings. Tribology International, 52, pp.7-16.

[37] Lu, X. and Khonsari, M.M., 2007. An experimental investigation of dimple effect on the stribeck curve of journal bearings. Tribology letters, 27(2), p.169.

[38] Tala-Ighil, N., Maspeyrot, P., Fillon, M. and Bounif, A., 2007. Effects of surface texture on journal-bearing characteristics under steady-state operating conditions. Proceedings of the Institution of Mechanical Engineers, Part J: Journal of Engineering Tribology, 221(6), pp.623-633.

[39] Wang, X., Kato, K., Adachi, K. and Aizawa, K., 2003. Loads carrying capacity map for the surface texture design of SiC thrust bearing sliding in water. Tribology International, 36(3), pp.189-197.

[40] Akbarzadeh, A. and Khonsari, M.M., 2018. Effect of untampered plasma coating and surface texturing on friction and running-in behavior of piston rings. Coatings, 8(3), p.110.

[41] Grabon, W., Pawlus, P., Wos, S., Koszela, W. and Wieczorowski, M., 2018. Evolutions of cylinder liner surface texture and tribological performance of piston ring-liner assembly. Tribology International, 127, pp.545-556.

[42] Morris, N., Rahmani, R., Rahnejat, H., King, P.D. and Howell-Smith, S., 2016. A numerical model to study the role of surface textures at top dead center reversal in the piston ring to cylinder liner contact. Journal of Tribology, 138(2), p.021703.

[43] Grabon, W., Pawlus, P., Wos, S., Koszela, W. and Wieczorowski, M., 2017. Effects of honed cylinder liner surface texture on tribological properties of piston ring-liner assembly in short time tests. Tribology International, 113, pp.137-148.

[44] Borghi, A., Gualtieri, E., Marchetto, D., Moretti, L. and Valeri, S., 2008. Tribological effects of surface texturing on nitriding steel for high-performance engine applications. Wear, 265(7-8), pp.1046-1051.

[45] Killian, M., 2009. Efficiency Improvement through Reduction in Friction and Wear in Powertrain Systems. Eaton Corporation.

[46] S.-C. Vlădescu, A. Olver, I. Pegg e T. Reddyhoff, 2016. Combined friction and wear reduction in a reciprocating contact through laser surface texturing. Wear 358, pp.51-61.

[47] Vlădescu, S.C., Ciniero, A., Tufail, K., Gangopadhyay, A. and Reddyhoff, T., 2017. Looking into a laser textured piston ring-liner contact. Tribology International, 115, pp.140-153.

[48] Yu, X.Q., Liu, M.H., Wang, Z.H., Peng, P.Y. and Cai, R.L., 2006. Experimental investigation on friction performance of mechanical seals with a laser-textured seal face. In Materials Science Forum (Vol. 532, pp. 81-84). Trans Tech Publications.

[49] Blatter, A., Maillat, M., Pimenov, S.M., Shafeev, G.A., Simakin, A.V. and Loubnin, E.N., 1999. Lubricated sliding performance of laser-patterned sapphire. Wear, 232(2), pp.226-230.

[50] Křupka, I., Vrbka, M. and Hartl, M., 2008. Effect of surface texturing on mixed lubricated non-conformal contacts. Tribology International, 41(11), pp.1063-1073.

[51] Zhang, H., Zhang, D.Y., Hua, M., Dong, G.N. and Chin, K.S., 2014. A study on the tribological behavior of surface texturing on babbitt alloy under mixed or starved lubrication. Tribology Letters, 56(2), pp.305-315.

[52] Guangneng, D., Junfeng, Z., Huabin, Y., Zhongrong, Z. and Youbai, X., 2008. Study on tribological properties of pseudoelastic Ti-Ni alloys with laser surface micro-convexes. RARE METAL MATERIALS AND ENGINEERING, 37(3), pp.444-447.

[53] Zum Gahr, K.H., Mathieu, M. and Brylka, B., 2007. Friction control by surface engineering of ceramic sliding pairs in water. Wear, 263(7-12), pp.920-929.

[54] Tauviqirrahman, M., Muchammad, Jamari and Schipper, D.J., 2014. Numerical study of the load-carrying capacity of lubricated parallel sliding textured surfaces including wall slip. Tribology transactions, 57(1), pp.134-145.

[55] Sagbas, B. and Durakbasa, M.N., 2013. Effect of surface patterning on frictional heating of vitamin E blended UHMWPE. Wear, 303(1), pp.313-320.

[56] Tomanik, E., 2013. Modelling the hydrodynamic support of cylinder bore and piston rings with laser textured surfaces. Tribology international, 59, pp.90-96.

[57] Scaraggi, M., 2012. Textured surface hydrodynamic lubrication: Discussion. Tribology Letters, 48(3), pp.375-391.

[58] Saka, N., Tian, H. and Suh, N.P., 1989. Boundary lubrication of undulated metal surfaces at elevated temperatures. Tribology Transactions, 32(3), pp.389-395.

[59] Suh, N.P., Mosleh, M. and Howard, P.S., 1994. Control of friction. Wear, 175(1-2), pp.151-158.

[60] Nosonovsky, M. and Bhushan, B., 2007. Multiscale friction mechanisms and hierarchical surfaces in nano-and bio-tribology. Materials Science and Engineering: R: Reports, 58(3-5), pp.162-193.

[61] Voevodin, A.A. and Zabinski, J.S., 2006. Laser surface texturing for adaptive solid lubrication. Wear, 261(11-12), pp.1285-1292.

[62] Pettersson, U. and Jacobson, S., 2003. Influence of surface texture on boundary lubricated sliding contacts. Tribology International, 36(11), pp.857-864.

[63] Lin, N., Li, D., Zou, J., Xie, R., Wang, Z. and Tang, B., 2018. Surface texture-based surface treatments on Ti6Al4V titanium alloys for tribological and biological applications: A mini review. Materials, 11(4), p.487.

[64] Hupp, S.J., 2004. A tribological study of the interaction between surface micro texturing and viscoelastic lubricants (Doctoral dissertation, Massachusetts Institute of Technology).

[65] Wang, X., Kato, K., Adachi, K. and Aizawa, K., 2001. The effect of laser texturing of SiC surface on the critical load for the transition of water lubrication mode from hydrodynamic to mixed. Tribology International, 34(10), pp.703-711.

[66] Wang, X., Adachi, K., Otsuka, K. and Kato, K., 2006. Optimization of the surface texture for silicon carbide sliding in water. Applied Surface Science, 253(3), pp.1282-1286.

[67] Mourier, L., Mazuyer, D., Lubrecht, A.A. and Donnet, C., 2006. Transient increase of film thickness in micro-textured EHL contacts. Tribology International, 39(12), pp.1745-1756.

[68] Braun, D., Greiner, C., Schneider, J. and Gumbsch, P., 2014. Efficiency of laser surface texturing in the reduction of friction under mixed lubrication. Tribology international, 77, pp.142-147.

[69] Galda, L., Pawlus, P. and Sep, J., 2009. Dimples shape and distribution effect on characteristics of Stribeck curve. Tribology International, 42(10), pp.1505-1512.

[70] Erdemir, A., 2005. Review of engineered tribological interfaces for improved boundary lubrication. Tribology International, 38(3), pp.249-256.

[71] Hsu S., Wang X., Ives L.K., Zhang H., Liang Y., Ying C., 2005. An Integrated Surface Modification of Engineering Materials for Heavy Vehicle Applications, FY 2005 Progress Report on Heavy Vehicle Propulsion Materials, prepared by Oak Ridge National Laboratory for US Department of Energy, pp. 231-235, URL: http://www1.eere.energy.gov/vehiclesandfuels/pdfs/hv_propulsion_05/5d_hsu.pdf.

[72] Holmberg, K., Siilasto, R., Laitinen, T., Andersson, P. and Jäsberg, A., 2013. Global energy consumption due to friction in paper machines. Tribology International, 62, pp.58-77.

[73] Holmberg, K. and Erdemir, A., 2017. Influence of tribology on global energy consumption, costs and emissions. Friction, 5(3), pp.263-284.

[74] Etsion, I. and Sher, E., 2009. Improving fuel efficiency with laser surface textured piston rings. Tribology International, 42(4), pp.542-547.

[75] Ronen, A., Etsion, I. and Kligerman, Y., 2001. Friction-reducing surface-texturing in reciprocating automotive components. Tribology Transactions, 44(3), pp.359-366.

[76] Holmberg, K. and Mathews, A., 1994. Coatings tribology: a concept, critical aspects and future directions. Thin Solid Films, 253(1-2), pp.173-178.

[77] Varenberg, M., Ryk, G., Yakhnis, A., Kligerman, Y., Kondekar, N. and McDowell, M.T., 2016. Mechano-Chemical Surface Modification with Cu 2 S: Inducing Superior Lubricity. Tribology Letters, 64(2), p.28.

[78] Gachot, C., Rosenkranz, A., Hsu, S.M. and Costa, H.L., 2017. A critical assessment of surface texturing for friction and wear improvement. Wear, 372, pp.21-41.

[79] Ryk, G., Kligerman, Y. and Etsion, I., 2002. Experimental investigation of laser surface texturing for reciprocating automotive components. Tribology Transactions, 45(4), pp.444-449.

[80] Ryk, G. and Etsion, I., 2006. Testing piston rings with partial laser surface texturing for friction reduction. Wear, 261(7), pp.792-796.

[81] Etsion, I., 2004. Improving tribological performance of mechanical components by laser surface texturing. Tribology letters, 17(4), pp.733-737.

[82] Kovalchenko, A., Ajayi, O., Erdemir, A., Fenske, G. and Etsion, I., 2005. The effect of laser surface texturing on transitions in lubrication regimes during unidirectional sliding contact. Tribology International, 38(3), pp.219-25.

[83] Henry, Y., Bouyer, J. and Fillon, M., 2015. An experimental analysis of the hydrodynamic contribution of textured thrust bearings during steady-state operation: A comparison with the untextured parallel surface configuration. Proceedings of the Institution of Mechanical Engineers, Part J: Journal of Engineering Tribology, 229(4), pp.362-375.

[84] Etsion, I., Halperin, G., Brizmer, V. and Kligerman, Y., 2004. Experimental investigation of laser surface textured parallel thrust bearings. Tribology Letters, 17(2), pp.295-300.

[85] Dumitru, G., Romano, V., Weber, H.P., Haefke, H., Gerbig, Y. and Pflüger, E., 2000. Laser microstructuring of steel surfaces for tribological applications. Applied Physics A, 70(4), pp.485-487.

[86] Wang, W.Z., Huang, Z., Shen, D., Kong, L. and Li, S., 2013. The effect of triangle-shaped surface textures on the performance of the lubricated point-contacts. Journal of Tribology, 135(2), p.021503.

[87] Echávarri Otero, J., Guerra Ochoa, E., Bellón Vallinot, I. and Chacón Tanarro, E., 2017. Optimising the design of textured surfaces for reducing lubricated friction coefficient. Lubrication Science, 29(3), pp.183-199.

[88] Varenberg, M., Halperin, G. and Etsion, I., 2002. Different aspects of the role of wear debris in fretting wear. Wear, 252(11-12), pp.902-910.

[89] Yan, D., Qu, N., Li, H. and Wang, X., 2010. Significance of dimple parameters on the friction of sliding surfaces investigated by orthogonal experiments. Tribology Transactions, 53(5), pp.703-712.

[90] Schneider, J., Braun, D. and Greiner, C., 2017. Laser textured surfaces for mixed lubrication: influence of aspect ratio, textured area and dimple arrangement. Lubricants, 5(3), p.32.

[91] Chen, P., Xiang, X., Shao, T., La, Y. and Li, J., 2016. Effect of triangular texture on the tribological performance of die steel with TiN coatings under lubricated sliding condition. Applied Surface Science, 389, pp.361-368.

[92] Sedlaček, M., Podgornik, B., Ramalho, A. and Česnik, D., 2017. Influence of geometry and the sequence of surface texturing process on tribological properties. Tribology International, 115, pp.268-273.

[93] Segu, D.Z., Choi, S.G., hyouk Choi, J. and Kim, S.S., 2013. The effect of multi-scale laser textured surface on lubrication regime. Applied Surface Science, 270, pp.58-63.

[94] Segu, D.Z. and Kim, S.S., 2014. Influence on friction behavior of micro-texturing under lubricated non-conformal contact. Meccanica, 49(2), pp.483-492.

[95] Zhang, Y., Zhang, X., Wu, T. and Xie, Y.B., 2016. Effects of surface texturing on the tribological behavior of piston rings under lubricated conditions. Industrial Lubrication and Tribology, 68(2), pp.158-169.

[96] Shen, C. and Khonsari, M.M., 2016. The effect of laser machined pockets on the lubrication of piston ring prototypes. Tribology International, 101, pp.273-283.

[97] Vladescu, S.C., Medina, S., Olver, A.V., Pegg, I.G. and Reddyhoff, T., 2016. Lubricant film thickness and friction force measurements in a laser surface textured reciprocating line contact simulating the piston ring–liner pairing. Tribology International, 98, pp.317-329.

[98]Vladescu, S.C., Olver, A.V., Pegg, I.G. and Reddyhoff, T., 2015. The effects of surface texture in reciprocating contacts–An experimental study. Tribology International, 82, pp.28-42.

[99] Profito, F.J., Vladescu, S.C., Reddyhoff, T. and Dini, D., 2017. Experimental validation of a mixed-lubrication regime model for textured piston-ring-liner contacts. Materials Performance and Characterization, 6(2), pp.112-129.

[100] Vlădescu, S.C., Ciniero, A., Tufail, K., Gangopadhyay, A. and Reddyhoff, T., 2018. Optimization of pocket geometry for friction reduction in piston–liner contacts. Tribology Transactions, 61(3), pp.522-531.

[101] Galda, L., Dzierwa, A., Sep, J. and Pawlus, P., 2010. The effect of oil pockets shape and distribution on seizure resistance in lubricated sliding. Tribology Letters, 37(2), pp.301-311.

[102] Koszela, W., Dzierwa, A., Galda, L. and Pawlus, P., 2012. Experimental investigation of oil pockets effect on abrasive wear resistance. Tribology International, 46(1), pp.145-153.

[103] Rahmani, R., Shirvani, A. and Shirvani, H., 2007. Optimization of partially textured parallel thrust bearings with square-shaped micro-dimples. Tribology Transactions, 50(3), pp.401-406.

[104] Rahmani, R., Mirzaee, I., Shirvani, A. and Shirvani, H., 2010. An analytical approach for analysis and optimisation of slider bearings with infinite width parallel textures. Tribology International, 43(8), pp.1551-1565.

[105] Ji, J., Fu, Y. and Bi, Q., 2014. The influence of partially textured slider with orientation ellipse dimples on the behavior of hydrodynamic lubrication. Industrial Lubrication and Tribology, 66(2), pp.161-167.

[106] Uddin, M.S. and Liu, Y.W., 2016. Design and optimization of a new geometric texture shape for the enhancement of hydrodynamic lubrication performance of parallel slider surfaces. Biosurface and Biotribology, 2(2), pp.59-69.

[107] Brunetière, N. and Tournerie, B., 2012. Numerical analysis of a surface-textured mechanical seal operating in mixed lubrication regime. Tribology International, 49, pp.80-89.

[108] Zhou, Y., Zhu, H., Zhang, W., Zuo, X., Li, Y. and Yang, J., 2015. Influence of surface roughness on the friction property of textured surface. Advances in Mechanical Engineering, 7(2), p.1687814014568500.

[109] Ma, C., Duan, Y., Yu, B., Sun, J. and Tu, Q., 2017. The comprehensive effect of surface texture and roughness under hydrodynamic and mixed lubrication conditions. Proceedings of the Institution of Mechanical Engineers, Part J: Journal of Engineering Tribology, 231(10), pp.1307-1319.

[110] Siripuram, R.B. and Stephens, L.S., 2004. Effect of deterministic asperity geometry on hydrodynamic lubrication. Journal of tribology, 126(3), pp.527-534.

[111] Syed, I. and Sarangi, M., 2014. Hydrodynamic lubrication with deterministic micro textures considering fluid inertia effect. Tribology International, 69, pp.30-38.

[112] Kligerman, Y., Etsion, I. and Shinkarenko, A., 2005. Improving tribological performance of piston rings by partial surface texturing. Journal of Tribology, 127(3), pp.632-638.

[113] Liu, C., Lu, Y.J., Zhang, Y.F., Li, S. and Müller, N., 2017. Numerical study on the lubrication performance of compression ring-cylinder liner system with spherical dimples. PloS one, 12(7), p.e0181574.

[114] Yin, B., Xu, B., Jia, H., Zhou, H., Fu, Y. and Hua, X., 2017. Effects of the array modes of laser-textured micro-dimples on the tribological performance of cylinder liner–piston ring. Proceedings of the Institution of Mechanical Engineers, Part J: Journal of Engineering Tribology, p.1350650117732718.

[115] Usman, A. and Park, C.W., 2017. Numerical investigation of tribological performance in mixed lubrication of textured piston ring-liner conjunction with a non-circular cylinder bore. Tribology International, 105, pp.148-157.

[116] Morris, N., Leighton, M., De la Cruz, M., Rahmani, R., Rahnejat, H. and Howell-Smith, S., 2015. Combined numerical and experimental investigation of the micro-hydrodynamics of chevron-based textured patterns influencing conjunctional friction of sliding contacts. Proceedings of the Institution of Mechanical Engineers, Part J: Journal of Engineering Tribology, 229(4), pp.316-335.

[117] Pettersson, U., 2005. Surfaces designed for high and low friction (Doctoral dissertation, Institutionen för teknikvetenskaper).

[118] Blau, P.J., Qu, J., 2004. Laser Surface Texturing of Lubricated Ceramic Parts. Progress Report on Heavy Vehicle Propulsion Materials, pp. 123-128, URL: http://www1.eere.energy.gov/vehiclesandfuels/pdfs/hv_propulsion_04/4k_blaulaser.pdf

[119] De la Guerra Ochoa, E., Otero, J.E., Tanarro, E.C., Morgado, P.L., Lantada, A.D., Munoz-Guijosa, J.M. and Sanz, J.M., 2013. Optimising lubricated friction coefficient by surface texturing. Proceedings of the Institution of Mechanical Engineers, Part C: Journal of Mechanical Engineering Science, 227(11), pp.2610-2619.

[120] Nakatsuji, T. and Mori, A., 2001. The tribological effect of electrolytically produced micro-pools and phosphoric compounds on medium carbon steel surfaces in rolling-sliding contact. Tribology transactions, 44(2), pp.173-178.

[121] Xiaolei, W. and Kato, K., 2003. Improving the anti-seizure ability of SiC seal in water with RIE texturing. Tribology letters, 14(4), pp.275-280.

[122] Zhang, J. and Meng, Y., 2012. A study of surface texturing of carbon steel by photochemical machining. Journal of Materials Processing Technology, 212(10), pp.2133-2140.

[123] Parreira, J.G., Gallo, C.A. and Costa, H.L., 2012. New advances on maskless electrochemical texturing (MECT) for tribological purposes. Surface and Coatings Technology, 212, pp.1-13.

[124] Xuan, Z.H.O.U., Ningsong, Q.U., Zhibao, H.O.U. and Gai, Z.H.A.O., 2018. Electrochemical micromachining of microgroove arrays on phosphor bronze surface for improving the tribological performance. Chinese Journal of Aeronautics, 31(7), pp.1609-1618.

[125] Kortikar, S.N., 2004. Fabrication and characterization of deterministic microasperities on thrust surfaces. (Master's Thesis, University of Kentucky)

[126] Schneider, Y.G., 1984. Formation of surfaces with uniform micropatterns on precision machine and instruments parts. Precision engineering, 6(4), pp.219-225.

[127] Wos, S., Koszela, W. and Pawlus, P., 2015. Tribological behaviours of textured surfaces under conformal and non-conformal starved lubricated contact conditions. Proceedings of the Institution of Mechanical Engineers, Part J: Journal of Engineering Tribology, 229(4), pp.398-409.

[128] Wos, S., Koszela, W. and Pawlus, P., 2016. Determination of oil demand for textured surfaces under conformal contact conditions. Tribology International, 93, pp.602-613.

[129] Abhishek, K., Hiremath, S.S. and Karunanidhi, S., 2018. A novel approach to produce holes with high degree of cylindricity through Micro-Abrasive Jet Machining (μ-AJM). CIRP Journal of Manufacturing Science and Technology, 21, pp.110-119.

[130] Pettersson, U. and Jacobson, S., 2006. Tribological texturing of steel surfaces with a novel diamond embossing tool technique. Tribology international, 39(7), pp.695-700.

[131] Nakano, M., Korenaga, A., Korenaga, A., Miyake, K., Murakami, T., Ando, Y., Usami, H. and Sasaki, S., 2007. Applying micro-texture to cast iron surfaces to reduce the friction coefficient under lubricated conditions. Tribology letters, 28(2), pp.131-137.

[132] Greco, A., Raphaelson, S., Ehmann, K., Wang, Q.J. and Lin, C., 2009. Surface texturing of tribological interfaces using the vibromechanical texturing method. Journal of manufacturing science and engineering, 131(6), p.061005.

[133] Šamánek, O., Zimmerman, M., Svoboda, P., Křupka, I. and Vrbka, M., 2010. Influence of surface texturing on lubricant film formation and surface fatigue. Engineering Mechanics, 17(1), pp.27-36.

[134] Vrbka, M., Křupka, I., Svoboda, P., Šperka, P., Navrat, T., Hartl, M. and Nohava, J., 2011. Effect of shot peening on rolling contact fatigue and lubricant film thickness within mixed lubricated non-conformal rolling/sliding contacts. Tribology International, 44(12), pp.1726-1735.

[135] Cho, M.H. and Park, S., 2011. Micro CNC surface texturing on polyoxymethylene (POM) and its tribological performance in lubricated sliding. Tribology International, 44(7-8), pp.859-867.

[136] Moshkovith, A., Perfiliev, V., Gindin, D., Parkansky, N., Boxman, R. and Rapoport, L., 2007. Surface texturing using pulsed air arc treatment. Wear, 263(7-12), pp.1467-1469.

[137] Vincent, C., Monteil, G., Barriere, T. and Gelin, J.C., 2008. Control of the quality of laser surface texturing. Microsystem Technologies, 14(9-11), pp.1553-1557.

[138] Du, D., He, Y.F., Sui, B., Xiong, L.J. and Zhang, H., 2005. Laser texturing of rollers by pulsed Nd: YAG laser. Journal of Materials Processing Technology, 161(3), pp.456-461.

[139] Gao, Y., Wu, B., Zhou, Y. and Tao, S., 2011. A two-step nanosecond laser surface texturing process with smooth surface finish. Applied Surface Science, 257(23), pp.9960-9967.

[140] Neves, D., Diniz, A.E. and de Lima, M.S.F., 2006. Efficiency of the laser texturing on the adhesion of the coated twist drills. Journal of Materials Processing Technology, 179(1-3), pp.139-145.

[141] Yadav, G., Tiwari, S. and Jain, M.L., 2018. Tribological analysis of extreme pressure and anti-wear properties of engine lubricating oil using four ball tester. Materials Today: Proceedings, 5(1), pp.248-253.

[142] Grabon, W., Koszela, W., Pawlus, P. and Ochwat, S., 2013. Improving tribological behaviour of piston ring–cylinder liner frictional pair by liner surface texturing. Tribology International, 61, pp.102-108.

[143] Kim, B., Chae, Y.H. and Choi, H.S., 2014. Effects of surface texturing on the frictional behavior of cast iron surfaces. Tribology International, 70, pp.128-135.

[144] Rosenkranz, A., Szurdak, A., Gachot, C., Hirt, G. and Mücklich, F., 2016. Friction reduction under mixed and full film EHL induced by hot micro-coined surface patterns. Tribology International, 95, pp.290-297.

[145] Majumdar B.C., 1999. Introduction to Tribology of Bearings. Wheeler Publishing.

[146] Wu, Z., Xing, Y., Huang, P. and Liu, L., 2017. Tribological properties of dimple-textured titanium alloys under dry sliding contact. Surface and Coatings Technology, 309, pp.21-28.

[147] Sun, Q., Hu, T., Fan, H., Zhang, Y. and Hu, L., 2015. Dry sliding wear behavior of TC11 alloy at 500° C: influence of laser surface texturing. Tribology International, 92, pp.136-145.

[148] Patir, N. and Cheng, H.S., 1978. An average flow model for determining effects of three-dimensional roughness on partial hydrodynamic lubrication. Journal of lubrication Technology, 100(1), pp.12-17.

[149] Patir, N. and Cheng, H.S., 1979. Application of average flow model to lubrication between rough sliding surfaces. Journal of Lubrication Technology, 101(2), pp.220-229.

[150] Wu, C. and Zheng, L., 1989. An average Reynolds equation for partial film lubrication with a contact factor. Journal of tribology, 111(1), pp.188-191.

[151] Meng, F., Wang, Q.J., Hua, D. and Liu, S., 2010. A simple method to calculate contact factor used in average flow model. Journal of Tribology, 132(2), p.024505.

[152] Greenwood, J.A. and Tripp, J.H., 1970. The contact of two nominally flat rough surfaces. Proceedings of the institution of mechanical engineers, 185(1), pp.625-633.

[153] Akalin, O. and Newaz, G.M., 2001. Piston ring-cylinder bore friction modeling in mixed lubrication regime: part I—analytical results. Journal of tribology, 123(1), pp.211-218.

[154] Hu, Y., Cheng, H.S., Arai, T., Kobayashi, Y. and Aoyama, S., 1994. Numerical simulation of piston ring in mixed lubrication—a nonaxisymmetrical analysis. Journal of tribology, 116(3), pp.470-478.

[155] Mishra, P.C., Balakrishnan, S. and Rahnejat, H., 2008. Tribology of compression ring-to-cylinder contact at reversal. Proceedings of the Institution of Mechanical Engineers, Part J: Journal of Engineering Tribology, 222(7), pp.815-826.

[156] Gao, L., Yang, P., Dymond, I., Fisher, J. and Jin, Z., 2010. Effect of surface texturing on the elastohydrodynamic lubrication analysis of metal-on-metal hip implants. Tribology International, 43(10), pp.1851-1860.

[157] Gu, C., Meng, X., Xie, Y. and Li, P., 2016. A study on the tribological behavior of surface texturing on the nonflat piston ring under mixed lubrication. Proceedings of the Institution of Mechanical Engineers, Part J: Journal of Engineering Tribology, 230(4), pp.452-471.

[158] Gu, C., Meng, X., Xie, Y. and Yang, Y., 2016. Effects of surface texturing on ring/liner friction under starved lubrication. Tribology International, 94, pp.591-605.

[159] Tomanik, E., 2008. Friction and wear bench tests of different engine liner surface finishes. Tribology International, 41(11), pp.1032-1038.

Appendix

Method of numerical solution

The appendix gives the idea of the solution procedure for the modified Reynolds equation and asperity contact model.

Finite difference method (FDM) is used to solve the Reynolds differential equation. The modified Reynolds equation by taking account of fluid flow factors can be given as:

$$\frac{\partial}{\partial x}\left(\phi_x \frac{h^3}{\mu}\frac{\partial \bar{p}}{\partial x}\right)+\frac{\partial}{\partial x}\left(\phi_z \frac{h^3}{\mu}\frac{\partial \bar{p}}{\partial z}\right)=6U\phi_c \frac{\partial h}{\partial x}+6\sigma\frac{\partial \phi_s}{\partial x}+12\phi_c \frac{\partial h}{\partial x} \tag{A 1}$$

Expanding the terms in equation (A 1)

$$\frac{\partial \phi_x}{\partial x}h^3\frac{\partial \bar{p}}{\partial x}+3h^2\phi_x\frac{\partial h}{\partial x}\frac{\partial \bar{p}}{\partial x}+h^3\phi_x\frac{\partial^2 \bar{p}}{\partial x^2}+\frac{\partial \phi_z}{\partial z}h^3\frac{\partial \bar{p}}{\partial z}+3h^2\phi_z\frac{\partial h}{\partial z}\frac{\partial \bar{p}}{\partial z}+h^3\phi_z\frac{\partial^2 \bar{p}}{\partial z^2}$$

$$=6\mu U\phi_c\frac{\partial h}{\partial x}+6\mu U\sigma\frac{\partial \phi_s}{\partial x} \tag{A 2}$$

The differentials can be approximated by central difference method as:

$$\frac{\partial \bar{p}}{\partial x}=\frac{\bar{p}(i,j+1)-\bar{p}(i,j-1)}{2\Delta x} \qquad \frac{\partial \bar{p}}{\partial z}=\frac{\bar{p}(i+1,j)-\bar{p}(i-1,j)}{2\Delta z}$$

$$\frac{\partial \phi_x}{\partial x}=\frac{\phi_x(i,j+1)-\phi_x(i,j-1)}{2\Delta x} \qquad \frac{\partial \phi_z}{\partial z}=\frac{\phi_z(i+1,j)-\phi_z(i-1,j)}{2\Delta z}$$

$$\frac{\partial h}{\partial x}=\frac{h(i,j+1)-h(i,j-1)}{2\Delta x} \qquad \frac{\partial h}{\partial z}=\frac{h(i+1,j)-h(i-1,j)}{2\Delta z}$$

$$\frac{\partial \phi_s}{\partial x}=\frac{\phi_s(i,j+1)-\phi_s(i,j-1)}{2\Delta x}$$

$$\frac{\partial^2 \bar{p}}{\partial x^2}=\frac{\bar{p}(i,j+1)-\overline{2p}(i,j)+\bar{p}(i,j-1)}{\Delta x^2} \qquad \frac{\partial^2 \bar{p}}{\partial z^2}=\frac{\bar{p}(i+1,j)-\overline{2p}(i,j)+\bar{p}(i-1,j)}{\Delta z^2}$$

Then equation (A 2) will become

$$h^3(i,j)\frac{\phi_x(i,j+1)-\phi_x(i,j-1)}{2\Delta x}\frac{\bar{p}(i,j+1)-\bar{p}(i,j-1)}{2\Delta x}+3h^2(i,j)\phi_x(i,j)\frac{h(i,j+1)-h(i,j-1)}{2\Delta x}\frac{\bar{p}(i,j+1)-\bar{p}(i,j-1)}{2\Delta x}$$

$$+h^3(i,j)\phi_x(i,j)\frac{\bar{p}(i,j+1)-\overline{2p}(i,j)+\bar{p}(i,j-1)}{\Delta x^2}+h^3(i,j)\frac{\phi_z(i+1,j)-\phi_z(i-1,j)}{2\Delta z}\frac{\bar{p}(i+1,j)-\bar{p}(i-1,j)}{2\Delta z}$$

$$+3h^2(i,j)\phi_z(i,j)\frac{h(i+1,j)-h(i-1,j)}{2\Delta z}\frac{\bar{p}(i+1,j)-\bar{p}(i-1,j)}{2\Delta z}+h^3(i,j)\phi_z(i,j)\frac{\bar{p}(i+1,j)-\overline{2p}(i,j)+\bar{p}(i-1,j)}{\Delta z^2}$$

$$=6\mu U\phi_c\frac{h(i,j+1)-h(i,j-1)}{2\Delta x}+6\mu U\sigma\frac{\phi_s(i,j+1)-\phi_s(i,j-1)}{2\Delta x} \quad \text{(A 3)}$$

Arranging the terms and solving for $\bar{p}(i,j)$ will give

$$\bar{p}(i,j)=\frac{Ax_1+Ax_2+Ax_3+Bz_1+Bz_2+Bz_3-CC-DD}{EE} \quad \text{(A 4)}$$

Here,

$$Ax_1=\frac{\phi_x(i,j+1)-\phi_x(i,j-1)}{2\Delta x}\frac{\bar{p}(i,j+1)-\bar{p}(i,j-1)}{2\Delta x} \quad \text{(A 5)}$$

$$Bz_1=\frac{\phi_z(i+1,j)-\phi_z(i-1,j)}{2\Delta z}\frac{\bar{p}(i+1,j)-\bar{p}(i-1,j)}{2\Delta z} \quad \text{(A 6)}$$

$$Ax_2=\frac{3\phi_x(i,j)}{h(i,j)}\frac{h(i,j+1)-h(i,j-1)}{2\Delta x}\frac{\bar{p}(i,j+1)-\bar{p}(i,j-1)}{2\Delta x} \quad \text{(A 7)}$$

$$Bz_2=\frac{3\phi_z(i,j)}{h(i,j)}\frac{h(i+1,j)-h(i-1,j)}{2\Delta z}\frac{\bar{p}(i+1,j)-\bar{p}(i-1,j)}{2\Delta z} \quad \text{(A 8)}$$

$$Ax_3=\phi_x(i,j)\frac{\bar{p}(i,j+1)+\bar{p}(i,j-1)}{\Delta x^2} \quad \text{(A 9)}$$

$$Bz_3=\phi_z(i,j)\frac{\bar{p}(i+1,j)+\bar{p}(i-1,j)}{\Delta z^2} \quad \text{(A 10)}$$

$$CC=\frac{6\mu U\phi_c}{h^3(i,j)}\frac{h(i,j+1)-h(i,j-1)}{2\Delta x} \quad \text{(A 11)}$$

$$DD = \frac{6\mu U\sigma}{h^3(i,j)} \frac{\phi_s(i,j+1) - \phi_s(i,j-1)}{2\Delta x} \quad \text{(A 12)}$$

$$EE = 2\left(\frac{\phi_x(i,j)}{\Delta x^2} + \frac{\phi_z(i,j)}{\Delta z^2} \right) \quad \text{(A 13)}$$

The Gauss-Seidel iterative scheme is employed to solve equation (A 4) for mean hydrodynamic pressure. The pressure at any mesh point (*i, j*) is expressed in terms of pressure of four adjacent points. The iteration method starts by assuming the pressure at all these mesh points corresponds to respective boundaries as given in section 5.1.4.The equation (A 4) is solved for all the mesh points by satisfying the preset pressure convergence of 10^{-6}. As the pressures were assumed in the beginning, equation (A 4) will not be satisfied. Therefore, the error at the point (*i, j*) is

$(error)_{i,j}$= RHS of equation (A 4) - $\bar{p}(i,j)$ (A 14)

The new pressure can be computed as

$$\bar{p}(i,j)_{new} = \bar{p}(i,j)_{old} + (error)_{i,j} \times erf \quad \text{(A 15)}$$

Where, *erf* is the relaxation factor for pressure convergence. The relaxation factor may be over relaxation or under relaxation based on the stability of numerical solution. Once the pressure is balanced, the fluid film pressure determined.

After calculating the fluid film pressure, the asperity pressure is determined as discussed in section 5.1.2.

$$p_{asp} = K'E'F_{2.5}(H) \quad \text{(A 16)}$$

The asperity pressure is determined by using equation (A 16) for given conditions. Later, the fluid film pressure and asperity pressure are utilized to determine the total load support (W) as given in Eq. (5.28). This generated load should equate it to the total applied load (W_1) with a load convergence value of 10^{-3}. If the load balance criterion is not met, then the minimum fluid film thickness can be adjusted as:

$$h_0^n = h_0^o + (W_1 - W)\,Rel \quad \text{(A 17)}$$

Where Rel is the relaxation factor for load convergence. The relaxation factor can be assumed based on the numerical stability of the solution.

A code has to be generated to solve equations (A 4) and (A 16) numerically. Any programming platforms such as C, C++ and MATLAB can be used. Nowadays, MATLAB is popular for providing the easier syntax for coding.

Outcome of the research

1. Journals

- **Venkateswara Babu, P.**, Ismail Syed, Satish Ben, B., 2020. Experimental and Numerical Studies of Positive Texture Effect on Friction Reduction of Sliding Contact under Mixed Lubrication. Institute of Mechanical Engineers Part J: Journal of Engineering Tribology (SCI-indexed, Accepted).
- **Venkateswara Babu P.**, Ismail Syed, Satish Ben Beera, 2019. Influence of positive texturing on friction and wear properties of piston ring-cylinder liner tribo pair under lubricated conditions. Industrial Lubrication and Tribology, Vol. 71 Issue: 4, pp.515-524. (SCI-indexed)
- **Venkateswara Babu, P.**, Ismail Syed, Satish Ben, B., 2020. Experimental investigation on effects of positive texturing on friction and wear reduction of piston ring/cylinder liner system. Materials Today Proceedings, Vol. 24, pp.1112-11121. (Scopus-indexed)

2. Book chapters

- **Babu, P.V**., Syed, I. and Ben, B.S., 2020. Optimization of Texture Geometry for Enhanced Tribological Performance in Piston Ring-Cylinder Liner Contact under Pure Hydrodynamic and Mixed Lubrication. In Innovative Product Design and Intelligent Manufacturing Systems (pp. 799-808). Springer, Singapore. (Scopus-indexed)

3. Conferences

- **Venkateswara Babu, P.**, Ismail Syed, Satish Ben, B., 2019. Modification of Surface Topography and Study of its Impact on Friction and Wear Reduction of Sliding Contact. The 2nd World Summit on Advances in Science, Engineering and Technology, Indiana University-Purdue University, Indianapolis, USA.
- **Venkateswara Babu, P.**, Ismail Syed, Satish Ben, B., 2019. Surface modification effect on tribological performance of sliding contact. International Conference on Advanced Functional Materials and Devices, NIT Warangal.
- **Venkateswara Babu, P.**, Ismail Syed, Satish Ben, B., 2019. Hydrodynamic Performance of Different Shapes of Surface Textured Parallel Sliding Contact. Emerging Trends in Mechanical Engineering, NIT Warangal.
- Yogesh Thakre, Syed Ismail, **P Venkateswara Babu**, 2017. Effect of Positive Textures Size on Tribological Performance of Piston ring/Cylinder liner assembly. 9th International Conference on Industrial Tribology, Tribology Society of India, Kolkata.